氧化釔、氧化鈣、氧化鈰含量對鈦金屬與氧化鋯高溫擴散介面反應之影響

研 究 生：張耀文　　指導教授：林健正

國 立 交 通 大 學

材 料 科 學 與 工 程 學 系

摘 要

以熱壓法製備不同組成之 Y_2O_3/ZrO_2 複合材料，Y_2O_3 固溶於 ZrO_2 裡形成固溶體或者與 ZrO_2 反應形成 $Zr_3Y_4O_{12}$。Y_2O_3/ZrO_2 複合材料與鈦金屬進行 1700°C/10 min 之熔融擴散反應後，發現於 ZrO_2 中添加 30 vol%以上的 Y_2O_3 對於鈦側的介面反應會有很好的抑制效果，鈦側反應物 β'-Ti(Zr, O)形貌會變的非常細而且量非常少。於 ZrO_2 內添加 30 vol%以上的 Y_2O_3，氧化鋯側靠近原始介面處發現有 Y_2O_3 的晶粒重新析出，原因為由鈦側沿著氧化鋯晶界進入此區域的 Ti 液固溶了大量的 ZrO_2，而 Y_2O_3 與 Ti 不會反應，使得原來熱壓 30 vol% Y_2O_3-ZrO_2 陶瓷試片時固溶於 ZrO_2 裡的 Y_2O_3 晶粒重新析出。在各組介面試片裡氧化鋯側遠離原始介面處皆發現有 α-Zr 之析出，生成量以 10 vol%Y_2O_3 最多，並且隨著 Y_2O_3 含量增加而減少，α-Zr 析出的原因為 ZrO_2 缺氧所致。

以熱壓法製備不同組成 CaO-stabilized ZrO_2，CaO 固溶於 ZrO_2 裡形成固

溶體或者與 ZrO_2 反應形成 $CaZr_4O_9$。不同組成鈣安定氧化鋯與鈦金屬進行 1550°C/6 h 之固態擴散反應後，發現於 ZrO_2 中添加 5 mol%的 CaO 對於鈦側的介面反應有較好的抑制效果，原因為在鈦側有一層厚度約 2 μm 的 TiO，此 layer 的形成可以有效阻擋 Ti 與 Zr 的相互擴散。而在 9 mol% CaO 與 17 mol% CaO-ZrO_2 介面試片裡，由於 Ti、O、Zr 相互擴散劇烈的結果造成鈦側有 α-Ti(O)、β'-Ti(Zr, O)和 Ti_2ZrO 反應生成物，其中在 17 mol% CaO-ZrO_2 的介面試片發現一層厚度較薄的(β'-Ti + α-Ti)。在 9 mol% CaO 與 17 mol% CaO-ZrO_2 二組介面試片裡發現在氧化鋯側靠近原始介面處會有一層(β'-Ti + $CaZrO_3$)，$CaZrO_3$ 形成的原因為由鈦側擴散至此區域的 Ti 固溶了大量的 ZrO_2，CaO 不與 Ti 反應而會維持在殘留的 ZrO_2 基材中，使得氧化鋯基材 CaO/ZrO_2 的比例漸漸提高至 1:1 而形成斜方晶相的 $CaZrO_3$。在 17 mol% CaO-ZrO_2 介面試片裡，(β'-Ti + $CaZrO_3$)為 diffusion zone，$CaZrO_3$ 的形貌為柱狀並且幾乎平行於 O 與 Zr 的擴散方向。在各組介面試片裡氧化鋯側遠離原始介面處皆發現有 α-Zr 析出於 ZrO_{2-x} 晶界上，並且隨著 CaO 含量增加而減少。在 17 mol% CaO-ZrO_2 介面試片裡，由於 CaO 固溶於 ZrO_2 裡會產生較多異質的氧空孔，使得此區域的 *c*-ZrO_{2-x} 為 stable。

以粉末燒結法製備不同組成之 CeO_2/ZrO_2 系陶瓷材料，由於在高溫低氧分壓的環境下進行燒結，其中一部份的 CeO_2 固溶於 ZrO_2 裡形成固溶體或者與 ZrO_2 反應形成 $Ce_2Zr_3O_{10}$，另一部份的 CeO_2 則會還原成 Ce_2O_3 並且與 ZrO_2 反應形成 $Ce_2Zr_2O_7$。$Ce_2Zr_2O_7$ 是一個有氧空孔的結構，氧化鋯側的氧離子可以藉由氧空孔快速擴散至鈦側，因此在觀察不同組成之 CeO_2/ZrO_2 與鈦金屬進行 1550°C/4 h 之固態擴散反應後，發現 30 mol%

CeO_2-ZrO_2 的試片與 Ti 的介面反應最為嚴重，原因為在這組介面試片裡，氧化鋯側靠近原始介面處會形成一層非常厚的(β'-Ti + $Ce_2Zr_2O_7$)，$Ce_2Zr_2O_7$ 的生成機構為由鈦側擴散至此區域的 Ti 對 O 與 Zr 有非常大的親和力，使得 $Ce_2Zr_3O_{10}$ 產生相變化所形成。在 10 mol% CeO_2-ZrO_2 介面試片裡，Ti 側反應層的(α-Ti + Ti_2ZrO)形貌與 Y_2O_3/ZrO_2 及 CaO/ZrO_2 二組系統有很大的不同，原因為 Ce 與 Zr 同為+4 價，因此 10 mol% CeO_2 固溶於 ZrO_2 中並不會產生異質的氧空孔，而 Y_2O_3 與 CaO 固溶於 ZrO_2 裡時因為異價陽離子的取代而產生較多異質的氧空孔，因此 10 mol% CeO_2-ZrO_2 的介面試片裡氧化鋯側氧離子擴散至鈦側的速度會比另外二組系統慢許多，因此造成(α-Ti + Ti_2ZrO)靠近原始介面處析出。當 ZrO_2 中添加 CeO_2 的比例超過 50 mol%時，發現氧化鋯側靠近原始介面處有 secondary CeO_2 析出，其生成機構為高溫時 $Ce_2Zr_3O_{10}$ 分解成 CeO_2 與 ZrO_2 二相，而擴散至此區域的 Ti 固溶大量 ZrO_2 形成 α-Ti + β-Ti，因此 cooling 下來後使得 secondary CeO_2 析出，實驗並發現 CeO_2 添加的比例達到 50 mol%時，鈦側只有 α-Ti(O)，並無其它的反應層，其結果顯示由於 secondary CeO_2 的析出可以有效阻擋氧化鋯側 Zr 離子往鈦側擴散，對於鈦側的介面反應會有較好的抑制效果。

Dependence of Yttria, Calcia and Ceria Contents on the Interfacial Reaction between Titanium and Zirconia-Containing Ceramics

Yao-Wen Chang, Ph. D.
Department of Materials Science and Engineering,
National Chiao Tung University, Hsinchu, Taiwan

Prof. Chien-Cheng Lin, Advisor

Abstract

Various Y_2O_3/ZrO_2 samples were fabricated by hot pressing, whereby Y_2O_3 was mutually dissolved or reacted with ZrO_2 as a solid solution or $Zr_3Y_4O_{12}$. Hot pressed samples were allowed to react with Ti melt at 1700°C for 10 min in argon. Microstructural characterization was conducted using x-ray diffraction and analytical electron microscopy. The Y_2O_3/ZrO_2 samples became more stable with increasing Y_2O_3 since Y_2O_3 was hardly reacted and dissolved with Ti melt. The incorporation of more than 30 vol% Y_2O_3 could effectively suppress the reactions in the Ti side, where only a very small amount of α-Ti and β'-Ti was found. When ZrO_2 was dissolved into Ti on the zirconia side near the original interfaces, Y_2O_3 re-precipitated in the samples containing 30-70 vol% Y_2O_3, because the solubility of Y_2O_3 in Ti was very low. In the region far from the original interface, α-Zr, Y_2O_3, and/or residual $Zr_3Y_4O_{12}$ were found in the samples containing more than 50 vol% Y_2O_3 and the amount of α-Zr decreased with increasing Y_2O_3.

ZrO_2 samples with various CaO contents were fabricated by hot-pressing, whereby CaO was dissolved by and/or reacted with ZrO_2 to form a solid solution and/or $CaZr_4O_9$, respectively. After a reaction with Ti at 1550°C for 6 h in argon, the interfacial microstructures were characterized using x-ray diffraction and analytical electron microscopy. Experimental results were very different from those previously found in the Y_2O_3-ZrO_2 system. The 5 mol% CaO-ZrO_2 sample was relatively stable due to the formation of a thin TiO layer acting as a diffusion barrier phase. However, α-Ti(O), β'-Ti(Zr, O) and/or Ti_2ZrO were found in 9 or 17 mol% CaO-ZrO_2 due to extensive interdiffusion of Ti, O, and Zr with a much thinner (β'-Ti + α-Ti) layer in 17 mol% CaO-ZrO_2 than in 9 mol% CaO-ZrO_2. Because CaO was hardly dissolved into Ti, it fully remained in the residual ZrO_2, leading to the formation of spherical $CaZrO_3$ in 9 mol% CaO-ZrO_2 and columnar $CaZrO_3$ in 17 mol% CaO-ZrO_2. In the region far from the original interface, abundant intergranular α-Zr was formed in 5 or 9 mol% CaO-ZrO_2. Scattered α-Zr and $CaZrO_3$ were found in 17 mol% CaO-ZrO_2 because a high concentration of extrinsic oxygen vacancies, which were created by the substitution of Ca^{+2} for Zr^{+4}, effectively retarded the reduction of zirconia.

Ceramics with various CeO_2/ZrO_2 ratios were sintered at 1400ºC/4 h in air. The sintered bodies, consisting of CeO_2, ZrO_2, $Ce_2Ze_3O_{10}$ and/or $Ce_2Ze_2O_7$, were taken into reaction with Ti at 1550°C for 4 h in argon. Microstructural characterization was conducted using x-ray diffraction and analytical electron microscopy. Both dissolution and reaction-oxidation were the predominant mechanisms controlling the interface reactions. Because CeO_2 was hardly dissolved into Ti, the CeO_2/ZrO_2 samples became more stable with increasing CeO_2. The incorporation of more than 50

mol% CeO_2 effectively suppressed the interfacial reactions in the Ti side without the formation of β'-Ti(Zr, O). In 10 mol% CeO_2-ZrO_2, selected dissolution of ZrO_2 into Ti gave rise to the formation of a diffusion zone with a columnar shaped $Ce_2Zr_3O_{10}$. In the 30-50 mol% CeO_2-ZrO_2 samples, Ce^{+4} was reduced to Ce^{+3} after reaction with Ti so that $Ce_2Zr_3O_{10}$ was transformed into $Ce_2Ze_2O_7$. Secondary CeO_2 was re-precipitated at the interface between Ti and the samples containing 50-70 mol% CeO_2. A reaction affected zone existed on the ceramic side far from the original interface due to the outward diffusion of oxygen. In the reaction affected zone, ZrO_2 was reduced into α-Zr and ZrO_{2-x}, while CeO_2 was reduced into $Ce_2Zr_2O_7$ and Ce_2O_3, depending upon the relative amounts of CeO_2 and ZrO_2. The effect of mass transport and contituent phases (e.g., CeO_2 and $Ce_2Zr_2O_7$) on the phase transformation in various reaction layers are elucidated.

誌 謝

博士研究生涯中，首先要感謝指導教授林健正老師，在實驗上給予許多教導與建議，讓學生了解做研究該有的態度與思考，使得學生能順利完成博士學位，在此並由衷的感謝博士學位口試委員們在論文的指導與建議。

感謝所有畢業與在學的精密陶瓷實驗室夥伴們，因為有了你們研究生活才會多采多姿。感謝璞玉計劃小組所有姑娘們，你們的加油打氣讓我備感窩心，也預祝璞玉計劃新校區推動順利成功。

最後要感謝我最親愛的爸爸、媽媽與女朋友燕玲，有了你們在生活上以及精神上全力的支持我與鼓勵我，才能讓我順利完成博士論文，在此獻給所有關心我以及我所關心的人，願大家都平安、健康!

Contents

List of Tables

List of Figures

Chapter 1
Introduction

1.1 Titanium and its Alloys

Ti and its alloy (i.e., Ti6Al4V) are widely used in the aerospace, chemical processing industries, golf club heads, and microelectronics because they have excellent properties such as high tensile strength, light weight, and good corrosion resistance. Moreover, commercially pure titanium and some titanium alloys are biologically compatible with human tissues and bones.

In the past, titanium industry has been dependent on the aerospace market. Recently, titanium alloy development has focused on the industrial application such as in the sport fields. Growth of titanium demand is according to the productions of golf clubs and has forced the technical improvements and downward the cost.[1] Strategies in today are to improve the manufacturing processes and to offer new product forms or more cost effective products.[2]

1.2 Casting of Titanium

Castings are usually produced by molten titanium with vacuum arc melting (VAR) in a water-cooled copper crucible. A simplified scheme[3] of one type of titanium casting process is shown in Fig.1.1. A major disadvantage of the VAR process using a water-cooled copper crucible is the potential hazard it presents. The close proximity of the water to molten metal creates a problem of leakage whereby explosive hydrogen is generated by water in

touch with the molten metal. Therefore, a ceramic crucible used in the vacuum induction melting (VIM) with no need of cooling water could be of great advantage. Because titanium is a highly reactive metal, how to control the interfacial reactions between titanium and ceramic crucible and/or mold is of great concern related to the investment casting.

1.3 Interfacial Reactions During Casting

Kahveci and Welsch[4] have indicated that the ductility of α-Ti is influenced by interstitial oxygen and the toughness also decreased with the increase in oxygen and nitrogen until the material eventually becomes quite brittle. The α-Ti usually forms at the surface of titanium casting, which is called α-casing, resulting in a hardening layer. Because the α-casing is detrimental to its mechanic properties, it must be removed by chemical milling. However, this treatment can increase the manufacturing cost and chemical pollution. Therefore, how to well control the interfacial reactions is very important to casting technology.

1.4 Previous Researches on the Interfacial Reactions between Titanium and Ceramics

Because some refractory materials could be used on the melting applications as well as investment casting for titanium, the interfacial reactions between refractory materials and titanium were extensively investigated in the last few decades.[5-13] Most of the studies attempted to find a suitable material being used in titanium casting or melting. However, the mechanisms of interfacial reactions were not fully elucidated yet. Saha *et. al*.[12] had found that the microhardness profile or the oxygen could be as an index for the

evaluation of the reactivity. Espie *et. al*.[14] indicated that titanium could dissolve zirconia to form the solid solution of α-Ti(O) and affected free energy of the titanium. Ruh[10] reported that up to 10 mol% of each O and Zr could be retained in the solid solution of Ti at temperatures ranging from 1200°C to 2000°C, while the solubility of Ti in ZrO_2 was less than 4 at%. Zirconia would transform into the oxygen deficient zirconia, causing the blackening of zirconia after reaction without the formation of new phase.[8,10] Base on the phase diagram of Zr-O system,[15] α-Zr and ZrO_{2-x} coexisted at high temperatures. The α-Zr could precipitate from the metastable ZrO_{2-x}. However, most of the studies indicated that the ZrO_2 would transform into the oxygen deficient zirconia (ZrO_{2-x}) during reaction.

1.5 Purposes of This Research

Interfacial reactions between metal and ceramic play an important role in the determination of the manufacture processing of titanium and mechanical properties.[16,17] If an inert crucible material were developed, a significant reduction in the cost of titanium ingots would have been achieved. In the present study, we characterized the interface microstructure in order to shed light on the formation mechanisms of reaction layers between titanium and zirconia. Effect of Yttria, Calcia and Ceria contents on the interfacial reaction between titanium and zirconia were completely elucidated.

1.6 Thesis Outline

Chapter 1 describes the basic applications of titanium and its alloy, casting of titanium, and interfacial reactions during casting. It also reviews the previous literatures talking about interfacial reaction between titanium and

zirconia.

In this study, the interfaces between titanium and various Y_2O_3/ZrO_2, CaO/ZrO_2, and CeO_2/ZrO_2 samples after reaction at high temperatures were characterized using analytical scanning electron microscopy (SEM), analytical transmission electron microscopy (TEM), both attached with an energy-dispersive spectrometer (EDS), X-ray diffraction (XRD), and electron probe microanalyses (EPMA).

Chapter 2 describes the various Y_2O_3/ZrO_2 samples were hot-pressed and allowed to react with Ti melt at 1700°C for 10 min. The Y_2O_3/ZrO_2 samples became more stable with increasing Y_2O_3 since Y_2O_3 was hardly reacted and dissolved with Ti melt. The incorporation of more than 30 vol% Y_2O_3 could effectively suppress the reactions in the Ti side, where only a very small amount of α-Ti and β'-Ti was found. When ZrO_2 was dissolved into Ti on the zirconia side near the original interfaces, Y_2O_3 re-precipitated in the samples containing 30-70 vol% Y_2O_3, because the solubility of Y_2O_3 in Ti was very low. In the region far from the original interface, α-Zr, Y_2O_3, and/or residual $Zr_3Y_4O_{12}$ were found in the samples containing more than 50 vol% Y_2O_3 and the amount of α-Zr decreased with increasing Y_2O_3.

Chapter 3 studies the interfacial reactions between titanium and various calcia-stabilized zirconia at 1550°C for 6 h. The 5 mol% $CaO-ZrO_2$ sample was relatively stable due to the formation of a thin TiO layer acting as a diffusion barrier phase. However, α-Ti(O), β'-Ti(Zr, O) and/or Ti_2ZrO were found in 9 or 17 mol% $CaO-ZrO_2$ due to extensive interdiffusion of Ti, O,

and Zr with a much thinner (β'-Ti + α-Ti) layer in 17 mol% CaO-ZrO_2 than in 9 mol% CaO-ZrO_2. Because CaO was hardly dissolved into Ti, it fully remained in the residual ZrO_2, leading to the formation of spherical $CaZrO_3$ in 9 mol% CaO-ZrO_2 and columnar $CaZrO_3$ in 17 mol% CaO-ZrO_2. In the region far from the original interface, abundant intergranular α-Zr was formed in 5 or 9 mol% CaO-ZrO_2. Scattered α-Zr and $CaZrO_3$ were found in 17 mol% CaO-ZrO_2 because a high concentration of extrinsic oxygen vacancies, which were created by the substitution of Ca^{+2} for Zr^{+4}, effectively retarded the reduction of zirconia.

Chapter 4 studies the interfacial reactions between titanium and various CeO_2/ZrO_2 samples at 1550°C/4 h. Both dissolution and reaction-oxidation were the predominant mechanisms controlling the interface reactions. Because CeO_2 was hardly dissolved into Ti, the CeO_2/ZrO_2 samples became more stable with increasing CeO_2. The incorporation of more than 50 mol% CeO_2 effectively suppressed the interfacial reactions in the Ti side without the formation of β'-Ti(Zr, O). In 10 mol% CeO_2-ZrO_2, selected dissolution of ZrO_2 into Ti gave rise to the formation of a diffusion zone with a columnar shaped $Ce_2Zr_3O_{10}$. In the 30-50 mol% CeO_2-ZrO_2 samples, Ce^{+4} was reduced to Ce^{+3} after reaction with Ti so that $Ce_2Zr_3O_{10}$ was transformed into $Ce_2Ze_2O_7$. Secondary CeO_2 was re-precipitated at the interface between Ti and the samples containing 50-70 mol% CeO_2. A reaction affected zone existed on the ceramic side far from the original interface due to the outward diffusion of oxygen. In the reaction affected zone, ZrO_2 was reduced into α-Zr and ZrO_{2-x}, while CeO_2 was reduced into $Ce_2Zr_2O_7$ and Ce_2O_3, depending upon the relative amounts of CeO_2 and ZrO_2. The effect of mass transport and contituent phases (e.g., CeO_2 and $Ce_2Zr_2O_7$)

on the phase transformation in various reaction layers are fully elucidated.

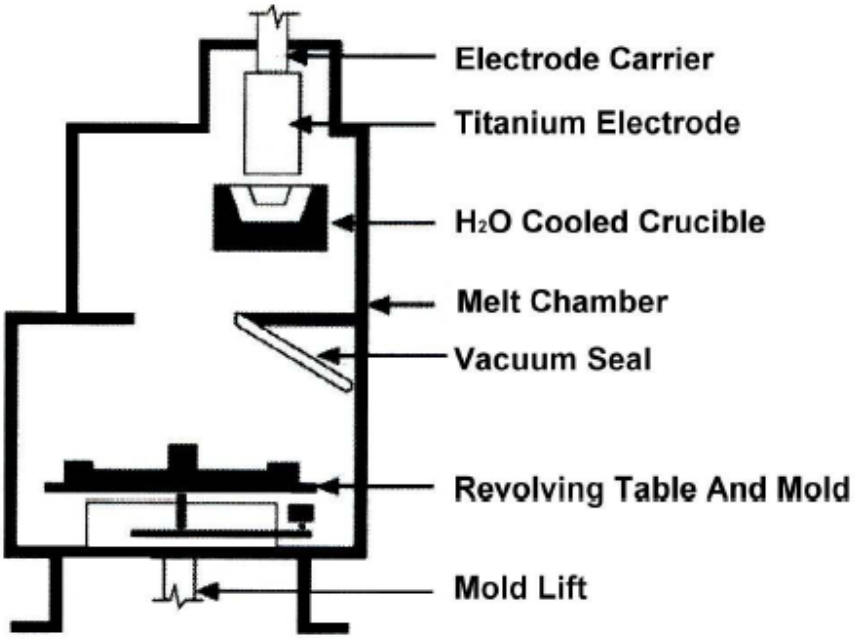

Fig. 1.1 Schematic of a vacuum casting furnace used for making titanium castings.

Chapter 2

Effect of Yttria on Interfacial Reactions Between Titanium Melt and Hot-Pressed Yttria/Zirconia Composites at 1700°C

2.1 Introduction

The majority of ceramic materials seriously react with titanium and titanium alloys during casting, resulting in an α-casing and the deterioration of mechanical properties. Because no suitable ceramic crucible is available, titanium and titanium alloys are usually melted in a water-cooled copper crucible by consumable electrode vacuum arc melting (VAR) instead of vacuum induction melting (VIM). However, there are some drawbacks to the VAR process, including the high cost of the equipment, scrape recycle, and long cycle time. If a suitable crucible material were available, the VIM process would be feasible in industry. Furthermore, titanium castings need to be chemically milled in order to remove the reaction products on their surface. If the interfacial reactions between titanium and ceramic mold were well controlled, the chemical milling of the so-called α-casing would not be required. Therefore, determining how to control the interfacial reactions between titanium melt and some ceramic materials is of great interest.

Extensive studies have been carried out on the interfacial reactions between titanium melt and zirconia molds and/or crucibles in the last few decades.[4,8,9,13,18-21] Saha and Jacob[13] indicated that a brittle α-case was

formed at the surface of titanium parts and thus adversely affected their mechanical properties. Weber[9,20] found a feather-like eutectic phase and blackened zirconia after titanium alloys reacted with a zirconia crucible. Zhu *et al.*[21] claimed that there were two distinct chemical reaction layers at the interface between titanium melt and zirconia after reaction at 1700°C. Holcombe and Serandos[22] stated that the composite crucible of W and Y_2O_3 revealed little contamination after reaction with titanium melt.

Recently, Lin and his colleagues[23-29] have thoroughly investigated the interfacial reaction mechanisms between titanium (or titanium alloys) and 3Y-ZrO_2 using analytical transmission electron microscopy. The lamellar orthorhombic Ti_2ZrO and the ordered titanium suboxide (Ti_3O) were formed in the α-Ti(Zr, O) at the interface between Ti melt and 3Y-ZrO_2 after reaction at 1750°C.[23] For the Ti/3Y-ZrO_2 diffusion couple, both lamellar orthorhombic Ti_2ZrO and spherical hexagonal Ti_2ZrO were found in α-Ti(Zr, O) after annealing at 1550°C.[24,26,27] In addition, the orientation relations of acicular α-Ti and β'-Ti were determined to be $[2\bar{1}\bar{1}0]_{\alpha\text{–Ti}}$ //$[001]_{\beta'\text{-Ti}}$ and $(0001)_{\alpha\text{–Ti}}$ //$(100)_{\beta'\text{-Ti}}$ in combination of $[2\bar{1}\bar{1}0]_{\alpha\text{–Ti}}$ //$[021]_{\beta'\text{-Ti}}$ and $(0001)_{\alpha\text{–Ti}}$ //$(1\bar{1}2)_{\beta'\text{-Ti}}$, respectively. Lin and Lin[25] also found the intergranular α-Zr, twinned *t'*-ZrO_{2-x}, lenticular *t*-ZrO_{2-x}, and ordered *c*-ZrO_{2-x} on the zirconia side far from the interface between Ti and 3Y-ZrO_2 after annealing at 1550°C.

Various ratios of Y_2O_3/ZrO_2 samples were attempted in this study to achieve better control over the reactions on the titanium side as well as the ceramic side. The powder mixtures of Y_2O_3/ZrO_2 were hot pressed and then allowed to react with titanium melt at 1700°C for 10 min in argon. Various

reaction layers at the interface between titanium melt and Y_2O_3/ZrO_2 samples were characterized using analytical scanning electron microscopy and analytical transmission electron microscopy. The effect of Y_2O_3 on the interfacial reactions between Ti melt and Y_2O_3/ZrO_2 samples will be elucidated in this study.

2.2 Experimental Procedures

The starting powders used were zirconia (> 99.95 wt% ZrO_2+HfO_2 with HfO_2 accounting for approximately 2%-3% of this total, < 0.002 wt% SiO_2, < 0.002 wt% Al_2O_3, < 0.005 wt% Fe_2O_3, < 0.005 wt% TiO_2, < 0.002 wt% CaO; 0.5 μm in average; Toyo Soda Mfg. Co., Tokyo, Japan), yttria (> 99.9 wt% Y_2O_3 with trace rare earth oxides < 0.001 wt% CeO_2, < 0.001 wt% Pr_6O_{11}, < 0.01 wt% Nd_2O_3, < 0.003 wt% Sm_2O_3, < 0.005 wt% Tb_4O_7, < 0.005 wt% Dy_2O_3, < 0.001 wt% CaO, < 0.001 wt% Fe_2O_3 and other traces in balance; 0.5 μm in average; NYC Ltd., Fukuoka, Japan), and commercially pure titanium (with a nominal composition of 99.31 wt% Ti, 0.3 wt% Fe, 0.25 wt% O, 0.1 wt% C, 0.03 wt% N, 0.01 wt% H., 60-70 μm average in diameter, Alfa Aesar, Ward Hill, MA).

Powder mixtures with various Y_2O_3/ZrO_2 ratios were dispersed in the ethanol solvent. The pH of the suspension was adjusted to 11 by adding NH_4OH, and the suspension was ultrasonically vibrated about 10 min (Model XL-2020, Sonicator, Heat Systems Inc., Farmingdale, NY). The suspension was dried in an oven at 150°C, ground with an agate mortar and pestle, and then the mixtures were passed through 80 mesh. Samples with various Y_2O_3/ZrO_2 ratios were prepared by hot pressing in a graphite furnace

at 1550°C-1600°C for 30 min in an Ar atmosphere (Model HP50-MTG-7010, Thermal Technology Inc., Santa Rosa, CA). Oxygen-deficient zirconia was formed in the as hot-pressed samples. To avoid the inaccuracy, samples were annealed in air at 1300ºC for 1 h so that stoichiometric zirconia was obtained.

The hot press conditions, compositions, relative densities, and designations of Y_2O_3/ZrO_2 samples are listed in Table 2.1. The Y_2O_3/ZrO_2 samples contained 10, 30, 50, 70, 90 and 100 vol% Y_2O_3, respectively, and were balanced with ZrO_2. The sample consisting of 10 vol% Y_2O_3 and 90 vol% ZrO_2 was designated as 10Y90Z, and so on. The apparent densities of all Y_2O_3/ZrO_2 powder mixtures were measured using gas pycnometry with 99.99% pure helium (Model MultiVolume Pycnometer 1305, Micromeritics, Norcross, GA). The bulk densities of the hot-pressed Y_2O_3/ZrO_2 samples were determined by the Archimedes method using water as an immersion medium. For a non-porous powder, the apparent density approximates the true density and can be used as the reference point in calculating the percentage of the theoretic density of a hot-pressed body. The relative densities of the hot-pressed samples were calculated as follows: relative density = (bulk density/apparent density) × 100%.

Hot-pressed samples were cut and machined to dimensions of about 10 × 10 × 5 mm. A bulk specimen was vertically placed into the zirconia crucible, and then tightly packed with commercially pure titanium powder. The crucible was put in an electric resistance furnace (Model No. 4156, Centorr Inc., Nashua, New Hampshire, UK) with tungsten mesh heating elements.

The chamber was evacuated to 10^{-4} torr and then refilled with argon. The cycle of evacuation and purging with argon was repeated three times. The temperature was increased to 1700°C at a heating rate of 10°C/min, held at 1700°C for 10 min and then cooled to room temperature in the furnace. The bulk specimen was fully immersed in the titanium melt above the melting point of titanium (1668°C), resulting in an interfacial reaction between Ti and Y_2O_3/ZrO_2 composites.

The phase identification of Ti and Y_2O_3/ZrO_2 samples was performed using an x-ray diffractometer (XRD, Model MXP18, Mac Science, Yokohama, Japan). The operating conditions of x-ray diffraction were CuK_α radition at 50 kV and 150 mA, and a scanning rate of 2° /min.

A scanning electron microscope (SEM, Model JSM 6500F, JEOL Ltd., Tokyo, Japan) was used for the microstructural observation on the interfaces between Ti and various Y_2O_3/ZrO_2 samples. Cross-sectional SEM specimens were cut and ground using standard procedures and finally polished using diamond pastes of 6, 3, and 1 μm in sequence.

The compositions of various phases in the reaction layers were measured by an electron probe microanalyzer (EPMA, JXA-8800M, JEOL Ltd., Tokyo, Japan) with an atomic number, absorption, and fluorescence correction (ZAF) program.[30] The operating conditions for EPMA were as follows: the accelerating voltage was 15 kV, the probe current was 1.5×10^{-8} A, and the beam diameter was 1 μm.

The interfacial microstructures were also characterized using a transmission

electron microscope (TEM, Model Tecnai 20, Philips, Eindhoven, Holland) equipped with an energy dispersive x-ray spectrometer (EDS, Model ISIS 300, Oxford Instrument Inc., London, UK). Cross-sectional TEM specimens were cut and then ground down to ~80 μm with a diamond matted disk, polished with diamond pastes of 6, 3, and 1 μm in sequence, and dimpled to a thickness of 50 μm. Finally the TEM specimens were ion milled by a precision ion miller (Model 691, Gatan Inc., Pleasanton, CA). Quantitative analyses of individual phases in the reaction layers were conducted by the Cliff-Lorimer standardless technique.[31]

2.3 Results and Discussion

2.3.1 XRD Analyses

Figure 2.1 shows the x-ray diffraction spectra of various Y_2O_3/ZrO_2 samples as well as pure Y_2O_3 after hot pressing. These spectra were arranged for Y_2O_3, 90Y10Z, 70Y30Z, 50Y50Z, 30Y70Z, and 10Y90Z, respectively, in a sequence from top to bottom. X-ray phases of these hot-pressed Y_2O_3/ZrO_2 samples are summarized in Table I. In the hot-pressed 90Y10Z, all of the zirconia was dissolved in yttria such that only cubic Y_2O_3 was detected. The hot-pressed 70Y30Z consisted of rhombohedral $Zr_3Y_4O_{12}$ and cubic Y_2O_3, while the XRD spectrum of the hot-pressed 50Y50Z showed only rhombohedral $Zr_3Y_4O_{12}$ peaks.[32] As for the hot-pressed 30Y70Z, only the cubic ZrO_2 phase was detected because all of the Y_2O_3 went into solid solution in zirconia. In other words, the cubic ZrO_2 was fully stabilized in 30Y70Z. However, *c*-ZrO_2, *t*-ZrO_2 and *m*-ZrO_2 were found in 10Y90Z or in a partially stabilized ZrO_2. In general, Y_2O_3 was mutually dissolved or reacted with ZrO_2 as a solid solution or $Zr_3Y_4O_{12}$ in hot-pressed Y_2O_3/ZrO_2

samples. Pascual and Durán[32] found Y_6ZrO_{11} after sintering at 2000°C for 3 h and subsequent prolonged annealing. However, Y_6ZrO_{11} was not found in this study because the equilibrium was probably not established.

2.3.2 SEM and TEM Analyses

Figures 2.2(a)-(f) display backscattered electron images of the cross-sections normal to the interfaces of Ti and various Y_2O_3/ZrO_2 samples after reaction at 1700°C for 10 min. Titanium is shown to the left of the micrograph, while zirconia is on the right-hand side. Arrows indicate the original interfaces of Ti and individual Y_2O_3/ZrO_2 samples. The original interfaces were deliberately located according to the characteristic K_α X-ray maps of yttrium (not shown), which was relatively immobile with respect to Zr, O, and Ti, etc. The large pores in the ceramic side, as shown in Figs. 2.2(a) and (b), were attributed to the Kirkendall effect since Zr and O diffused to the titanium side more rapidly than Ti diffused to the zirconia side.

Figure 2.2 indicates that extensive reactions took place at the interface between Ti and 10Y90Z. It was previously reported that needle-like α-Ti and some lamellar phases were usually found in the titanium side because of the interfacial reactions between Ti and ZrO_2.[23,24,26,27] However, only a limited reaction took place on the titanium side at the interface between Ti and those samples containing more than 30 vol% Y_2O_3, while 90Y10Z and pure Y_2O_3 reacted minimally with Ti melt. This indicated that interfacial reactions were effectively suppressed in those samples containing more than 30 vol% Y_2O_3. This fact plays an important role in the engineering respect of Ti castings such that a controlled interfacial reaction results in a lower amount of α-casing and thus better mechanical properties. Even though the

system became more stable with increasing Y_2O_3, several reaction layers were found on the zirconia side after interfacial reactions between Ti and various Y_2O_3/ZrO_2 samples. Microstructures of the reaction layers at the interface between Ti and various Y_2O_3/ZrO_2 samples were characterized using SEM/EDS and TEM/EDS and the results are listed in Table II. The details will be described below.

(A) Reaction layer "I" on the metal side

The reaction layer "I" was observed on the metal side of the interfaces between Ti and Y_2O_3/ZrO_2 samples containing less than 70 vol% Y_2O_3 as shown in Figs. 2.2(a)-(d). An α-Ti phase with a small amount of oxygen in solid solution was to the left of reaction layer "I". The reaction layer "I" consisted of β'-Ti(Zr, O) and/or acicular α-Ti(Zr, O) in the α-Ti matrix. A clear comparison could be made with Fig. 2.3, displaying the backscattered electron images of the reaction layer "I" in 10Y90Z, 30Y70Z, and 50Y50Z, respectively, at higher magnification. As shown in Fig. 3(a) together with Fig. 2.2(a), a large amount of β'-Ti(Zr, O) and acicular α-Ti(Zr, O) were precipitated in the α-Ti matrix at the interface between Ti and 10Y90Z. However, a relatively small amount of β'-Ti and acicular α-Ti existed at the interface between Ti and 30Y70Z [Fig. 2.3(b)] and only very few β'-Ti at the interface between Ti and 50Y50Z [Fig. 2.3(c)]. For comparison, several reaction layers consisting of α-Ti(Zr, O), β'-Ti(Zr, O) and Ti_2ZrO were found in the diffusion couple of Ti and 3Y-ZrO_2 after reactions ranging from 1400ºC to 1550ºC.[24,26,27]

(B) Reaction layer "II" on the ceramic side

Figure 2.4 shows the backscattered electron image of reaction layers "II" on

the outermost ceramic side of Ti/10Y90Z after reaction at 1700°C for 10 min. β'-Ti (bright), acicular α-Ti (dark), and spherical *c*-ZrO_{2-x} coexisted in reaction layer "II" at the interface between Ti and 10Y90Z, where zirconia was extensively dissolved in titanium. Based on EPMA results, β'-Ti in reaction layer "II" consisted of 43.98 at% Ti, 25.97 at% Zr, and 30.05 at% O, indicating that β'-Ti was stabilized by dissolving a significant amount of Zr. Concurrently, zirconia was retained as a cubic phase because it dissolved as high as 10.7 at% Y as a stabilizer. This was consistent with the results found by Zhu *et al.,*[21] indicating that Y was retained in cubic zirconia, when Y_2O_3-stabilized zirconia was reacted with molten titanium. Lin and Lin[26,27] also indicated a two-phase region of β'-Ti and *c*-ZrO_2 in the Ti/3Y-ZrO_2 diffusion couple after reaction at 1550ºC. It was believed that reaction layer "II" was formed because titanium melt infiltrated along the grain boundaries of 10Y90Z.

(C) Reaction layers "III" and "IV" on the ceramic side

Microstructures of reaction layers "III" and "IV" at the interface between Ti and 30Y70Z were very different from those of the corresponding reaction layers previously found in the Ti/ZrO_2 diffusion couples [26,27]. Figure 2.5 demonstrates the microstructural variations in reaction layers "III" and "IV", as well as the observation that reaction layer "III" consisted of α-Ti, acicular α-Ti, β'-Ti, and Y_2O_3 at the interface between Ti and 30Y70Z after reaction at 1700°C for 10 min. Acicular α-Ti was found in β'-Ti as indicated by the arrow in Fig. 2.5(a). Based on EPMA analyses, the β'-Ti consisted of 57.92 at% Ti, 20.31 at% Zr, and 21.77 at% O, while the composition of acicular α-Ti was measured as 52.63 at% Ti, 13.86 at% Zr, and 33.51 at% O. Because β'-Ti had a larger Zr/O ratio than α-Ti, β'-Ti looked brighter than

α-Ti in backscattered electron images. The composition of Y_2O_3 was measured as 5.93 at% Ti, 34.51 at% Y, 4.50 at% Zr, and 55.06 at% O, indicating a significant amount of Ti and Zr in solid solution.

Figure 2.5(b) displays the backscattered electron image of reaction layer "IV" at the interface between Ti and 30Y70Z after reaction at 1700°C for 10min. Reaction layer "IV" in 30Y70Z consisted of acicular α-Ti, β'-Ti, and Y_2O_3. β'-Ti was Ti with zirconium and oxygen in solid solution, consisting of 52.9 at.% Ti, 27.6 at.% Zr, and 19.5 at.% O, while Y_2O_3 was composed of 3.0 at.% Ti, 37.1 at.% Y, 1.6 at.% Zr, and 58.3 at.% O, respectively. All compositions were measured using EPMA. Reaction layer "IV" dissolved a larger amount of Zr in Ti than reaction layer "III". It was thus inferred that reaction layer "IV" was likely to be stabilized as the β phase at 1700°C because Zr is an effective β-stabilizer. During cooling, β-Ti was transformed into β'-Ti accompanied by the precipitation of acicular α-Ti in the β'-Ti matrix.[33]

As 30Y70Z reacted with Ti melt, a large amount of Zr and O from 30Y70Z were dissolved in titanium, giving rise to the formation of Y_2O_3 due to the very limited solubility of yttrium in titanium. The precipitation of Y_2O_3 was increased with an increasing Y_2O_3/ZrO_2 ratio. It was noted that no interfacial reactions were found at the interface between Ti and 90Y10Z after reaction at 1700ºC for 10 min. It was concluded that increasing Y_2O_3 content was useful for better controlling the interfacial reactions.

In the case of the Ti/ZrO_2 diffusion couple, Lin and Lin[26,27] found previously that acicular α-Ti precipitated in the β'-Ti matrix of the titanium side .

However, acicular α-Ti and the β'-Ti matrix existed in reaction layers "III" and "IV" of the ceramic side in this study. This was attributed to the infiltration of titanium melt into the ceramic side, whereby the reactions between Ti and ZrO_2 took place. In contrast, the faster diffusion of O and Zr into the titanium side led to the formation of the (α-Ti + β'-Ti) layers in the Ti-ZrO_2 diffusion couple.

Figure 2.6(a) shows the bright field image of the cross-section normal to the interface of Ti and 30Y70Z after reaction at 1700°C for 10 min. The orientation relationship of acicular α-Ti and β'-Ti was identified to be $[2\bar{1}\,\bar{1}\,0]_{\alpha\text{–Ti}}$ //$[001]_{\beta'\text{-Ti}}$ and $(0001)_{\alpha\text{–Ti}}$ //$(100)_{\beta'\text{-Ti}}$ as indicated in Fig. 2.6(b) in agreement with the results presented by Lin and Lin.[26,27] The selected-area diffraction pattern depicted in Fig. 2.6(c) indicated the existence of the cubic Y_2O_3 in reaction layer "IV."

Microstructural evolution of reaction layer "III" at the interface between Ti and 30Y70Z at 1700ºC is schematically displayed in Fig. 2.7(a). Upon heating to 1700ºC, titanium melt infiltrated and dissolved a large amount of Zr and O, resulting in the formation of a two-phase (α-Ti + β-Ti) layer. Because the solubility of yttrium in titanium is quite limited, it remained as Y_2O_3 [the center of Fig. 2.7(a)]. During cooling, the β-Ti was transformed into orthorhombic β'-Ti, where a small amount of acicular α-Ti was precipitated [the right of Fig. 2.7(a)]. Figure 2.7(b) displays a proposed model of microstructural evolution in reaction layer "IV" at the interface between Ti and 30Y70Z at 1700ºC. Because less titanium melt infiltrated into reaction layer "IV," Ti dissolved more concentrated Zr and O and existed as β-Ti during heating at 1700ºC. As the solubility of yttrium in

titanium was quite limited, Y_2O_3 was retained in the matrix of β-Ti at high temperatures [the center of Fig. 2.7(b)]. During cooling, the cubic β-Ti was transformed into orthorhombic β'-Ti where acicular α-Ti was precipitated in this reaction layer [Fig. 2.7(b), right side].

(D) Reaction layer "V" on the ceramic side

Figures 2.8(a)-(c) show the bright field images of reaction layer "V" on the ceramic side far from the original interfaces of Ti and 10Y90Z, 30Y70Z, and 50Y50Z, respectively, after reaction at 1700°C for 10 min. Figure 2.8(a) demonstrates that *t*-ZrO_{2-x} with two variants was precipitated in *c*- ZrO_{2-x} at the interface between Ti and 10Y90Z after reaction at 1700°C for 10 min. Because Y_2O_3 was completely retained in ZrO_2, no free Y_2O_3 was found in 10Y90Z. Figure 2.8(b) shows several α-Zr particles were embedded in *c*-ZrO_{2-x} in reaction layer "V" of 30Y70Z after reaction at 1700°C for 10min. The composition of α-Zr was measured using EPMA, indicating that it contained 2.43 at% Y, 69.14 at% Zr, and 28.43 at% O. Figure 2.8(c) shows the bright field image of reaction layer "V" in 50Y50Z after reaction at 1700°C for 10min. Residual $Zr_3Y_4O_{12}$ was found and its crystal structure was identified to be rhombohedral based on the inset selected-area diffraction pattern, as shown in the upper right corner of Fig. 2.8(c). Figure 2.8(d) shows an EDS spectrum of this ternary compound. The average composition was calculated from six measurements to be 15.88 at% Zr, 22.08 at% Y, and 62.04 at% O in correspondence with the composition of $Zr_3Y_4O_{12}$.

It was believed that the oxidation-reduction reaction rather than dissolution was the predominant reaction mechanism in reaction layer "V".

Dissolution did not play a significant role, as the titanium was not detected by EDS in reaction layer "V". The oxidation-reduction reaction between Ti and ZrO_2 resulted in the formation of metastable oxygen-deficient zirconia (ZrO_{2-x}). It was inferred that α-Zr precipitated from the supersaturated *c*-ZrO_{2-x}, accompanied with an increasing O/Zr ratio in ZrO_{2-x}.[15] Furthermore, the amount of α-Zr decreased with increasing amounts of Y_2O_3 because Y_2O_3 could effectively suppress the reaction between Ti and ZrO_2.

2.3.3 A General Discriptions of Interfacial Reaction Layers

According to the above discussion, the reaction layers were formed at the interface between titanium and yttria/zirconia samples after reaction at 1700°C for 10 min (summarized in Table 2.2). Briefly speaking, extensive reactions occurred at the interface between Ti and 10Y90Z as previous studies indicated.[24-27] However, interfacial reactions were effectively suppressed by incorporating more than 30 vol% Y_2O_3. The interfaces were increasingly stable with the amount of Y_2O_3 because Y_2O_3 functioned as a reaction barrier phase. On the metal side, β'-Ti and acicular α-Ti were observed in the α-Ti matrix of reaction layer "I" after Ti reacted with 10Y90Z or 30Y70Z, although only a small amount of β'-Ti was found in the α-Ti matrix of reaction layer "I" for the cases of 50Y50Z and 70Y30Z. Furthermore, no reaction layer "I" was formed for the cases of 90Y10Z and pure Y_2O_3. In the outermost ceramic region, β'-Ti and α-Ti were found along with c-ZrO_{2-x} in reaction layer "II" of 10Y90Z, while β'-Ti and α-Ti were found along with Y_2O_3 in reaction layers "III" and "IV" of 30Y70Z, 50Y50Z, and 70Y30Z. Free Y_2O_3 existed in reaction layers "III" and "IV" due to a very limited solubility of Y_2O_3 in Ti when ZrO_2 was completely dissolved in Ti. On the ceramic side far from the original interface, dense

α-Zr was formed in addition to residual ZrO_2 in reaction layer "V" of 10Y90Z and 30Y70Z, where α-Zr was excluded from metastable *c*-ZrO_{2-x}. However, α-Zr was formed in reaction layer "V" of 70Y30Z and 90Y10Z, because oxygen in ZrO_2 was extracted by Ti through the oxidation-reduction mechanism. The amount of α-Zr decreased with increasing amounts of Y_2O_3. Although Y_2O_3 was dissolved into ZrO_2 as a solid solution or reacted with ZrO_2 as $Zr_3Y_4O_{12}$ during hot pressing, Y_2O_3 was reprecipitated, due to the oxidation-reduction mechanism and strong affinity of O and Zr to Ti, in 50Y50Z and 70Y30Z after reaction at 1700ºC for 10 min. It was also noted that some $Zr_3Y_4O_{12}$ grains were retained in 50Y50Z after reaction at 1700ºC for 10 min.

2.4 Conclusions

1. The incorporation of more than 30 vol% Y_2O_3 significantly suppressed reactions at the interfaces between Ti and various Y_2O_3/ZrO_2 samples. In contrast, an extensive reaction occurred at the interface between Ti and 10Y90Z (or a partially stabilized ZrO_2) as mentioned previously.
2. On the metal side, β'-Ti and acicular α-Ti were observed in the α-Ti matrix after Ti melt reacted with 10Y90Z or 30Y70Z at 1700ºC for 10 min. However, only a very small amount of β'-Ti was found in the α-Ti matrix after Ti reacted with 50Y50Z or 70Y30Z. Ti was almost kept intact after reaction with 90Y10Z or Y_2O_3 at 1700ºC for 10 min.
3. After reaction at 1700ºC for 10 min, β'-Ti, α-Ti and *c*-ZrO_{2-x} were found in the outermost region of 10Y90Z, while β'-Ti, α-Ti and Y_2O_3 existed in the outermost region of 30Y70Z, 50Y50Z, and 70Y30Z. The formation of Y_2O_3 in this region was caused by the extensive dissolution of ZrO_2 in

Ti together with a very limited solubility of Y_2O_3.

4. Dense α-Zr was formed along with residual ZrO_2 (cubic and/or tetragonal) or Y_2O_3 far from the original interface after reaction with Ti at 1700ºC for 10 min. The amount of α-Zr decreased with increasing amounts of Y_2O_3.
5. Y_2O_3, existing as a solid solution or $Zr_3Y_4O_{12}$ after hot pressing, was reprecipitated in 50Y50Z and 70Y30Z far from the original interface after reaction at 1700ºC for 10 min. This was due to the oxidation-reduction reaction and the strong Ti affinity of O and Zr.
6. Some $Zr_3Y_4O_{12}$ grains were retained in the sample containing 50 vol% Y_2O_3 after reaction at 1700ºC for 10 min.

Table 2.1 Designations, Compositions, Hot-Pressing Conditions, Relative Densities and XRD Phases of Hot Pressed Y_2O_3/ZrO_2 Samples

Specimens	**Composition (vol%)**	**Hot-pressing conditions**	**Relative Densities**	**XRD Phases**
10Y90Z	10% Y_2O_3 + 90% ZrO_2	1550℃/30min/1 atm Ar	98.0%	*c*-ZrO_2, *t*-ZrO_2, *m*-ZrO_2
30Y70Z	30% Y_2O_3 + 70% ZrO_2	1550℃/30min/1 atm Ar	98.6%	*c*-ZrO_2
50Y50Z	50% Y_2O_3 + 50% ZrO_2	1550℃/30min/1 atm Ar	98.8%	$Zr_3Y_4O_{12}$
70Y30Z	70% Y_2O_3 + 30% ZrO_2	1550℃/30min/1 atm Ar	98.1%	Y_2O_3, $Zr_3Y_4O_{12}$
90Y10Z	90% Y_2O_3 + 10% ZrO_2	1600℃/30min/1 atm Ar	98.1%	Y_2O_3
100Y0Z	100% Y_2O_3	1600℃/30min/1 atm Ar	98.3%	Y_2O_3

Table 2.2 Reaction Layers Formed at the Interfaces of Ti and Y_2O_3/ZrO_2 Samples after Reaction at 1700°C/10 min

Specimens	Interface reaction layers and phases				Reaction layer "V" in the Ceramic side
	Ti side		Ceramic side		
10Y90Z	I	α-Ti, β′-Ti + acicular α-Ti	II	β′-Ti + acicular α-Ti, *c*-ZrO_{2-x}	*c*-ZrO_{2-x}, *t*-ZrO_{2-x}, α-Zr
30Y70Z	I	α-Ti, β′-Ti + acicular α-Ti	III	Y_2O_3, α-Ti, β′-Ti + acicular α-Ti	*c*-ZrO_{2-x}, α-Zr
			IV	Y_2O_3, β′-Ti + acicular α-Ti	
50Y50Z	I	α-Ti, β′-Ti	III	Y_2O_3, α-Ti, β′-Ti + acicular α-Ti	Y_2O_3, $Zr_3Y_4O_{12}$, α-Zr
			IV	Y_2O_3, β′-Ti + acicular α-Ti	
70Y30Z	I	α-Ti, β′-Ti	III	Y_2O_3, α-Ti, β′-Ti + acicular α-Ti	Y_2O_3, α-Zr
90Y10Z	Insignificant interfacial reaction				Y_2O_3, α-Zr
100Y0Z	Insignificant interfacial reaction				Y_2O_3

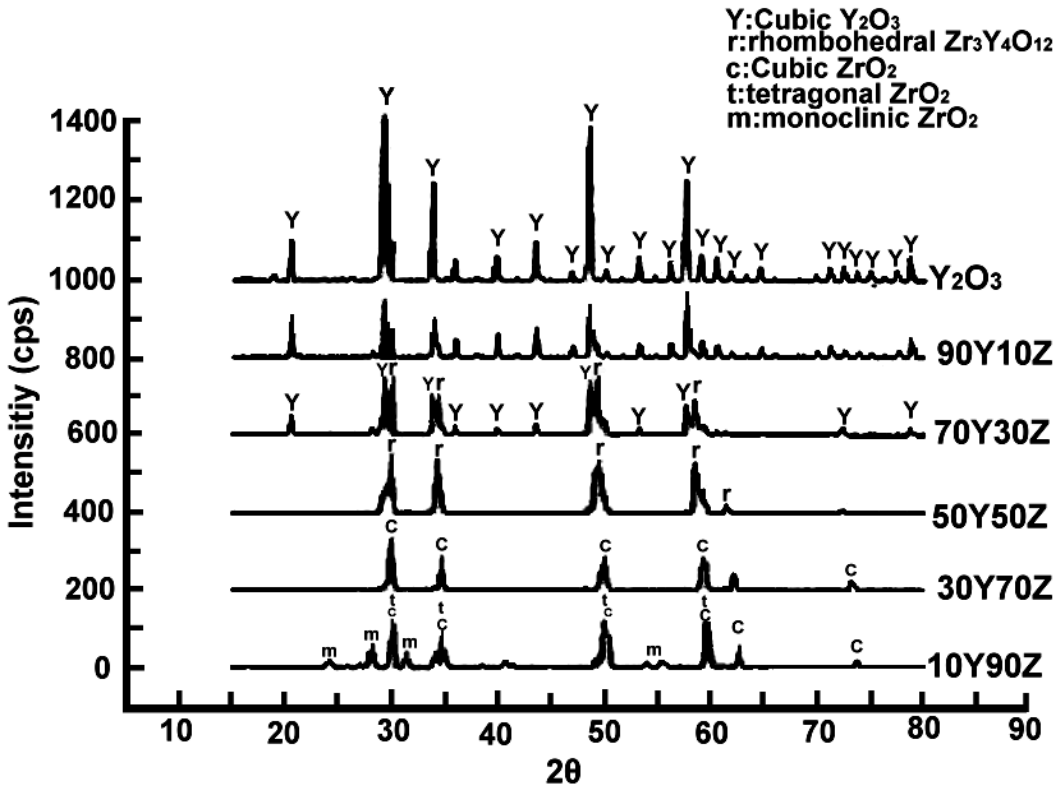

Fig. 2.1 X-ray diffraction spectra of as hot-pressed Y_2O_3/ZrO_2 samples.

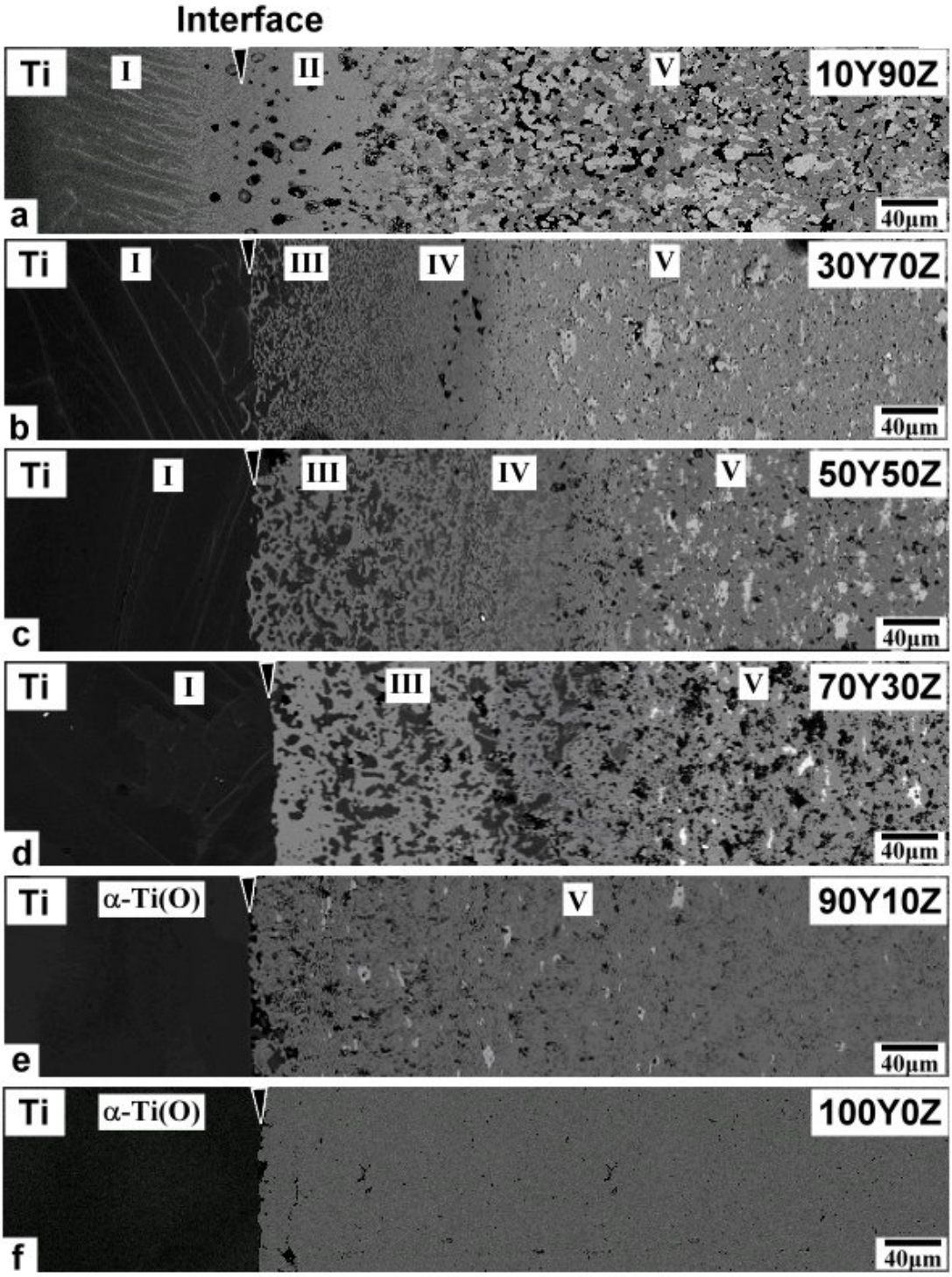

Fig. 2.2 (a)-(f) Backscattered electron images of the cross section between Ti and Y_2O_3/ZrO_2 samples after reaction at 1700°C for 10 min. Arrows indicate the original interfaces between Ti and Y_2O_3/ZrO_2 samples.

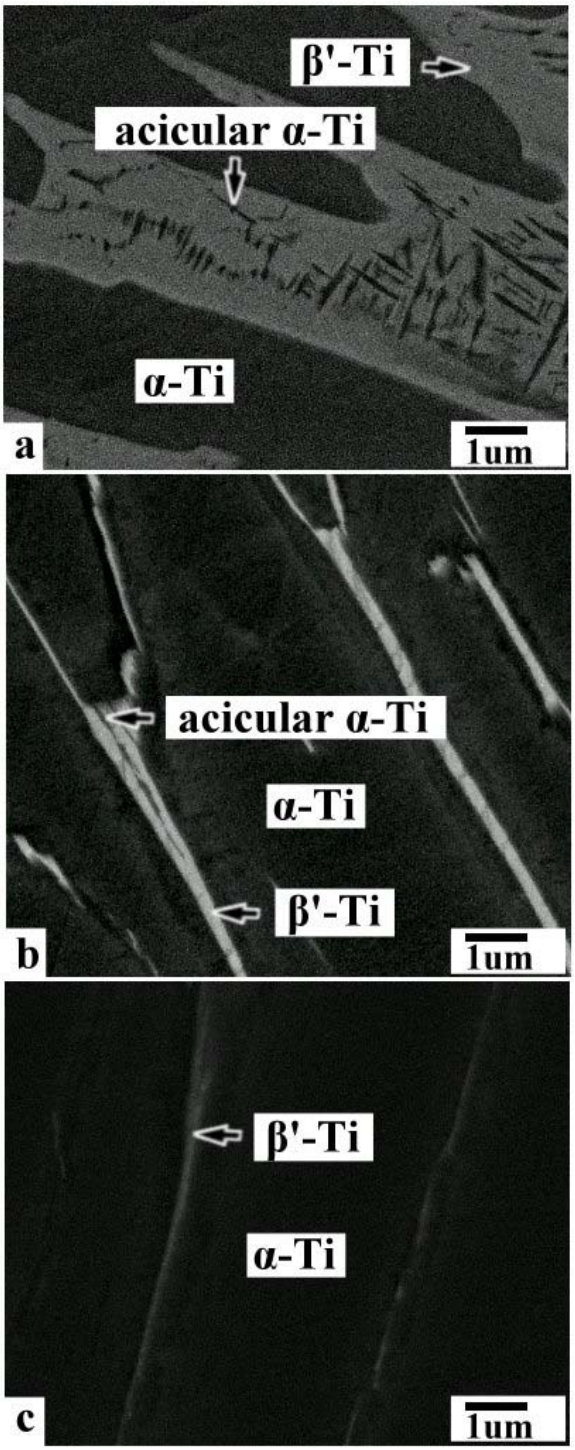

Fig. 2.3 Backscattered electron images of reaction layer "I" in the titanium side at the interface between (a) Ti and 10Y90Z, (b) Ti and 30Y70Z, and (c) Ti and 50Y50Z after reaction at 1700°C for 10 min.

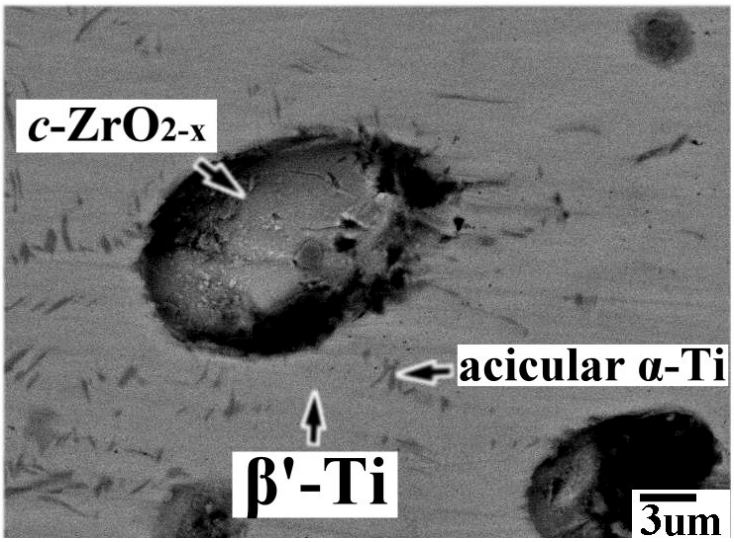

Fig. 2.4 Backscattered electron image of reaction layer "II" at the interface between Ti and 10Y90Z after reaction at 1700°C for 10 min.

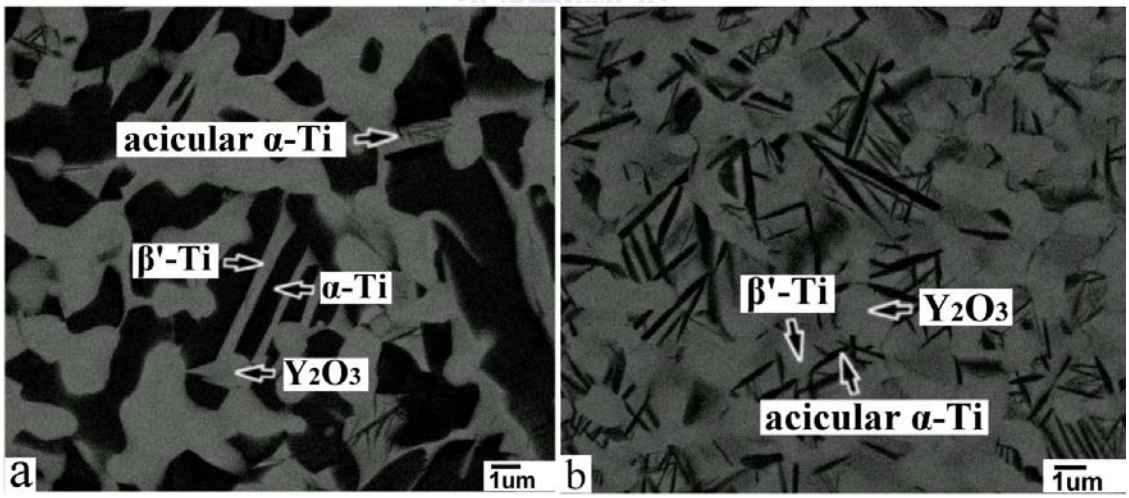

Fig. 2.5 Backscattered electron images of (a) reaction layer "III" and (b) reaction layer "IV" at the interface between Ti and 30Y70Z after reaction at 1700°C for 10 min.

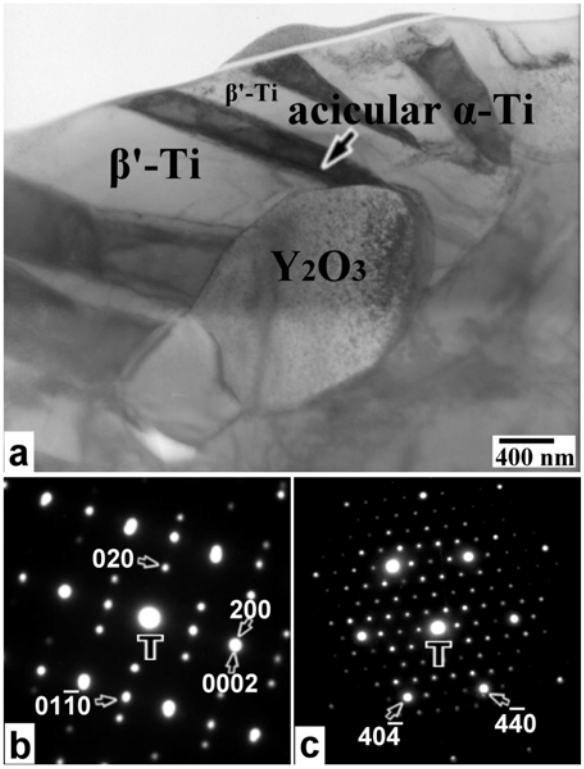

Fig. 2.6 (a) Bright-field image of reaction layer "IV" at the interface between Ti and 30Y70Z after reaction at 1700°C for 10 min; (b) selected-area diffraction patterns of acicular α-Ti and the matrix β'-Ti; (c) a selected-area diffraction pattern of the Y_2O_3 with the zone axis [111].

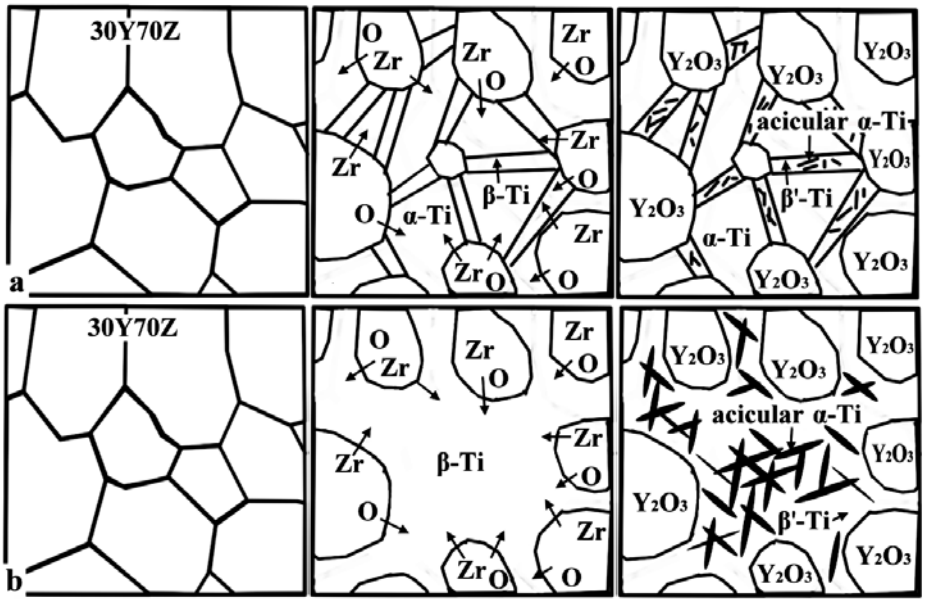

Fig. 2.7 Schematic diagrams showing the microstructural evolution of (a) reaction layer "III" and (b) reaction layer "IV" at the interface between Ti and 30Y70Z at various stages.

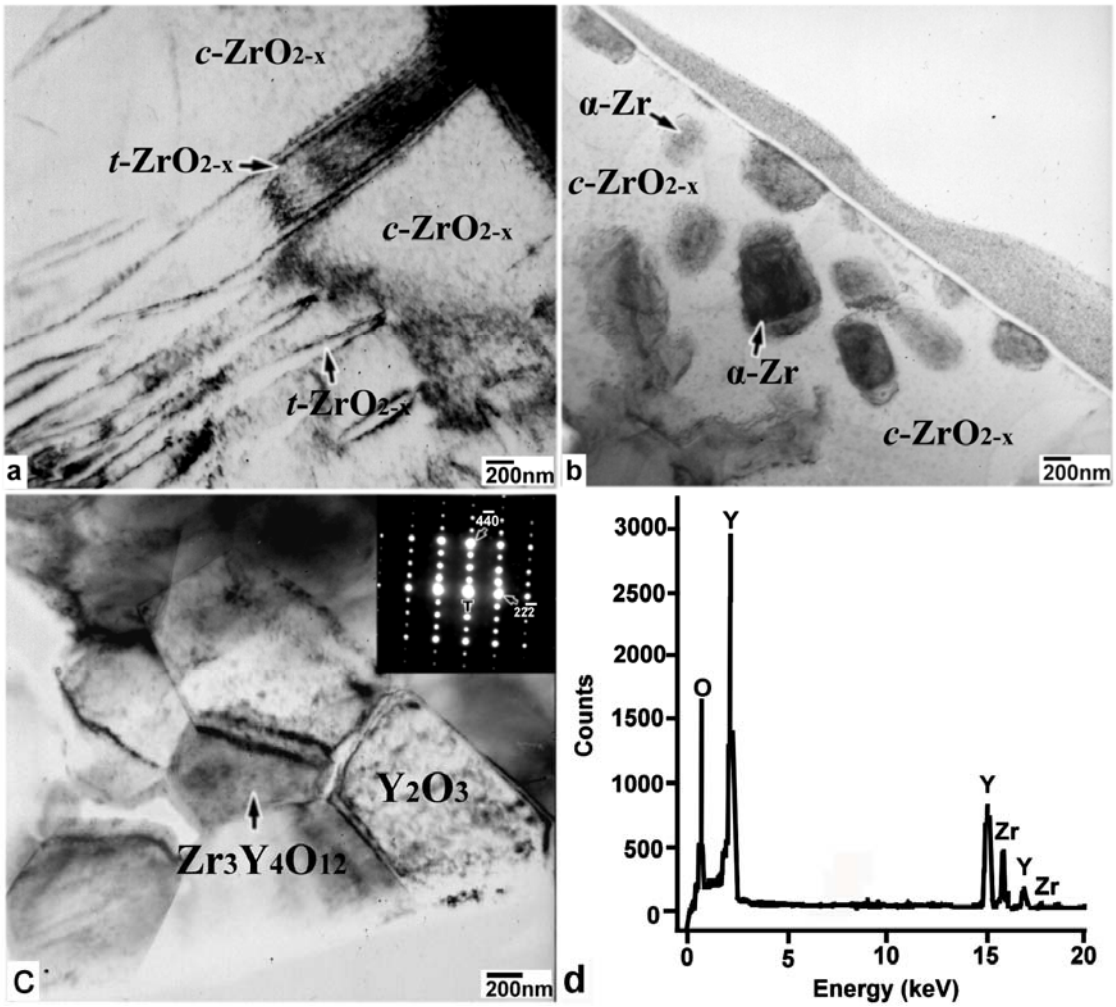

Fig. 2.8 Bright-field images of reaction layer "V" in the zirconia side far away from the interface between (a) Ti and 10Y90Z, (b) Ti and 30Y70Z, and (c) Ti and 50Y50Z after reaction at 1700°C for 10 min. The inset in the upper right-hand corner of Fig. 8(c) is the selected-area diffraction pattern of $Zr_3Y_4O_{12}$ with the zone axis [112]; (d) an energy dispersive spectrum of $Zr_3Y_4O_{12}$.

Chapter 3

Compositional Dependence of Phase Formation Mechanisms at the Interface Between Titanium and Calcia-Stabilized Zirconia at 1550°C

3.1 Introduction

Because titanium alloys have high tensile strength and toughness, light weight, and extraordinary corrosion resistance, they are widely applied to some parts of aircraft, medical devices, golf club heads, consumer electronics, etc. Titanium alloys are usually melted in a water-cooled copper crucible by the consumable electrode vacuum arc-melting (VAR),[34] because the ceramic crucible used in the vacuum induction melting (VIM) seriously reacts with titanium.[35] However, high cost of the equipment, scrape recycle, and long cycle time are some of drawbacks for the VAR process. Moreover, the reaction between the ceramic mold and titanium parts during invest casting inevitably results in the α-casing and resultant deterioration of mechanical properties. Therefore, how to control the interfacial reactions between titanium and some ceramic materials are of great concerns.

In the past several decades, extensive studies have been performed on the reactions between titanium and zirconia.[4,8-10,13,18,20,36] Economos and Kingery[8] found that titanium penetrated along the grain boundaries of ZrO_2 to form black oxygen-deficient zirconia. Ruh[10] indicated that up to approximately 10 mol% zirconia could be dissolved in titanium, while the

residual zirconia became oxygen-deficient zirconia. Saha *et al*.[36] also revealed that the oxygen of zirconia was readily extracted and dissolved into the titanium to form α-Ti(O).

Recently, Lin and his colleagues[24-27,37] have thoroughly investigated the phase formation mechanisms and microstructural evolution at the interface between titanium (or titanium alloys) and 3Y-ZrO_2 (or various ratios of Y_2O_3/ZrO_2) using analytical electron microscopy. α-Ti(O), β'-Ti (Zr, O) and/or Ti_2ZrO were formed near the original interface due to the dissolution of ZrO_2 into Ti and vice versa. Both lamellar orthorhombic Ti_2ZrO and spherical hexagonal Ti_2ZrO were found in α-Ti(Zr, O) after reaction at 1550°C.[24] The orientation relations of the acicular α-Ti and the β'-Ti were $[2\bar{1}\bar{1}0]_{\alpha-Ti}$ // $[001]_{\beta'-Ti}$ and $(0001)_{\alpha-Ti}$ // $(100)_{\beta'-Ti}$ in combinations of $[2\bar{1}\bar{1}0]_{\alpha-Ti}$ // $[021]_{\beta'-Ti}$ and $(0001)_{\alpha-Ti}$ // $(1\bar{1}2)_{\beta'-Ti}$, respectively.[26] Lin and Lin[25] also found intergranular α-Zr, twinned *t*'-ZrO_{2-x}, lenticular *t*-ZrO_{2-x}, and/or ordered *c*-ZrO_{2-x} in the zirconia side far from the interface between Ti and 3Y-ZrO_2 after reaction at 1550°C. Concerning the reaction of the Ti melt with various Y_2O_3/ZrO_2 samples at 1700°C,[37] the incorporation of more than 30 vol% Y_2O_3 in ZrO_2 could effectively suppress the reactions on the Ti side, where only a very small amount of α-Ti and β'-Ti was found. Furthermore, Y_2O_3 re-precipitated in the samples containing 30-70 vol% Y_2O_3 because the solubility of Y_2O_3 in Ti was very low.

The yttria partially stabilized zirconia (Y-PSZ) has been considered as one of the most popular industrial ceramic materials because of its good fracture toughness. Because Y_2O_3 is much more expensive than CaO or MgO, the zirconia crucibles used in casting industry are frequently made from CaO- or

MgO-stabilized zirconia instead. In this study, powder mixtures with various CaO/ZrO_2 ratios were hot-pressed and then allowed to react with titanium at 1550°C for 6 h in argon. The reaction layers at the interface were characterized using analytical scanning electron microscopy and analytical transmission electron microscopy. The effect of CaO on the interfacial reactions between Ti and CaO/ZrO_2 samples is elucidated.

3.2 Experimental Procedures

Starting powders were zirconia (> 99.14 wt% ZrO_2+HfO_2, with HfO_2 accounting for approximately 1.84% of this total, < 0.5 wt% SiO_2, < 0.11 wt% Y_2O_3, < 0.08 wt% Na_2O, < 0.05 wt% Al_2O_3, < 0.05 wt% Fe_2O_3, < 0.03 wt% CaO, < 0.01 wt% MgO, < 0.005 wt% TiO_2, < 0.018 wt% U, < 0.007 wt% Th; 8.54 μm average particle size; Z-Tech LLC, Bow, NH), and calcia (> 99.9 wt% CaO, < 0.034 wt% Sr, < 0.02 wt% Mg, < 0.02 wt% Na, < 0.01 wt% K, < 0.005 wt% Ba, < 0.005 wt% Pb, < 0.003 wt% Fe, < 0.002 wt% Cd, < 0.001 wt% As; 10 μm average particle size; Ube Material Industries, Ltd., Chiba, Japan).

The CaO/ZrO_2 samples contained 5, 9, or 17 mol% CaO, with the balance being ZrO_2. The sample consisting of 5 mol% CaO and 95 mol% ZrO_2 was designated as 5C95Z, with the same notation used for the other samples. Powder mixtures were dispersed in ethanol. The pH of the suspension was adjusted to 11 by adding NH_4OH. The suspension was ultrasonically vibrated for 10 minutes (Model XL-2020, Sonicator, Heat Systems Inc., Farmingdale, NY), dried in an oven at 150°C, ground with an agate mortar and pestle, and then screened through an 80 mesh. Bulk specimens were

fabricated by hot-pressing in a graphite furnace at 1 atm argon (Model HP50-MTG-7010, Thermal Technology Inc., Santa Rosa, CA). As-hot pressed samples were blackened and were regarded as oxygen-deficient zirconia. They become stoichiometric after isothermal annealing at 1300°C for 1 h.

The apparent densities of CaO/ZrO_2 powder mixtures were measured using a gas pycnometer (Model MultiVolume Pycnometer 1305, Micromeritics, Norcross, GA) with 99.99% pure helium. Bulk densities of hot-pressed CaO/ZrO_2 samples were determined by the Archimedes method using water as an immersion medium. The relative densities of the hot-pressed samples were calculated as follows: Relative density = (bulk density/true density) × 100%. For a non-porous powder, the apparent density approximates the true density and can be used as the reference point in calculating the relative density. The hot press conditions, compositions, relative densities, and designations of CaO/ZrO_2 samples are listed in Table 3.1.

Commercially pure titanium plates (99.7% purity, Alfa Aesar, Ward Hill, MA) were brought to react with hot-pressed CaO/ZrO_2 samples at 1550°C for 6 h in argon. First, bulk CaO/ZrO_2 samples and titanium plates were cut and machined to dimensions of 10 × 10 × 5 mm. Their surfaces were ground and polished with a diamond paste and subsequently ultrasonically cleaned in acetone. One titanium specimen was inserted between two pieces of a CaO/ZrO_2 sample to produce a sandwiched type, and the sandwich was then placed into the aforementioned graphite furnace. The furnace was initially prepared by first being pressurized to 5 MPa, then

evacuated to 2×10^{-4} Torr, and filled with argon to 1 atmospheric pressure. This cycle of evacuation and purging was repeated at least three times. After the sample insertion, the furnace temperature was raised to 1000°C at a heating rate of 30°C/min, to 1550°C at 25°C/min, and then held at 1550°C for 6 h. Thereafter, the temperature was lowered to 1000°C at a cooling rate of 25°C/min, and finally, the furnace was cooled down to room temperature.

The phase identification of the as hot-pressed CaO/ZrO_2 samples was performed using an x-ray diffractometer (XRD, Model MXP18, Mac Science, Yokohama, Japan). The operating conditions of the x-ray diffraction were Cu K_α radiation at 50 kV and 150 mA and a scanning rate of 2 degrees/min.

A scanning electron microscope (SEM, Model JSM 6500F, JEOL Ltd., Tokyo, Japan), which was equipped with an energy dispersive x-ray spectrometer (EDS, Model ISIS 300, Oxford Instrument Inc., London, UK), was used for the microstructural observation of the interfaces between Ti and various CaO/ZrO_2 samples. Cross-sectional SEM specimens were cut and ground using standard procedures and finally polished using diamond pastes of 6, 3, and 1 μm in sequence.

The cross-sectional specimens of the interfaces between Ti and various CaO/ZrO_2 samples for transmission electron microscopy (TEM) were prepared by two different methods. Firstly, they were cut perpendicular to the interface and then polished, dimpled, and subsequently ion-beam-thinned using a precision ion-polishing system (PIPS, Model 691, Gatan, San

Francisco, CA). The details of this traditional technique for preparing cross-sectional TEM specimens were described in a previous study.[37] Secondly, the TEM samples were acquired by an innovative technique. A specific location on a metallographic sample was ion-bombarded using a focused ion beam (FIB, Model Nova 200, FEI Co., Hillsboro, OR). The FIB operating parameters were adjusted so that the electron beam was 5 kV from 98 pA to 1.6 nA, and the ion beam was 30 kV from 10 pA to 7 nA. A TEM specimen with a thickness of less than 100 nm was electron-transparent. The final TEM specimen was approximately 12 × 5 × 0.05 μm in size.

The interfacial microstructures were then characterized using a TEM (Model JEM 2100, JEOL Ltd., Tokyo, Japan) equipped with an EDS (Model ISIS 300, Oxford Instrument Inc., London, UK). Analyses of atomic configurations in various phases were performed using computer simulation software for crystallography (CaRIne Crystallography 3.1, Divergent S.A., COMPIEGNE, France). Chemical quantitative analyses for various phases were conducted by the Cliff-Lorimer standardless technique.[31] A conventional ZAF correction was operated using the LINK ISIS software.

3.3 Results and Discussion

3.3.1 XRD Analyses

Figure 3.1 shows the XRD spectra of various hot-pressed CaO/ZrO_2 samples. These spectra are arranged in the sequence of 17C83Z, 9C91Z, 5C95Z, from top to bottom. Monoclinic $CaZr_4O_9$[38-40] and cubic ZrO_2 were found in the hot-pressed 17C83Z, indicating that cubic ZrO_2 was fully stabilized by 17

mol% CaO. While *c*-ZrO_2, *t*-ZrO_2 and *m*-ZrO_2 were found in 9C91Z, the 5C95Z consisted of *t*-ZrO_2 and *m*-ZrO_2. This indicates that CaO was dissolved by or reacted with ZrO_2 to form a solid solution and/or $CaZr_4O_9$, respectively, in hot-pressed CaO/ZrO_2 samples.

Though Hellmann and Stubican[40] found $Ca_6Zr_{19}O_{44}$ after sintering at 2000°C for 4 h and subsequent prolonged annealing, $Ca_6Zr_{19}O_{44}$ was not found at all in this study. It was noted that few $CaZr_4O_9$ were found in 5C95Z and 9C91Z. Furthermore, only a very small amount of $CaZr_4O_9$ was distributed along the grain boundaries of cubic zirconia in 17C83Z, as illustrated in Fig. 2. It was thus inferred that the equilibrium was not established after hot pressing. X-ray phases of these hot pressed CaO/ZrO_2 samples are summarized in Table I.

At the eutectoid temperature of CaO-ZrO_2 (1140°C),[40] the solid solution of ZrO_2 with more than 17 mol% CaO could decompose into cubic solid solution and two ordered phases (Φ_1: $CaZr_4O_9$,[38-40] and Φ_2:$Ca_6Zr_{19}O_{44}$).[40,41] However, the rates of decomposition to ordered phases are very slow at relatively low temperatures (< 1400°C).[40]

3.3.2 SEM and TEM Analyses

Figures 3.2(a)-(c) display the backscattered electron images of the cross-sections normal to the interfaces of Ti and various CaO/ZrO_2 samples. Titanium is shown on the left of the micrograph, while zirconia is on the right-hand side. The vertical arrows on the upper sides of individual figures indicate the original interfaces of Ti and individual CaO/ZrO_2 samples. The original interfaces were deliberately located according to the

characteristic K_α x-ray maps of calcium (not shown), which was relatively immobile compared with Zr, O, and Ti. The existence of pores in the ceramic side was attributed to the Kirkendall effect, as zirconium and oxygen diffused to the titanium side much more rapidly than titanium diffused toward the zirconia side.

Figure 3.2(a) indicates that only a limited reaction took place on the titanium side at the Ti/5C95Z interface, signifying that interfacial reactions were effectively suppressed. In the engineering respect of Ti castings, a well-controlled interfacial reaction between Ti and 5C95Z can result in a thinner α-casing and thus in better mechanical properties. However, extensive reactions took place at the Ti/9C91Z and Ti/17C83Z interfaces, as shown in Figs. 3.2(b) and (c). It was previously reported that needle-like α-Ti and some lamellar phases were usually found in the titanium side because of the interfacial reactions between Ti and 3Y-ZrO_2.[24,26,27] Even though the system became more stable with decreasing CaO, several reaction layers were found on the zirconia side after the interfacial reactions between Ti and various CaO/ZrO_2 samples. Microstructures of the reaction layers at the interface between Ti and various CaO/ZrO_2 samples were characterized using SEM/EDS and TEM/EDS, with the results listed in Table 3.2. Four dissimilarities of the interfacial microstructures were recognized after various CaO/ZrO_2 samples reacted with Ti. They are described below.

(A) Two TiO and t-ZrO_2 layers at the Ti/5C95Z interface vs. four complex layers of α-Ti, β'-Ti and Ti_2ZrO at the Ti/9C91Z and Ti/17C83Z interfaces

The two outermost layers were TiO and *t*-ZrO_{2-x} layers at the Ti/5C95Z interface. In contrast, the three distinct outermost layers were composed of α-Ti, β'-Ti, and Ti_2ZrO at the Ti/9C91Z or Ti/17C83Z interface. Figure 3.3(a) shows a bright-field image of a thin TiO reaction layer (about 2 μm thick) at the Ti/5C95Z interface. The arrow indicates the original interface between titanium (α-Ti) and zirconia (*t*-ZrO_{2-x}). Figures 3.3(b) and (c) show the selected area diffraction patterns (SADPs) of TiO with [001] and [011] zone axes, respectively. It can be seen that TiO has a B1(NaCl) structure. The EDS spectrum in Fig. 3(d) shows that TiO dissolved a small amount of Zr and was composed of 49.73 at.% Ti, 49.26 at.% O, and 1.01 at.% Zr. This indicates that titanium could not dissolve Ca in solid solution. Figure 3(e) shows the SADP of continuous *t*-ZrO_{2-x} phase with a zone axis of [111]. The EDS results indicate that *t*-ZrO_{2-x} was composed of 4.96 at% Ti, 2.72 at% Ca, 32.62 at% Zr, and 59.70 at% O.

Figure 3.4 shows the backscattered electron image of the reaction layers I and II at the Ti/17C83Z interface. Reaction layer I consisted of *α*-Ti (dark) and Ti_2ZrO (bright). Reaction layer II consisted of Ti_2ZrO (bright), *α*-Ti (dark), and *β′*-Ti (bright). Lin and Lin[24] reported that the Ti_2ZrO lamellae were precipitated from plate-like α-Ti by a eutectoid reaction during cooling. At high temperatures, the primary *α*-Ti dissolved a significant amount of oxygen and a relatively small amount of zirconium, forming metastable *α*-Ti, which could result in the precipitation of Ti_2ZrO during cooling. As more Zr was dissolved in α-Ti, β-Ti was formed, some of which was transformed into orthorhombic β'-Ti solid solution during cooling.

(B) A much thinner reaction layer III (β'-Ti+α-Ti) at the Ti/17C83Z interface than at the Ti/9C91Z interface

Figures 3.2(b) and (c) show a much thinner reaction layer III (β'-Ti+α-Ti) in 17C83Z than in 9C91Z, while their reaction layers (I+II) had approximately the same thickness. Reaction layer III, which dissolved a significant amount of zirconium (β stabilizer) and oxygen (α stabilizer), was composed of α-Ti + β-Ti with Zr and O in solid solution. Lin and Lin[26] indicated that the acicular α-Ti was precipitated from the β'-Ti matrix.

As described in the following section, a stable 1:1 $CaO \cdot ZrO_2$ compound (or $CaZrO_3$) was formed in the ceramic side as Ti and CaO/ZrO_2 samples were brought into contact at 1550°C for 6 h. Assuming that all of CaO was consumed to form $CaZrO_3$, 9C91Z and 17C83Z had 82 and 66 mol% of excess ZrO_2, respectively. Even though this assumption is not fully correct (i.e., some CaO went into the solid solution of ZrO_2), it was obvious that more excess ZrO_2 existed in 9C91Z than in 17C83Z. As a result, the thinner reaction layer III at the Ti/17C83Z interface was attributed to the fact that a smaller amount of excess ZrO_2 and a relatively large amount of stable $CaZrO_3$ were formed in the outermost ceramic region.

(C) Distinct morphologies of $CaZrO_3$ in reaction layer IV at the Ti/9C91Z and Ti/17C83Z interfaces

Figure 3.5 demonstrates the microstructural variations of reaction layers IV at the Ti/9C91Z and Ti/17C83Z interfaces. Both reaction layers IV consisted of $CaZrO_3$ (dark) and β'-Ti (bright). The $CaZrO_3$ phase was

sparse and isolated at the Ti/9C91Z interface, while the $CaZrO_3$ phase was dense and interconnected at the 17C83Z interface. As shown in Fig. 3.5(a), β'-Ti and a relatively small amount of spherical or worm-like $CaZrO_3$ existed in reaction layers IV at the Ti/9C91Z interface. While the excess ZrO_2 was dissolved into Ti at the Ti/9C91Z interface, ZrO_2 reacted with CaO and formed the compound $CaZrO_3$. Figure 3.5(b) displays the β'-Ti and a relatively large amount of columnar or worm-like $CaZrO_3$ coexisting in reaction layer IV at the Ti/17C83Z interface. The columnar $CaZrO_3$ was formed due to the outward diffusion of O and Zr away from metastable CaO fully stabilized *c*-ZrO_{2-x}. This was usually called as a diffusion zone, consisting of β'-Ti and columnar $CaZrO_3$. This result indicates that $CaZrO_3$ was a stable phase and was not significantly dissolved in Ti.

Figure 3.6(a) shows a bright-field image of reaction layer IV, consisting of β'-Ti and $CaZrO_3$, at the Ti/17C83Z interface. The arrow in the upper right corner indicates the interface between reaction layer IV and reaction layer V. Columnar β'-Ti and $CaZrO_3$ were aligned nearly perpendicular to the interface of reaction layers IV and V. The crystal structures of both $CaZrO_3$ and β'-Ti were identified to be orthorhombic from the superimposed SADPs, as shown in Fig. 3.6(b). With the diffraction spots being indexed in Fig. 3.6(b), the orientation relationships of $CaZrO_3$ and β'-Ti were thus recognized as follows: $[101]_{CaZrO3}$ // $[001]_{\beta'\text{-}Ti}$ and $(\bar{1}01)_{CaZrO3}$ // $(100)_{\beta'\text{-}Ti}$. Figure 3.6(c) shows the EDS spectrum of the $CaZrO_3$, revealing that it comprised 19.93 at.% Ca, 20.61 at.% Zr, and 59.46 at.% O. Figure 3.6(d) displays the $[101]_{CaZrO3}$ or $[001]_{\beta'\text{-}Ti}$ standard stereographic projection corresponding to the selected area diffraction patterns illustrated in Fig. 3.6(b). It indicates that the $(\bar{1}01)$ plane of $CaZrO_3$ is parallel to the (100)

plane of β'-Ti. Lin and Lin[28] reported that the reaction at 1750°C/7 min between zirconia and titanium melt caused the formation of several $CaZrO_3$ ovals embedded in α-Zr on the zirconia side. No specific orientation relationship was identified in previous studies.

(D) Distinct α-Zr and/or $CaZrO_3$ in reaction layer V

Figures 3.7 displays the backscattered electron images of reaction layer V on the zirconia side far away from the original interfaces. This layer could be termed as a reaction affected zone. Figure 3.7(a) displays that dense α-Zr grains existed along the grain boundaries of *c*-ZrO_{2-x} in reaction layer V of Ti/9C91Z. Dissolution did not play a significant role because the titanium was not detected by EDS in reaction layer V. A much denser α-Zr phase was found at the Ti/5C95Z interface, as shown in Fig. 3.2(a). In the other respect, very little α-Zr was found in reaction layer V of Ti/17C83Z, as shown in Fig. 3.7(b). In general, the amount of intergranular α-Zr decreases with increasing CaO content.

Figures 3.8(a)-(b) show two bright-field images of reaction layer V on the zirconia side far away from the original interfaces. Figure 3.8(a) shows the bright-field image of *m*-ZrO_{2-x}, (*t*+*m*)-ZrO_{2-x}, and α-Zr in the reaction layer V of Ti/5C95Z. As 5C95Z reacted with Ti, the metastable oxygen-deficient ZrO_{2-x} was transformed into *m*-ZrO_{2-x} and α-Zr. Several martensite lathes grew completely across the grain and became twinned *m*-ZrO_{2-x} (labeled as "m" in Fig. 3.8(a)) due to the stress concentrations at such a region.[42] Figure 3.8(b) shows a bright-field image of *c*-ZrO_{2-x}, $CaZrO_3$, and α-Zr in reaction layer V of Ti/17C83Z. The crystal structure of α-Zr was identified

to be hexagonal based upon the superimposed SADP, as shown in the upper right corner. In 17C83Z, ZrO_{2-x} was fully stabilized as a cubic phase because 17 mol% CaO was dissolved into ZrO_2 as a solid solution. This *c*-ZrO_{2-x} was so stable that no oxidation-reduction was able to take place between zirconia and titanium in reaction layer V. In order to maintain charge neutrality, an oxygen vacancy was created in the crystal lattice of zirconia for every substitution of Ca^{2+} for Zr^{4+}. As a result, there was 17 mol% of oxygen vacancies in 17C83Z if all of the CaO was consumed to form the solid solution of ZrO_2. It was also believed that the intergranular $CaZrO_3$ was found due to the decomposition of intergranular $CaZr_4O_9$ at the Ti/17C83Z interface.

Table 3.2 summarizes the formation of various reaction layers at the interface between titanium and various CaO/ZrO_2 samples after reaction at 1550°C for 6 h. The formation mechanisms of α-Ti, β'-Ti, Ti_2ZrO, ZrO_{2-x}, and α-Zr were described in detail previously. However, the following phases were not found in previous studies: (1) TiO and continuous *t*-ZrO_{2-x} in reaction layers I and IV of Ti/5C95Z; (2) $CaZrO_3$ in reaction layers IV and/or V of Ti/9C91Z and Ti/17C83Z. As also indicated in Table II, the formation mechanisms of various reaction layers are described as follows: (1) reaction layers I, II, and III were formed because of the outward diffusion of O and/or Zr away from zirconia; (2) reaction layer IV was formed because of the inward diffusion of Ti into zirconia together with the outward diffusion of O and Zr away from zirconia; (3) reaction layer V was formed because of the decomposition of metastable oxygen-deficient ZrO_{2-x} and/or $CaZr_4O_9$ as well as the outward diffusion of O away from ZrO_2.

3.3.3 Formation Mechanisms of TiO and Continuous t-ZrO_{2-x} at the Ti/5C95Z Interface

As mentioned above, TiO and continuous *t*-ZrO_{2-x} were found in reaction layers I and IV, respectively, at the Ti/5C95Z interface. The TiO reaction layer was formed due to the oxidation-reduction reaction between titanium and zirconia. Previous studies[26,27] reported that α-Ti(O) rather than a TiO layer was observed at the Ti/3Y-ZrO_2 interface after reaction at 1550°C for 6 h. It was inferred that 5 mol% CaO-ZrO_2 released oxygen atoms much more easily than 3Y-ZrO_2 did because the Ca−O bond is weaker than the Y−O bond. This thin TiO reaction layer functioned as a diffusion barrier phase[43] because Ti and Zr diffuse very slowly across the TiO reaction layer, resulting in a suppressed interfacial reaction between Ti and 5C95Z.

While oxygen-deficient zirconia was formed because of the oxidation-reduction between titanium and zirconia, the metastable zirconia with supersaturated oxygen vacancies had the tendency to decompose, leading to the formation of *α*-Zr along the grain boundaries. However, the dissolution of Ti^{+2} could stabilize the oxygen-deficient zirconia (or ZrO_{2-x}) due to the creation of extra oxygen vacancies. Therefore, continuous *t*-ZrO_{2-x} rather than *α*-Zr was found in the ceramic outer layer in 5C95Z.

It was noticeable that the TiO layer did not exist at the Ti/9C91Z and Ti/17C83Z interfaces. As mentioned above, almost all CaO and ZrO_2 went into a solid solution in as hot-pressed 9C91Z or 17C83Z. When these metastable solid solutions reacted with Ti at 1550ºC, the excess Zr and O had a great tendency to be excluded from the solid solution, with $CaZrO_3$ being left, and subsequently dissolved into Ti. Because TiO had a very

limited solubility of Zr as indicated in the ternary phase diagram of Ti-O-Zr,[13,14] the extended dissolution of both Zr and O into Ti (as α-Ti, β'-Ti and/or Ti_2ZrO) obviously excluded the possibility of the formation of the TiO layer at the Ti/9C91Z and Ti/17C83Z interfaces.

3.3.4 Formation Mechanisms of $CaZrO_3$ and α-Zr at the Ti/9C91Z and Ti/17C83Z Interfaces

Figure 3.9 shows schematically the formation mechanisms of $CaZrO_3$ and α-Zr at the Ti/9C91Z and Ti/17C83Z interfaces, respectively. Upon heating at 1550°C, the interfacial reactions resulted in the formation of a two-phase (β-Ti + $CaZrO_3$) layer. During cooling, cubic β-Ti was transformed into orthorhombic β'-Ti, where spherical or worm-like $CaZrO_3$ was formed.

Microstructural evolution in reaction layer IV at the Ti/9C91Z interface is schematically displayed in Fig. 3.9(a). As 9C91Z reacted with Ti at 1550°C for 6 h, increasing amounts of O and Zr from the CaO-ZrO_2 solid solution were gradually dissolved in titanium. Because CaO remained in the solid solution due to the very limited solubility of CaO in Ti, the increase in the ratio of CaO to ZrO_2 gave rise to the formation of $CaZrO_3$. The formation mechanisms of β'-Ti and $CaZrO_3$ in the case of Ti/9C91Z in the reaction layer IV can be expressed as follows:

$$0.09\ CaO + 0.91\ ZrO_2 \rightarrow (Ca_{0.09}Zr_{0.91})O_{1.91} \quad \text{during hot pressing} \qquad (1)$$

$$x\text{-Ti} + (Ca_{0.09}Zr_{0.91})O_{1.91} \rightarrow (x\text{-Ti} + 0.82\ Zr + 1.64\ O) + Ca_{0.09}Zr_{0.09}O_{0.27}$$
$$\rightarrow \beta'\text{-Ti (Zr, O)} + 0.09\ CaZrO_3 \qquad (2)$$

Figure 3.9(b) displays a proposed model of microstructural evolution in reaction layer IV at the Ti/17C83Z interface. As 17C83Z reacted with Ti at 1550°C for 6 h, titanium diffused into this region and dissolved a relatively small amount of O and Zr, which diffused out of the metastable ZrO_2 phase with supersaturated 17 mol% CaO in solid solution, leading to an appearance of a so-called diffusion zone. As the solubility of Ca in Ti was quite limited, Ca was retained in the residual ZrO_2, causing the formation of columnar $CaZrO_3$. This diffusion zone consisted of a two-phase (β-Ti + $CaZrO_3$) layer and was featured by the columnar $CaZrO_3$ parallel to the diffusion direction. The formation mechanisms of β'-Ti and $CaZrO_3$ in the case of Ti/17C83Z in the reaction layer IV can be expressed as follows:

$$0.17\ CaO + 0.83\ ZrO_2 \rightarrow (Ca_{0.17}Zr_{0.83})O_{1.83} \quad \text{during hot-pressing} \qquad (3)$$

$$x\text{-Ti} + (Ca_{0.17}Zr_{0.83})O_{1.83} \rightarrow (x\text{-Ti} + 0.66\ Zr + 1.32\ O) + Ca_{0.17}Zr_{0.17}O_{0.51}$$
$$\rightarrow \beta'\text{-Ti (Zr, O)} + 0.17\ CaZrO_3 \qquad (4)$$

Moreover, as O and Zr diffused out of $CaZr_4O_9$ previously formed during hot pressing, the ratio of CaO/ZrO_2 changed from 1:4 to 1:1. Consequently, $CaZr_4O_9$ was transformed into $CaZrO_3$. This reaction mechanism can be expressed by the following equation.

$$x\text{-Ti} + CaZr_4O_9 \rightarrow (x\text{-Ti} + 3Zr + 6\ O) + CaZrO_3$$
$$\rightarrow \beta'\text{-Ti (Zr, O)} + CaZrO_3 \qquad (5)$$

It is worth mentioning that a columnar $CaZrO_3$ phase was precipitated in 17C83Z from the $CaO\text{-}ZrO_2$ solid solution. As Zr and O of the $CaO\text{-}ZrO_2$

solid solutions in 17C83Z diffused outwards or were selectively dissolved into Ti, the matrix became enriched in CaO. There were two possibilities that $CaZrO_3$ were formed. For example, it might have entered into the two-phase (C_{SS} + $CaZrO_3$) region[39] and then would decompose into *c*-ZrO_2 and $CaZrO_3$ at 1550°C through the nucleation and growth mechanism. However, a diffusion zone was generally featured by columnar precipitates, which grew along the direction parallel to that of diffusion. For instance, Goward and Boone[44] observed a diffusion zone in the aluminized nickel-based superalloys. The morphology of $CaZrO_3$ at the Ti/17C83Z interface implied that it was a diffusion zone and thus excluded the possibility that $CaZrO_3$ was formed through a decomposition process. In other words, the diffusion of Zr and O atoms out of the *c*-ZrO_2 with 17 mol% CaO in solid solution was the primary formation mechanism of the columnar $CaZrO_3$ in the diffusion zone of 17C83Z.

Figure 3.9(c) illustrates the formation of intergranular α-Zr in reaction layer V of Ti/9C91Z. The oxygen-deficient zirconia entered into a two-phase (α-Zr + ZrO_{2-x}) region[33] because of the oxidation-reduction between Ti and zirconia at such a high temperature as 1550°C. It was obvious that the oxygen-deficient zirconia was metastable because of the supersaturation of oxygen vacancies. The exsolution of Zr from ZrO_{2-x} to the grain boundaries gave rise to the formation of intergranular α-Zr with oxygen in solid solution.

Figure 3.9(d) illustrates that less intergranular α-Zr(O) was formed in 17C83Z than in 9C91Z or 5C95Z. The $CaZr_4O_9$ in reaction layer V of Ti/17C83Z could be decomposed into $CaZrO_3$ and α-Zr(O), with O partially

dissolved into β'-Ti in reaction layer IV. The decomposition of $CaZr_4O_9$ could be expressed in terms of the following equation:

$$CaZr_4O_9 \rightarrow CaZrO_3 + 3\alpha\text{-}Zr_{\text{ (with O in solid solution)}} + 6O_{\text{ (partially dissolved in β'-Ti)}} \quad (6)$$

It is also believed that the enthalpy change ΔH for an extra oxygen vacancy significantly increased with increasing vacancy concentration. While the vacancy concentration increased with increasing concentration of CaO in solid solution, the tendency of extraction of oxygen from ZrO_2 by Ti also diminished with increasing CaO content. It was thus possible that ZrO_{2-x} did not become metastable or oxygen-vacancy supersaturated, so that very little α-Zr was found at the Ti/17C83Z interface.

3.3.5 Thermodynamic Calculation for the Formation of $CaZrO_3$ at the Ti/17C83Z Interface

The metastable solid solution will be decomposed when it is in contact with Ti. The thermodynamic values for the decomposition of 17C83Z are calculated as an example. In addition to four end solid solution phases, there are four intermediate stoichiometric compounds, i.e., *o*-$CaZrO_3$, *c*-$CaZrO_3$, $CaZr_4O_9$(Φ1), and $Ca_6Zr_{19}O_{44}$(Φ2), in the CaO-ZrO_2 binary system.[45] The thermodynamic values acquired were mainly focused on the intermediate compounds $CaZrO_3$ in previous studies,[46-50] while those for the other two intermediate phases (Φ1 and Φ2) are relatively insufficient. It was reported that the intermediate compounds Φ1 and Φ2 are stable at the temperatures 1408.5-1507.1 K and 1418.9-1625.6 K, respectively, and *c*-$CaZrO_3$ was stable above 2273K[51] according to the CaO-ZrO_2 phase

diagram proposed by Wang *et al.*[45] Based on these arguments and experimental results, only *o*-$CaZrO_3$ is considered among the four intermediate compounds.

Because of lack of the experimental information for solid solution phases with a wide range of compositions, it is assumed that the decomposition is governed by the following reaction for simplicity. In other words, the 17C83Z solid solution was first decomposed into $CaZrO_3$ and ZrO_2, and then the reduction and dissolution occurred between Ti and ZrO_2.

$$0.66\ Ti + Ca_{0.17}Zr_{0.83}O_{1.83} \rightarrow 0.66\ Ti + (0.66\ ZrO_2 + Ca_{0.17}Zr_{0.17}O_{0.51})$$
$$\rightarrow 0.66\ \alpha\text{-}TiO_x + 0.66\ ZrO_{2-x} + 0.17\ CaZrO_3 \qquad \Delta G_1 \qquad (7)$$

During hot pressing, ZrO_2 and CaO are mutually dissolved as a homogeneous solid solution phase for the sake of kinetics, which can be expressed as follows.

$$0.17\ CaO + 0.83\ ZrO_2 \rightarrow Ca_{0.17}Zr_{0.83}O_{1.83} \qquad \Delta G_2 \qquad (8)$$

Using solid electrolyte galvanic cells, the standard Gibbs free energies of formation of $CaZrO_3$ from CaO and ZrO_2 at different range of temperature were determined. The formation of $CaZrO_3$ can be expressed by the following equation:

$$CaO + ZrO_2 \rightarrow CaZrO_3 \qquad \Delta G_3 \qquad (9)$$

where $\Delta G_3 = -25.2\ (\pm 0.15) - 17.58\ (\pm 0.085) \times 10^{-3} T$ (kJ/mol) and T is the absolute temperature.[47] When T = 1550°C (1823K), $\Delta G_3 = -57.25$ (kJ/mol). The reduction and dissolution between Ti and ZrO_2 can be expressed by the following equation:

$$Ti + ZrO_2 \rightarrow \alpha\text{-}TiO_x + ZrO_{2-x} \qquad \Delta G_4 \qquad (10)$$

Therefore, $\Delta G_1 = -\Delta G_2 + 0.17\ \Delta G_3 + 0.66\ \Delta G_4$. The Gibbs free energy ΔG_4 can be estimated by taking into consideration the following equivalent defect reaction.

$$O_{O\ (\text{in zirconia})}^{X} \rightarrow V_{O\ (\text{in zirconia})}^{\bullet\bullet} + 2e'_{\ (\text{in zirconia})} + O_{i\ (\text{in titanium})}'' + 2h^{\bullet}_{\ (\text{in titanium})} \qquad \Delta G_5 \qquad (11)$$

This equivalent reaction is the combination of dissolution and reduction. Based upon the calculation by Lin and Lin,[25] $\Delta G_5 = \Delta G_{red} + \Delta G_{diss} = 0.54 - 379.30 = -378.76$ (kJ/mol) at 1550°C. Since $\Delta G_4 = x\Delta G_5$, $\Delta G_1 = -\Delta G_2 + 0.17\ \Delta G_3 + 0.66\ x\ \Delta G_5$,. Substituting $\Delta G_3 = -57.25$ kJ/mol and $\Delta G_5 = -378.76$ kJ/mol, $\Delta G_1 = -\Delta G_2 - 9.73 - 249.98\ x$ (kJ/mol). Since ΔG_2 is a positive value,[52] ΔG_1 must be negative.

Based upon the discussion mentioned above, the formation of $CaZrO_3$ and ZrO_{2-x} induced by the interfacial reaction between Ti and 17C83Z is thermodynamically favorable. This calculation is in good agreement with present experimental results, indicating the formation of $CaZrO_3$, α-Ti(O), and oxygen deficient ZrO_{2-x} in layer V. It is believed that extensive

diffusion between Ti, Zr, and O is more thermodynamically favorable and results in β'-Ti (O, Zr) and $CaZrO_3$ in layer IV at the Ti/17C83Z interface.

3.4 Conclusions

1. The phase formation mechanisms at the interface between Ti and ZrO_2 strongly depended upon the types of stabilizers as well as their amounts. This study shows the promising application of CaO-stabilized-ZrO_2 as molding ceramics for Ti and its alloys while being compared with previous studies conducted on the Ti/Y_2O_3-ZrO_2 interfaces.
2. The 5C95Z shows the best performance due to the formation of a thin layer of TiO which behaves as diffusion barrier between Ti and ZrO_2. In other words, the incorporation of 5 mol% CaO into ZrO_2 could effectively suppress the interfacial reactions between Ti and 5C95Z. However, more complex layers consisting of α-Ti, β'-Ti and Ti_2ZrO were found at interfaces such as Ti/9C91Z and Ti/17C83Z. This indicates that the zirconia with 5 mol% CaO in solid solution is one of the most potential candidates for crucible and mold materials in the Ti-casting industry.
3. Both β'-Ti and spherical $CaZrO_3$ were found at the Ti/9C91Z interface after reaction at 1550°C for 6 h because of extensive dissolution of O and Zr together with a very limited solubility of Ca in Ti.
4. The outward diffusion of Zr and O, which were subsequently dissolved into Ti, gave rise to a diffusion zone featuring columnar $CaZrO_3$ in the matrix of β'-Ti after the reaction between Ti and 17C83Z. This implies that $CaZrO_3$ is a stable phase and thus as a potential refractory when it is taken into contact with titanium alloys at high temperatures.

5. For 5C95Z and 9C91Z, a large amount of α-Zr grains were excluded from metastable oxygen-deficient ZrO_{2-x} on the zirconia side far away from the original interface. In this reaction affected zone, oxygen-deficient zirconia was partially stabilized as tetragonal in 5C95Z and fully stabilized as cubic in 9C91Z.
6. A very small amount of α-Zr and $CaZrO_3$ was found on grain boundaries of zirconia on the ceramic side far away from the original interface between Ti and 17C83Z. The amount of intergranular α-Zr decreased with increasing CaO content.

Table 3.1 Designations, Compositions, Hot-Pressing Conditions, Relative Densities and XRD Phases of Hot Pressed CaO/ZrO_2 Sample

Specimens	Composition (mol%)	Hot-Pressing Conditions	Relative Densities	XRD Phases
5C95Z	5% CaO + 95% ZrO_2	1600℃/30min/1 atm Ar	98.4%	*t*-ZrO_2, *m*-ZrO_2
9C91Z	9% CaO + 91% ZrO_2	1600℃/30min/1 atm Ar	98.9%	*c*-ZrO_2, *t*-ZrO_2, *m*-ZrO_2
17C83Z	17% CaO + 83% ZrO_2	1600℃/30min/1 atm Ar	98.0%	*c*-ZrO_2, $CaZr_4O_9$

Table 3.2 Thickness and Phases in Various Reaction Layers at the Interfaces of Ti and CaO/ZrO_2 Samples after Reaction at 1550°C for 6 h

CaO content	Reaction layers in the titanium side			Reaction layers in the zirconia side		
	Layer	Thickness (μm)	Phases	Layer	Thickness (μm)	Phases
5 mol%	I	2	TiO [(1)*]	IV	8	*t*-ZrO_{2-x} [(1)]
				V	very large	*t*-ZrO_{2-x}, *m*-ZrO_{2-x}, α-Zr [(1,4)]
9 mol%	I	8	α-Ti + Ti_2ZrO [(1,2)]	IV	90	$CaZrO_3$, β′-Ti [(1,2,3)]
	II	56	α-Ti + Ti_2ZrO + β′-Ti [(1,2)]	V	very large	*c*-ZrO_{2-x}, α-Zr [(1,4)]
	III	38	β′-Ti + acicular α-Ti [(1,2)]			
17 mol%	I	8	α-Ti + Ti_2ZrO [(1,2)]	IV	86	$CaZrO_3$, β′-Ti [(1,2,3)]
	II	56	α-Ti + Ti_2ZrO + β′-Ti [(1,2)]	V	very large	*c*-ZrO_{2-x}, $CaZrO_3$, α-Zr [(1,5)]
	III	14	β′-Ti + acicular α-Ti [(1,2)]			

*Note that the formation mechanisms of various reaction layers are indicated by the superscript numbers in parenthesis: [1] outward diffusion of O; [2] outward diffusion of Zr; [3] inward diffusion of Ti; [4] excluded from ZrO_{2-x}; [5] decomposition of $CaZr_4O_9$.

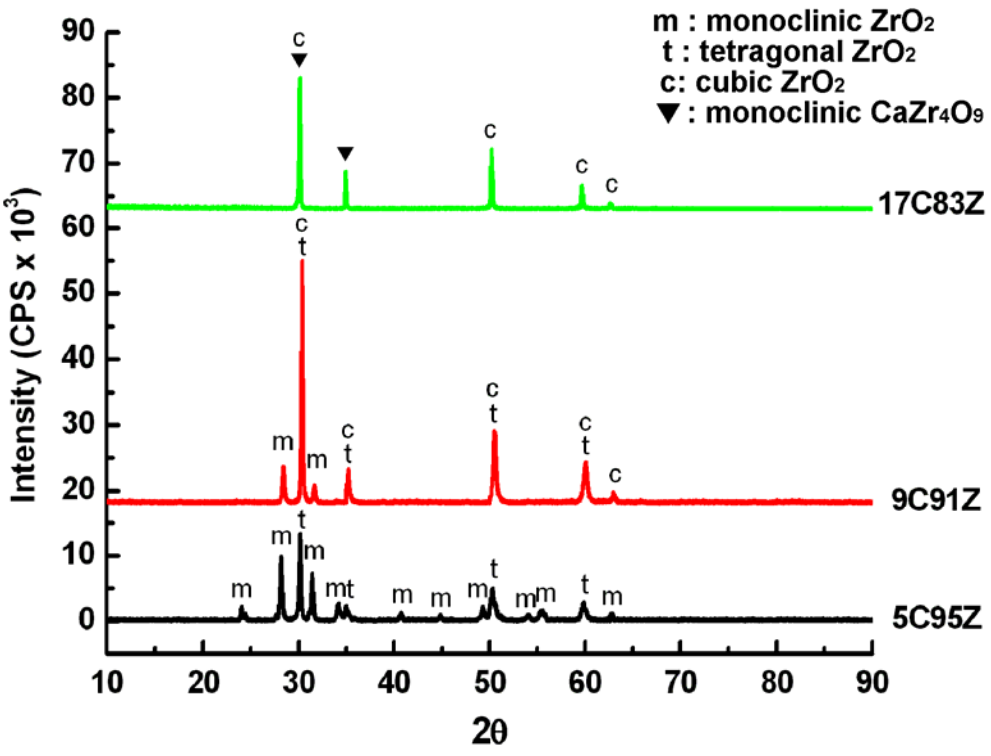

Fig. 3.1 X-ray diffraction spectra of as hot-pressed CaO/ZrO_2 samples.

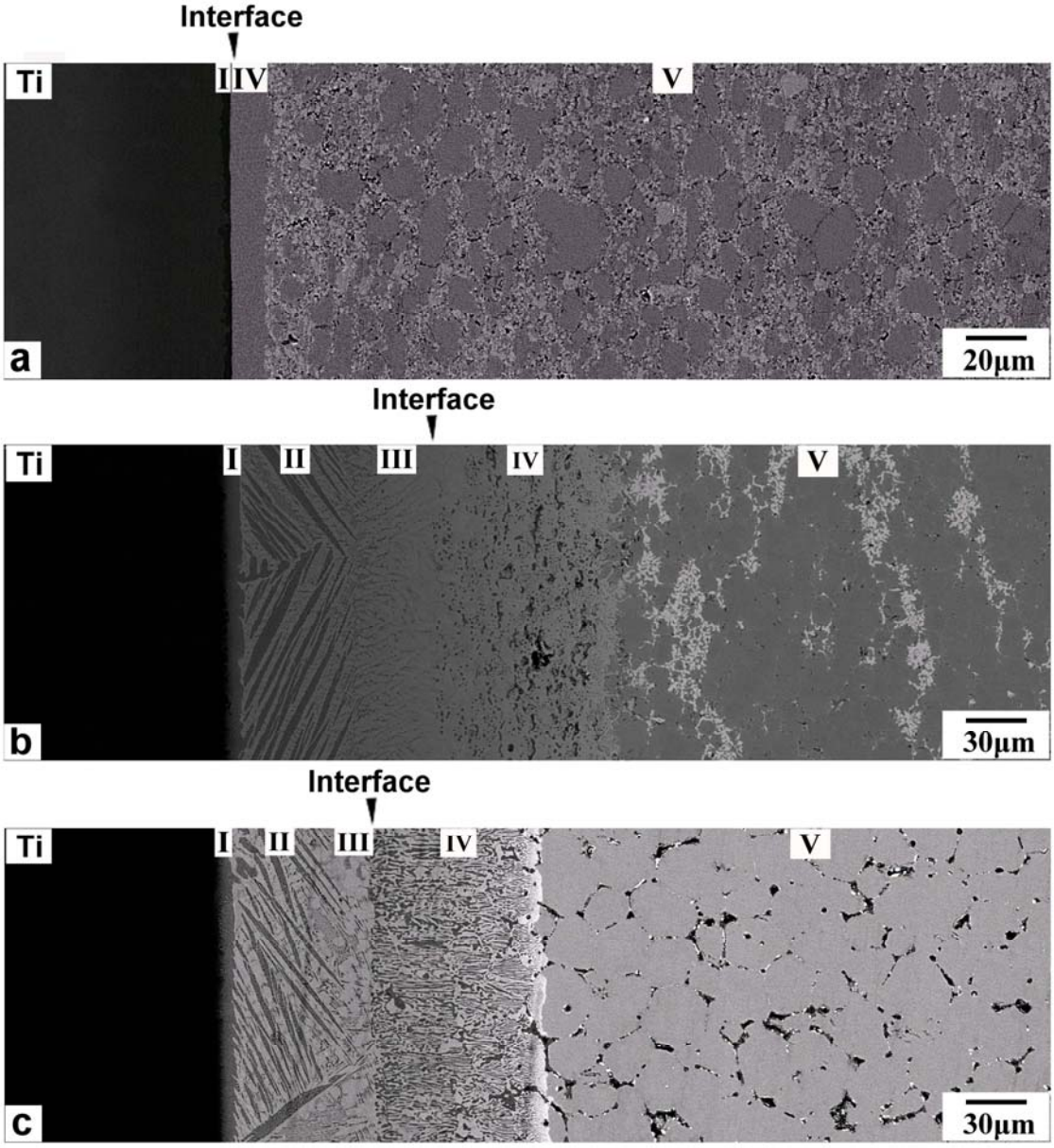

Fig. 3.2 The backscattered electron images of the interfaces between (a) Ti and 5C95Z, (b) Ti and 9C91Z, and (c) Ti and 17C83Z after reaction at 1550°C for 6 h. The arrows indicate the original interfaces between Ti and CaO/ZrO_2 samples before reaction.

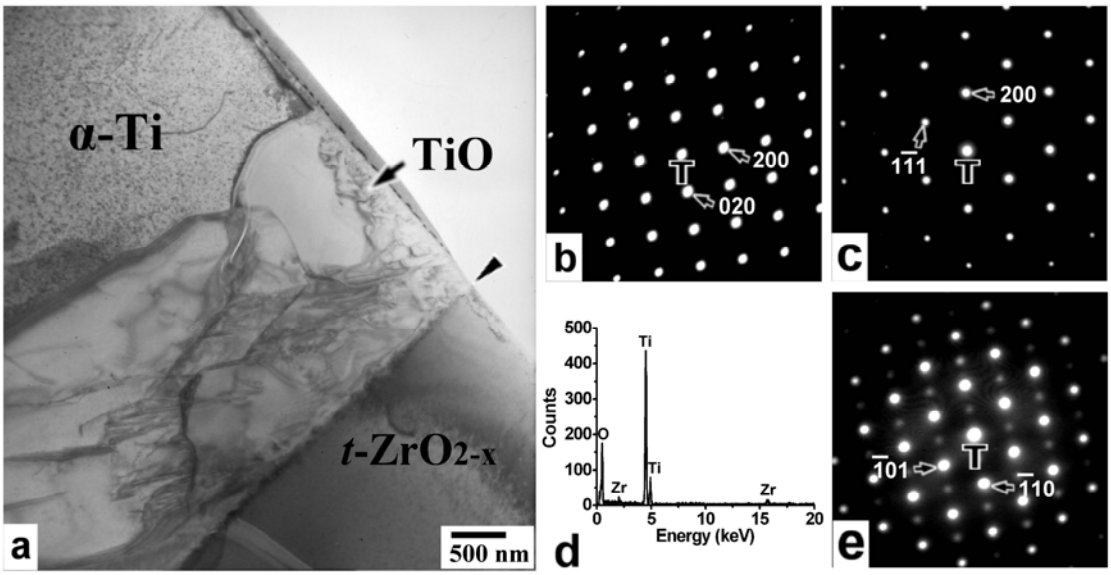

Fig. 3.3 (a) The bright-field image of reaction layers I and IV at the Ti/5C95Z interface after reaction at 1550°C for 6 h. The arrow indicates the original interface between Ti and 5C95Z prior to reaction; (b) and (c) selected area diffraction patterns (SADPs) of TiO along the [001] and [011] zone axes, respectively; (d) an energy dispersive spectrum of TiO; (e) a selected area diffraction pattern of t-ZrO_{2-x} along the zone axis [111].

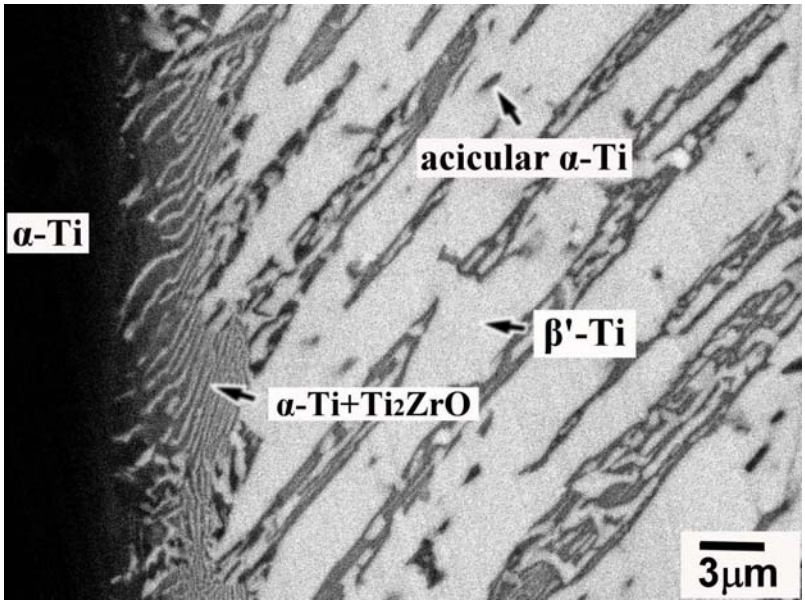

Fig. 3.4 The backscattered electron image of reaction layers I and II at the Ti/17C83Z interface after reaction at 1550°C for 6 h.

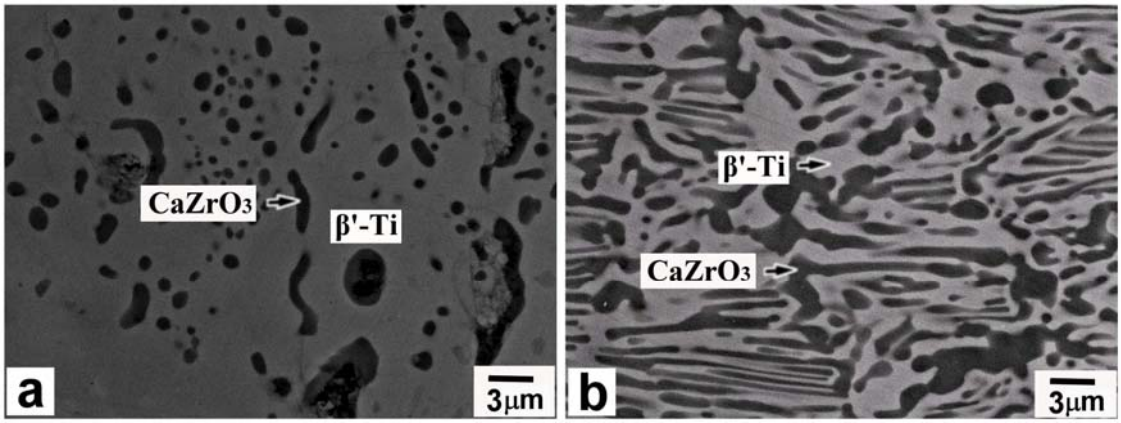

Fig. 3.5 The backscattered electron images of reaction layer IV at the interface between (a) Ti and 9C91Z, and (b) Ti and 17C83Z after reaction at 1550°C for 6 h.

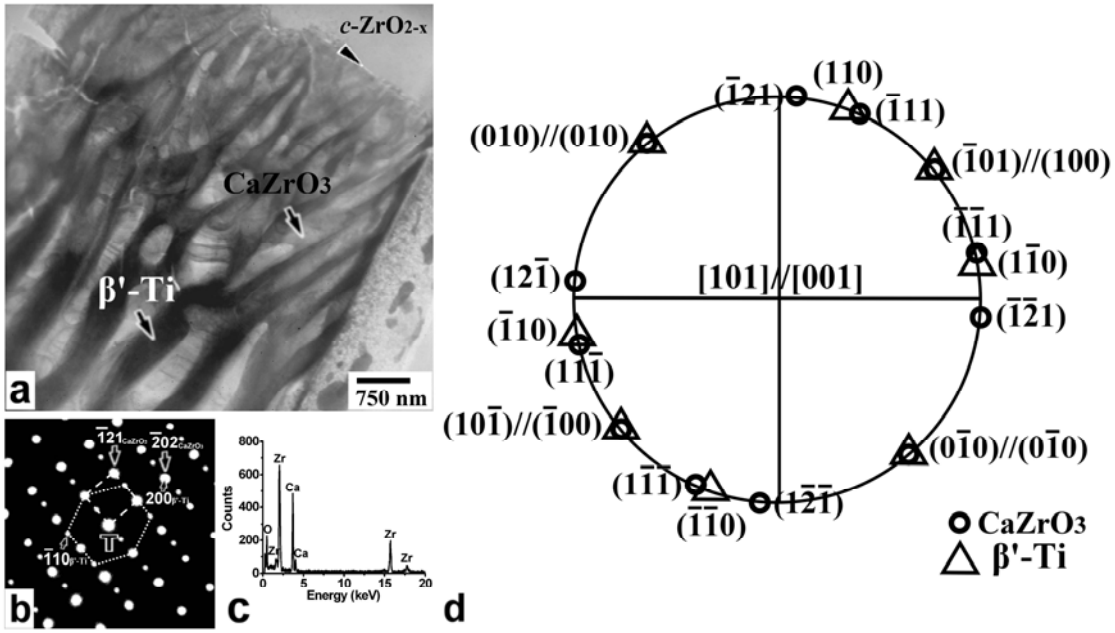

Fig. 3.6 (a) The bright-field image of reaction layers IV and V at the Ti/17C83Z interface after reaction at 1550°C for 6 h; (b) selected area diffraction patterns of the $CaZrO_3$ and β'-Ti, Z = $[101]_{CaZrO3}$ //$[001]_{β'-Ti}$; (c) an energy dispersive spectrum of $CaZrO_3$; (d) the standard stereographic projection with $[101]_{CaZrO3}$ //$[001]_{β'-Ti}$.

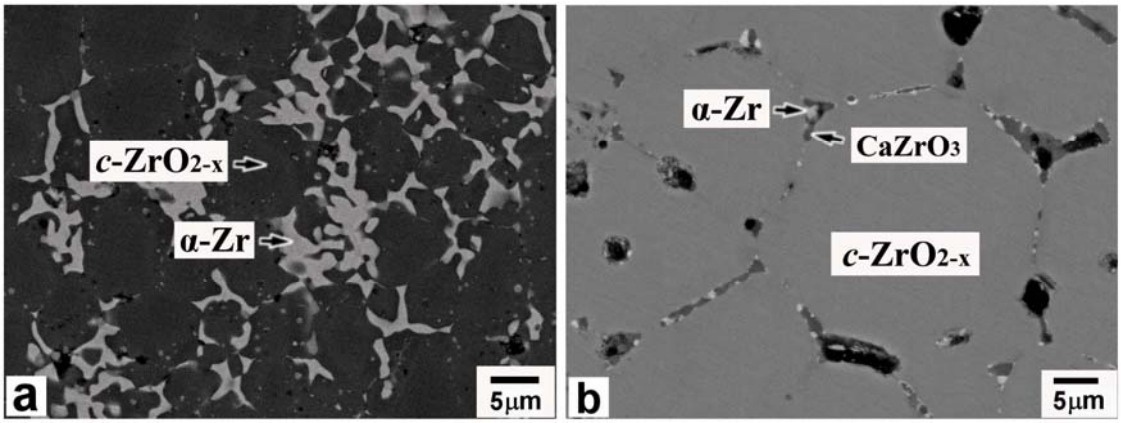

Fig. 3.7 The backscattered electron images of reaction layer V in the zirconia side far away from the original interface after reaction at 1550°C for 6 h between (a) Ti and 9C91Z and (b) Ti and 17C83Z.

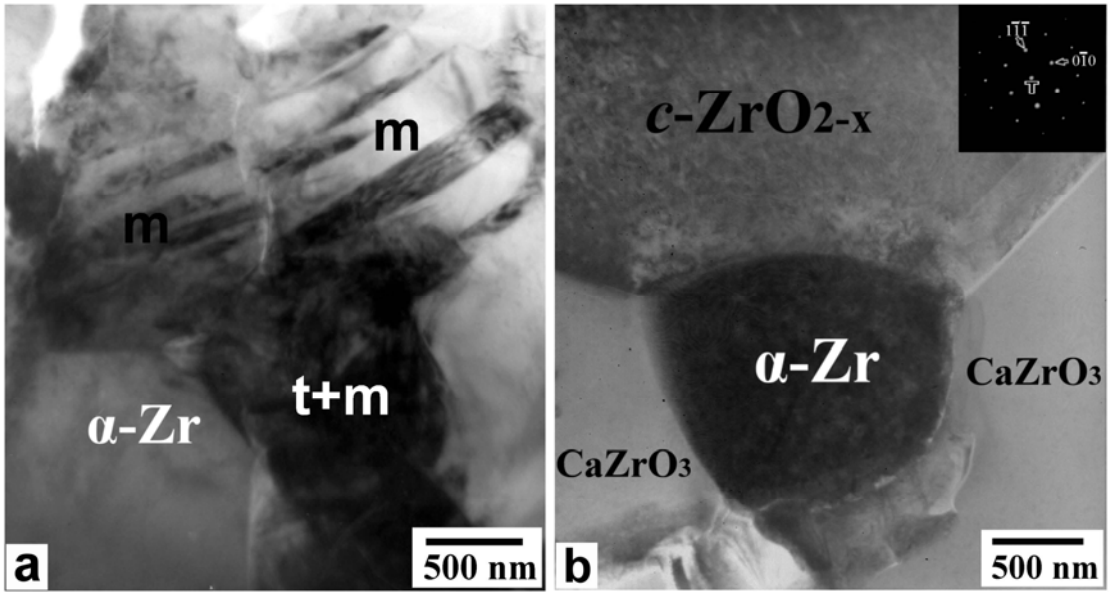

Fig. 3.8 Bright-field images of reaction layer V in the zirconia side far away from the original interface between (a) Ti and 5C95Z and (b) Ti and 17C83Z after reaction at 1550°C for 6 h. Inset in the upper right hand corner of Fig. 9(b) is a selected area diffraction pattern of α-Zr along the [101] zone axis.

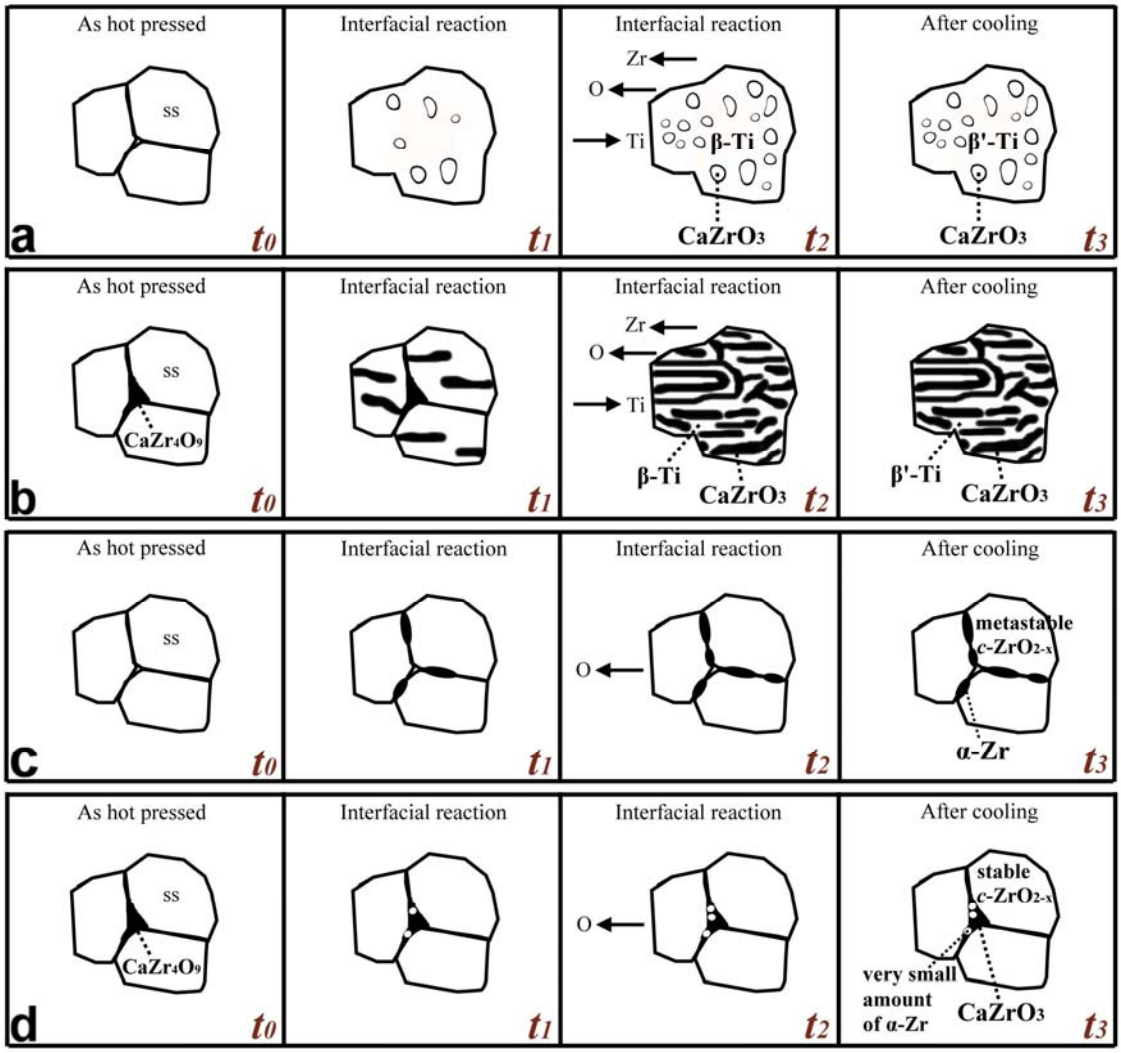

Fig. 3.9 Schematic diagrams showing the formation mechanisms of (a) $CaZrO_3$ in reaction layer IV at the Ti/9C91Z interface; (b) $CaZrO_3$ in reaction layer IV at the Ti/17C83Z interface; (c) α-Zr in reaction layer V in 9C91Z; (d) α-Zr in reaction layer V in 17C83Z at various intervals ($t_0 < t_1 < t_2 < t_3$). The arrows indicate the diffusion directions for the individual atoms of Ti, Zr, and O assuming Ti and ZrO_2 are on the left- and right- hand sides, respectively.

Chapter 4

Formation Mechanisms of Interfacial Reaction Layers Between Titanium and Ceria/Zirconia Ceramics at 1550°C

4.1 Introduction

High specific strength and good corrosion resistance have led to the large-scale use of titanium in the aerospace and chemical processing industries. However, they are extremely reactive to ceramics at high temperatures, resulting in chemical reaction affected surface. The interfacial reactions between titanium and ceramics play an important role in the titanium precision casting. The interstitial elements (e.g., C, N, O, H) from the ceramic mold have a great tendency to enter into the titanium alloys during casting and cause the deterioration of mechanical properties.

Many researches[9,10,12,18,53] have been working on the reactions of the titanium with various ceramic molds or crucibles in the last few decades. Weber *et al*.[9] presented an unspecified feather-like eutectic phase in the reaction zone of Ti and MgO-ZrO_2 crucible. Ruh[10] found that zirconium entered the titanium lattice substitutionally and oxygen went to interstitial positions during the reactions between zirconia and titanium at elevated temperatures. While previous studies had been focused on the reactions taking place in the metal side, the transformation in the ceramic side had not been well attended.

Recently, Lin and his colleagues[23-27,29,37] have thoroughly investigated the phase formation mechanisms and microstructural evolution at the interface between titanium (or titanium alloys) and 3Y-ZrO_2 (or various ratios of Y_2O_3/ZrO_2) using analytical electron microscopy. The α-Ti(O), β'-Ti(Zr, O) and/or Ti_2ZrO were formed near the original interface due to the dissolution of ZrO_2 into Ti. Both lamellar orthorhombic Ti_2ZrO and spherical hexagonal Ti_2ZrO were found in α-Ti(Zr, O) after reaction at 1550°C.[24] Lin and Lin[25] also found the intergranular α-Zr, twinned *t'*-ZrO_{2-x}, lenticular *t*-ZrO_{2-x}, and/or ordered *c*-ZrO_{2-x} in the zirconia side far from the interface between Ti and 3Y-ZrO_2 after reaction at 1550°C. Concerning the reaction of Ti melt with various Y_2O_3/ZrO_2 samples at 1700°C,[37] the incorporation of more than 30 vol% Y_2O_3 in ZrO_2 could effectively suppress the reactions in the Ti side. Y_2O_3 re-precipitated in the samples containing 30-70 vol% Y_2O_3, because the solubility of Y_2O_3 in Ti was very low.

As for the interfacial reaction of Ti with various CaO-stabilized-ZrO_2 samples at 1550°C,[54] the 5 mol% CaO-ZrO_2 sample shows the best performance due to the formation of a thin layer of TiO which behaves as diffusion barrier between Ti and ZrO_2. After the reaction between Ti and 17 mol% CaO-ZrO_2, the outward diffusions of Zr and O gave rise to a diffusion zone featuring columnar $CaZrO_3$. This implies that $CaZrO_3$ is a stable phase and thus as a potential refractory when it is taken into contact with titanium alloys at high temperatures. In the region far from the original interface, scattered α-Zr and $CaZrO_3$ were found in 17 mol% CaO-ZrO_2 because a high concentration of extrinsic oxygen vacancies, which were created by the substitution of Ca^{+2} for Zr^{+4}, effectively retarded the reduction of zirconia.

Although tetravalent dopants (Si, Ge, Ti, Sn, Ce, Th, and U) do not create anion vacancies, they still stabilize tetragonal zirconia.[55] The stabilization process of the tetragonal phase in the CeO_2–ZrO_2 system can be attributed to the fact that oversized tetravalent Ce^{4+} atoms dilate the cation network, leading to an increase of strain energy. Zirconia solid solutions with tetravalent oxides have been studied in some detail, including ZrO_2-CeO_2,[56] ZrO_2-TiO_2,[57,58] and ZrO_2-GeO_2[59]. Ce^{4+} is an oversized dopant, while Ti^{4+} and Ge^{4+} are undersized. Although their phase transformation temperature for tetragonal to monoclinic decrease with increasing dopant concentration,[59] the crystallographic variations are dependent on dopant sizes. The *cla* ratio of the tetragonal form decreases with increasing Ce^{4+} content and a cubic phase forms at high Ce concentrations.[56] On the other hand, the *cla* ratio increases with increasing Ti^{4+} and Ge^{4+} content and these tetragonal solid solutions do not approach the cubic form.[57-60] Phase diagrams of these systems are also dependent on dopant sizes. ZrO_2-CeO_2[56] shows a wide tetragonal solid solution region, so are the ZrO_2-UO_2[61] and ZrO_2-ThO_2 systems.[62]

It is well known that ceria-doped Ce-TZP (tetragonal zirconia polycrystal) exhibits high toughness and high resistance to low-temperature aging degradation, and is a good candidate ceramic for structural applications.[63-66] Heussner *et al.*[67] introduced phase-transformation-induced compressive surface stresses into Ce-TZP through the reduction of CeO_2, and found that the four-point-bending strength of sintered 12 mol% CeO_2 stabilized ZrO_2 increased from 240 to 545 MPa after annealing at 1400°C for 2 h in nitrogen. Ceria based ceramics, which have higher oxygen ion conductivity than yttria-stabilized zirconia, is one of the possible electrolytes for SOFCs at low

temperatures.[68] Extensive studies have been devoted to the effect of rare-earth oxide additions on the electrical and the mechanical properties of ceria based ceramics.[69-73] Because CeO_2 was cheaper than Y_2O_3, ceria-stabilized zirconia is considered as a candidate ceramic material applied in Ti-casting industry.

At present study, various ratios of CeO_2/ZrO_2 samples were attempted to achieve better control over the interface reactions with titanium The powder mixtures of CeO_2/ZrO_2 were sintered and then allowed to react with titanium at 1550°C for 4 h in argon. Various reaction layers at the interface between titanium and CeO_2/ZrO_2 samples were characterized using analytical scanning electron microscopy and analytical transmission electron microscopy. Finally, we would attempt to elucidate the effect of CeO_2 on the interfacial reactions between Ti and various CeO_2/ZrO_2 samples.

4.2 Experimental Procedures

Bulk CeO_2/ZrO_2 specimens used in this study were prepared from the starting powders of zirconia (> 99.95 wt% ZrO_2+HfO_2 with HfO_2 accounting for approximately 2%-3% of this total, < 0.02 wt% Fe_2O_3, < 0.02 wt% TiO_2, < 0.004 wt% SiO_2, < 0.004 wt% Al_2O_3, < 0.002 wt% CaO; 0.5 μm in average; Toyo Soda Mfg. Co., Ltd. Tokyo, Japan), and cercia (> 99.9 wt% CeO_2, < 0.04 wt% CaO, < 0.03 wt% SiO_2, < 0.02 wt% Fe_2O_3, < 0.01 wt% Na_2O_3; 0.5 μm in average; NYC, Ltd., Fukuoka, Japan) by sintering in air at 1400°C for 4 h at 5°C/min heating rate (Lindberg/Blue M STF54454C, Thermo Fisher Scientific Inc., Waltham Massachusetts, USA). Thereafter, the bulk CeO_2/ZrO_2 specimens and commercially pure titanium plates

(99.7% purity, Alfa Aesar, Ward Hill, MA) were cut and machined to dimensions of 10 × 10 × 4 mm. One titanium specimen was inserted in between two pieces of each CeO_2/ZrO_2 sample to produce a sandwiched type, were slightly pressed and annealed at 1550°C for 4 h in 1 atmosphere of Ar. The hot-pressing procedures of the sandwiched samples have been described in detailed elsewhere.[54]

The CeO_2/ZrO_2 samples contained 10, 30, 50, 70, and 100 mol% CeO_2, respectively, and were balanced with ZrO_2. The sample consisting of 10 mol% CeO_2 and 90 mol% ZrO_2 was designated as 10Ce90Zr, and so on. The designations, compositions, sintering conditions, and relative densities of CeO_2/ZrO_2 samples are listed in Table 4.1.

The phase identification of the sintered CeO_2/ZrO_2 samples was performed using an x-ray diffractometer (XRD, Model MXP18, Mac Science, Yokohama, Japan). The operating conditions of x-ray diffraction were Cu K_α radition at 50 kV and 150 mA, and a scanning rate of 2 degrees/min.

The cross-sectional SEM and TEM specimens perpendicular to the interface of titanium and ceria/zirconia ceramics were cut, ground, and polished by standard procedures.[54] Microstructures at the interface were observed using a high-resolution scanning electron microscope (SEM, Model JSM 6500F, JEOL Ltd., Tokyo, Japan) equipped with an energy dispersive x-ray spectrometer (EDS, Model ISIS 300, Oxford Instrument Inc., London, UK) and an analytical transmission electron microscope (TEM, Model JEM 2100, JEOL Ltd., Tokyo, Japan) equipped with an energy dispersive x-ray spectrometer (EDS, Model ISIS 300, Oxford Instrument Inc., London, UK).

Chemical quantitative analyses for various phases were conducted by the Cliff-Lorimer standardless technique.[31] A conventional ZAF correction procedure included in the LINK ISIS software was used for the quantitative analyses. Analyses of atomic configurations in various phases were performed using computer simulation software for crystallography (CaRIne Crystallography 3.1, Divergent S.A., France).

4.3 Results and Discussion

4.3.1 XRD Analyses

Figure 4.1 shows the x-ray diffraction spectra of various CeO_2/ZrO_2 samples as well as pure CeO_2 after sintering. X-ray phases of these sintered CeO_2/ZrO_2 samples are summarized in Table 4.1. In the 10Ce90Zr, all of the CeO_2 went into solid solution in zirconia such that only *t*-ZrO_2 and *m*-ZrO_2 were detected. Cubic-ZrO_2, *t*-ZrO_2, tetragonal $Ce_2Zr_3O_{10}$,[56,74,75] and cubic $Ce_2Ze_2O_7$[76,77] were found in both 30Ce70Zr and 50Ce50Zr. $Ce_2Ze_2O_7$ and *c*-CeO_2 phase were detected in 70Ce30Zr. Comparing 30Ce70Zr and 50Ce50Zr, the ratio of $Ce_2Zr_2O_7/Ce_2Zr_3O_{10}$ was significantly increased with an increase in the content of CeO_2. In the 100Ce, only cubic CeO_2 was detected. CeO_2 was mutually dissolved or reacted with ZrO_2 as a solid solution or $Ce_2Zr_3O_{10}$ and $Ce_2Ze_2O_7$ compounds in various sintered CeO_2/ZrO_2 samples.

The solid solution of CeO_2-ZrO_2 systems can be written as *c*-$Ce_{1-x}Zr_xO_2$. The dissolution of undersized Zr into CeO_2 severely distorts and destabilizes the oxygen sublattice. Under oxidizing conditions, the oxygen sublattice distortion and destabilization may be relieved by the clustering of CeO_2-rich

and ZrO_2-rich domains. As a result, a stable ordered compound in the CeO_2–ZrO_2 system is thermodynamically unlikely. It is thus supposed that $Ce_2Zr_3O_{10}$ decomposed into ZrO_2 (with CeO_2 in solid solution) and CeO_2 (with ZrO_2 in solid solution) at high temperatures such as 1400ºC and 1550ºC.

Destabilization of *c*-$Ce_{1-x}Zr_xO_2$ can also be relieved by the reduction of Ce^{4+} to Ce^{3+}. The reducibility of CeO_2 is enhanced by the dissolution of ZrO_2 into CeO_2. For every two Ce ions reduced, an oxygen vacancy is created to maintain charge neutrality. One eighth of tetrahedral interstitial oxygen ions were vacant and ordered in $Ce_2Zr_2O_7$. Oxygen vacancies are preferentially associated with Zr, lowering its coordination and providing a stabilization effect.

4.3.2 Oxidation state of Cerium and Extrinsic Oxygen Vacancies in the Sintered CeO_2/ZrO_2 Samples

Cerium is the second element of the lanthanide series. Its electronic configuration can be described as (Xe) $6s^25d^14f^1$. In such a configuration, the volume of 6s and 5d orbital are greater than that of the 4f orbital. Therefore, $6s^2$ and $5d^1$ electrons are the only ones participating for chemical bonds. For this reason, the valance of the lanthanide elements in their configurations is habitually 3+.[32] Reports on the redox behavior of CeO_2 and CeO_2-ZrO_2 solid solutions suggest that the reduction of Ce^{4+} to Ce^{3+} is favored under reducing environments in CeO_2-containing systems.

In the evaluation of the reduction energy of CeO_2, Vicario *et al.*[78] indicated that the calculated 2.28 eV is in satisfactory agreement with the

experimental value of 1.98 eV.[79] Negas *et al.*[80] pointed out that partial reduction of Ce^{4+} to Ce^{3+} took place at temperatures above 1400°C in air. The amount of Ce^{3+}, however, seemed to be small below 1600°C, so that the ternary system ZrO_2–CeO_2–Ce_2O_3 could be regarded as the pseudobinary system ZrO_2–CeO_2 below 1600°C in air.

The influence of oxygen partial pressure on the phase relation of solid solutions in Ce-Zr-O system is that the Ce^{+4} in a solid solution of ZrO_2 will be reduced to Ce^{+3} at increased temperature in reducing atmospheres (such as H_2, CO, and NH_4) or under a vacuum of 10^{-4} to 10^{-5} torr, or in an inert atmosphere (such as Ar and He) or in the atmosphere of flame furnaces with low oxygen partial pressure (for example, oxygen partial pressure 10^{-2} torr at 1400°C).[77,81]

In the as sintered samples, $Ce_2Zr_3O_{10}$ was formed in 30Ce70Z and 50Ce50Z because of the mutual dissolution between CeO_2 and ZrO_2. The reduction of Ce^{+4} to Ce^{+3} in ZrO_2 at a low oxygen partial pressure resulted in the formation of $Ce_2Ze_2O_7$ as a 1:2 Ce_2O_3 • ZrO_2 ternary compound in 30Ce70Z, 50Ce50Z, and 70Ce30Z.

4.3.3 Microstructures of Ti and Various Sintered CeO_2/ZrO_2 Samples

Figures 4.2(a)-(e) display the backscattered electron images (BEI) of the cross-sections normal to the interfaces of Ti and various CeO_2/ZrO_2 samples after reaction at 1550°C for 4 h. Titanium is shown to the left of the micrograph, while zirconia is on the right-hand side. The vertical arrows in the upper side of individual figures indicate the original interfaces of Ti and individual CeO_2/ZrO_2 samples. The original interfaces were deliberately

located according to the characteristic K_α x-ray maps of cerium (not shown), which was relatively immobile compared with respect to Zr, O, and Ti, etc.

Figure 4.2(a) and (b) indicated that extensive reactions took place at the interface between Ti and ZrO_2 containing 10 mol% and 30 mol% CeO_2. It was previously reported that needle-like α-Ti and some lamellar phases were usually found in the titanium side because of the interfacial reactions between Ti and ZrO_2.[23,24,26,27] However, only a limited reaction took place on the titanium side at the interface between Ti and those samples containing more than 50 mol% CeO_2, while pure CeO_2 reacted minimally with Ti after reaction at 1550°C for 4 h. This indicated that interfacial reactions were effectively suppressed in those samples containing more than 50 mol% CeO_2. This fact plays an important role in the engineering respect of Ti castings such that a controlled interfacial reaction results in a lower amount of α-casing and thus better mechanical properties. Even though the system became more stable with increasing CeO_2, several reaction layers as well as the reaction affected zone were found on the zirconia side after the interfacial reactions between Ti and various CeO_2/ZrO_2 samples. Microstructures of the reaction layers at the interface between Ti and various CeO_2/ZrO_2 samples were characterized using SEM/EDS and TEM/EDS and the results are listed in Table 4.2. Some details will be described below.

4.3.4 Phase Formation Mechanisms in the Metal Side

Formation of β'-Ti and Ti_2ZrO. Commercially pure titanium consists of the α-Ti phase. The microstructure does not change apparently after reaction when only the α-stabilizer (i.e., oxygen in this study) is dissolved into the α-Ti phase. Conversely, as a significant amount of the β-stabilizer (i.e., Zr

in this study) diffuses outward out of the ceramic side and is dissolved into the α-Ti phase, reaction layers consisting of α-Ti and β'-Ti are then be observed in the Ti side.

Figures 4.2 (a) and (b) indicate that reaction layers "I" and "II" exist in the titanium side at the Ti/10Ce90Zr and Ti/30Ce70Zr interfaces, respectively. However, no reaction layers were observed in the titanium side at the Ti/50Ce50Zr, Ti/70Ce30Zr, and Ti/100Ce interfaces, respectively, as shown in Figs. 4.2(c)-(e). It implies that the amount of Zr diffusing across the original Ti/50Ce50Zr and Ti/70Ce30Zr interface is negligible.

Figure 4.3 displays the backscattered electron images of reaction layer "II" at the Ti/10Ce90Zr and Ti/30Ce70Zr interfaces, respectively, at a higher magnification. As shown in Fig. 4.3(a) for the Ti/10Ce90Zr interface, reaction layer "II" consisted of the acicular α-Ti (dark) in β'-Ti (bright) matrix. It was worth noting that the lamellar Ti_2ZrO (bright) precipitated only in the α-Ti (dark) matrix very close to reaction layer "III". Morphologies of reaction layer "II" at the Ti/10Ce90Zr and Ti/30Ce70Zr interfaces were very different from those of the corresponding reaction layers previously found in the Ti/ZrO_2 diffusion couple.[24,26,27,37] For the latter cases, lamellar and/or spherical Ti_2ZrO was ubiquitous in the corresponding reaction layers.

Formation of reaction layer "II" at the Ti/10Ce90Zr interface. Few extrinsic oxygen vacancies were created in 10Ce90Zr because Zr^{+4} were replaced by another isovalent cation Ce^{+4}. For the lack of extrinsic oxygen vacancies, slow diffusion of O^{-2} anions as well as Zr^{+4} cations resulted in a

thinner reaction layer and a smaller concentration of Zr in the corresponding reaction layers as compared with the results obtained for Y_2O_3-ZrO_2 and CaO-ZrO_2 systems. $Ce_2Zr_3O_{10}$ was subsequently formed in reaction layer "III" of Ti/10Ce90Zr as the concentration of Ce increased, following the outward diffusion of O and Zr from the solid solution. A diffusion zone with the columnar phase was found as a result of the outward diffusion of O and Zr in reaction layer "III" at the Ti/10Ce90Zr interface as described below.

At high temperatures, α-Ti dissolved a large amount of O and Zr to become a metastable supersaturated solid solution, thus resulting in the precipitation of the lamellar Ti_2ZrO during cooling. The formation mechanisms of β'-Ti, α-Ti, and Ti_2ZrO in the reaction layer "II" at Ti/10Ce90Zr interface can be expressed as follows:

$$2Ti + xZr + yO \rightarrow \alpha\text{-}Ti(Zr, O) + \beta\text{-}Ti(Zr, O) \quad (1)$$

$$\alpha\text{-}Ti(Zr, O) \rightarrow \alpha\text{-}Ti(Zr, O) + Ti_2ZrO \quad (2)$$

$$\beta\text{-}Ti(Zr, O) \rightarrow \beta'\text{-}Ti(Zr, O) \quad (3)$$

Formation of reaction layer "II" at the Ti/30Ce70Zr interface. Reaction layer "II" consisted of acicular α-Ti in the *β'*-Ti (bright) matrix and *α*-Ti at Ti/30Ce70Zr interface. However, no Ti_2ZrO was found at reaction layer "II" at the Ti/30Ce70Zr interface as shown in Fig. 4.3(b). Morphology of the *α*-Ti at the Ti/30Ce70Zr interface was very different from that found at the Ti/10Ce90Zr interface. The β'/α ratio approximated to unit without the formation of Ti_2ZrO in the α-Ti at the Ti/30Ce70Zr interface. It was believed that the formation of $Ce_2Zr_2O_7$ in reaction layer "III," which is

based on the fluorite structure with an ordered oxygen vacances in the tetrahedral interstitial sites, causing much faster diffusion of oxygen anions and slow diffusion of Zr in $Ce_2Zr_2O_7$. With relative fast diffusion of oxygen with respect to Zr, the α-Ti in reaction layer "II" dissolved an excess of oxygen at high temperatures, while no Ti_2ZrO precipitated in the α-Ti matrix during cooling. The formation mechanisms of β'-Ti and α-Ti in the reaction layer "II" at Ti/30Ce70Zr interface can be expressed as follows:

$$2Ti + xZr + yO \rightarrow \alpha\text{-}Ti(O) + \beta\text{-}Ti(Zr, O) \rightarrow \alpha\text{-}Ti(O) + \beta'\text{-}Ti(Zr, O) \quad (4)$$

As shown in Fig. 4.2(c) and (d), there was no significant interfacial reaction layer in Ti side. Formation of the secondary CeO_2 functioned as a reaction barrier phase in the outermost ceramic region, resulting in a suppressed interfacial reaction between Ti and 50 mol% - 70 mol% CeO_2-ZrO_2.

Effect of $Ce_2Zr_2O_7$ and CeO_2. It is noted that $Ce_2Zr_2O_7$ is a fast diffusion path of O ions and a sluggish diffusion path of Zr cations. In addition, CeO_2 is hardly dissolved into Ti so that few Ce diffused into the metal side. Since CeO_2 can dissolve an extended amount of ZrO_2 in solid solution, it can act as a sink of Zr or as a diffusion barrier of Zr. While $Ce_2Zr_2O_7$ and CeO_2 are the major phases in the samples containing more than 50 mol% CeO_2, Zr and Ce are unlikely to diffuse outward into the Ti side. Consequently, the outward diffusion of oxygen from the ceramic side to titanium is one of the predominant mechanisms controlling the interface reaction between Ti and the ceramic samples containing more than 50 mol% CeO_2. Simultaneously, Ti diffused into the ceramic side and dissolved Zr and O there, leading the

formation of α-Ti and β'-Ti. After an extended dissolution of Zr and O in Ti, secondary CeO_2 was formed at the interface between Ti and 50Ce50Zr or between Ti and 70Ce30Zr.

4.3.5 Formation Mechanisms of $Ce_2Zr_3O_{10}$, $Ce_2Zr_2O_7$, and Secondary CeO_2 in the Ceramic Side

The phase transformation taking place in the ceramic side (reaction layers "III" and "IV") was caused by the outward diffusion of O and Zr and inward diffusion of Ti. As mentioned above, Ce is insoluble in Ti so that it does not diffuse outwards out of the ceramic side into the metal side. The dissolution of Zr into Ti gave rise to the formation of β'-Ti with Zr and O in solid solution. The relative diffusion rates of Zr and O had an effect of α/β' ratio in reaction layer "II."

Formation of $Ce_2Zr_3O_{10}$ at the Ti/10Ce90Zr interface. Figure 4.4(a) shows the backscattered electron image of reaction layer "III" at the Ti/10Ce90Zr interface. Zr and O diffused outwards from the 10Ce90Zr solid solution and were dissolved in titanium during reaction at 1550°C for 4 h. On the other hand, titanium diffused into the ceramic side, where it dissolved a significant amount of O and Zr. Both α-Ti and β-Ti were formed as Ti and ZrO_2 were mutually dissolved in either way mentioned above. However, CeO_2 remained in the solid solution because of the very limited solubility of CeO_2 in Ti, giving rise to the formation of 2:3 $CeO_2 \cdot ZrO_2$ ternary compound (or $Ce_2Zr_3O_{10}$) after reaction. The EDS results indicate that $Ce_2Zr_3O_{10}$ consisted of 13.11 at% Ce, 20.52 at% Zr, and 66.37 at% O. The formation mechanisms of α-Ti, β'-Ti, and $Ce_2Zr_3O_{10}$ in reaction layer "III" can be expressed as follows:

$$0.1\ CeO_2 + 0.9\ ZrO_2 \rightarrow (Ce_{0.1}Zr_{0.9})O_2 \qquad \text{during sintering} \qquad (5)$$

$$Ti + (Ce_{0.1}Zr_{0.9})O_2 \rightarrow (Ti + 0.75\ Zr + 1.5\ O) + Ce_{0.1}Zr_{0.15}O_{0.5}$$
$$\rightarrow x\ \alpha\text{-Ti (O, Zr)} + (1\text{-}x)\ \beta'\text{-Ti(Zr, O)} + 0.05\ Ce_2Zr_3O_{10} \qquad (6)$$

Figure 4.5(a) shows the bright-field image (BFI) of reaction layers "II" and "III" at the Ti/10Ce90Zr interface. Reaction layer "III" consisted of α-Ti, β'-Ti, and $Ce_2Zr_3O_{10}$. The arrow marked below the BFI micrograph indicates the original interface located between reaction layers "II" and "III" after reaction at 1550ºC/4 h. A large amount of spherical or worm-like $Ce_2Zr_3O_{10}$ existed in reaction layer "III." Figure 4.5(a) also shows Ti_2ZrO lamellae precipitated in the α-Ti matrix in the reaction layer "II." With the diffraction spots being indexed in Fig. 4.5(b), the orientation relationship of Ti_2ZrO and α-Ti was thus recognized as follows: $[110]_{Ti2ZrO}$ // $[0001]_{\alpha\text{-Ti}}$ and $(1\ \bar{1}\ 0)_{Ti2ZrO}$ // $(10\ \bar{1}\ 0)_{\alpha\text{-Ti}}$. Crystal structures of Ti_2ZrO and α-Ti were identified to be orthorhombic and hexagonal based upon the superimposed selected area diffraction patterns (SADPs), as shown in Fig. 4.5(b). Figure 4.5(c) shows the SADP of the $Ce_2Zr_3O_{10}$ phase along the zone axis of [001], of which the crystal structure was identified to be tetragonal.

Formation of $Ce_2Zr_2O_7$ at the Ti/30Ce70Zr interface. As shown in Fig. 4.2(b), a much thicker reaction layer "III" (β'-Ti + $Ce_2Ze_2O_7$) existed at the Ti/30Ce70Zr interface. On contact with Ti, $Ce_2Zr_3O_{10}$ was reduced into $Ce_2Zr_2O_7$ with the release of Zr and 3O. Formation of $Ce_2Zr_2O_7$, which one-eighth of tetrahedral interstitial sites were oxygen vacancies, causes the relatively fast diffusion of oxygen anion into Ti. A very thick (β'-Ti +

$Ce_2Ze_2O_7$) layer at Ti/30Ce70Zr interface was caused by the fast diffusion of O and the extensive inter-diffusion of Ti and O. Meanwhile, Zr diffused relatively slow in comparison with O so that a concentrated Zr existed in the matrix, leading to the formation of β-Ti(O, Zr) rather than α-Ti, Reaction layer "III", which dissolved a significant amount of zirconium (β stabilizer), was composed of β'-Ti solid solution and an interconnected stable $Ce_2Zr_2O_7$ phase as shown in Fig. 4.4(b). The EDS analyses showed that $Ce_2Zr_2O_7$ contained 18.21 at% Ce, 18.52 at% Zr, and 63.27 at% O. As O and Zr diffused out of $Ce_2Zr_3O_{10}$, formed previously during sintering, the $Ce_2Zr_3O_{10}$ decomposed in the expression of the following equation:

$$\begin{aligned} Ti + Ce_2Zr_3O_{10} &\rightarrow Ti + (Ce_2Zr_2O_7 + Zr + 3O) \\ &\rightarrow (Ti + Zr + 3\,O) + Ce_2Zr_2O_7 \\ &\rightarrow \beta'\text{-}Ti(Zr, O) + Ce_2Zr_2O_7 \end{aligned} \quad (7)$$

Figure 4.6(a) shows the BFI of the reaction layer "III" at the Ti/30Ce70Zr interface. Crystal structure of the $Ce_2Zr_2O_7$ phase was identified to be cubic based on the SADPs as shown in Fig. 4.6(b) and (c) with the zone axes of [111] and [001], respectively. The $Ce_2Zr_2O_7$ possesses the pyrochlore type structure (space group $Fd\bar{3}m$) in which one out of every eight oxygen ions is missing in the stoichiometric fluorite. The pyrochlore lattice can be explained as a cation-ordered and anion-deficient fluorite lattice. The ordering process transforms the symmetry of the lattice from $Fm\bar{3}m$ to $Fd\bar{3}m$ with doubling of the unit cell parameter. The ideal $Ce_2Zr_2O_7$ structure is described as an ordered cubic close-packed array of cations (16d and 16c sites) with the oxygen ions occupying seven-eighths of the

tetrahedral sites (48f and 8b sites). The oxygen vacancies in the remaining one-eighths of the tetrahedral sites (8a site) are also ordered.

Formation of secondary CeO_2 and $Ce_2Zr_2O_7$ at the Ti/50Ce50Zr interface. Figure 4.7(a) displays that reaction layer "III" at Ti/50Ce50Zr interface consisted of α-Ti, secondary CeO_2, and a minor β'-Ti. The EDS analyses indicate that the CeO_2 contained 32.14 at% Ce, 64.57 at% O, 1.21 at% Ti, and 2.08 at% Zr. The secondary CeO_2 were formed in reaction layer "III" after Zr and O rather than Ce in $Ce_2Zr_3O_{10}$ were selectively dissolved in Ti. Furthermore, it was evident that the inward diffusion of Ti into the ceramic region was the predominant mechanism. The worm-like morphology excluded the possibility that the secondary CeO_2 was formed through the outward diffusion of Zr and O.

Formation of the secondary CeO_2, which functioned as a reaction barrier phase, effectively retarded the diffusion of O and Zr so that a suppressed interfacial reaction was observed between Ti and 50Ce50Zr. Thus it was concluded that the interfacial reaction between Ti and 50Ce50Zr was better controlled. The formation mechanisms of α-Ti, β'-Ti, and secondary CeO_2 in the reaction layer "III" at the Ti/50Ce50Zr interface can be expressed as follows:

$$\begin{aligned} Ti + Ce_2Zr_3O_{10} &\rightarrow Ti + (2CeO_2 \cdot 3ZrO_2) \rightarrow 2CeO_2 + (Ti + 3ZrO_2) \\ &\rightarrow 2CeO_2 + x\ \alpha\text{-}Ti(O) + (1-x)\ \beta'\text{-}Ti(Zr, O) \end{aligned} \quad (8)$$

In contrast to reaction layer "III," a less amount of titanium diffused inwards into reaction layer "IV" so that β'-Ti was obtained with a relatively

concentrated O and Zr. The diffusion of O and Zr out of the $Ce_2Zr_3O_{10}$ led to an appearance of a so-called diffusion zone in the reaction layer "IV" at the Ti/50Ce50Zr interface as shown in Fig. 4.8(a). This diffusion zone was featured with the columnar phases. Reaction layer "IV" at the Ti/50Ce50Zr interface consisted of α-Ti, β'-Ti, secondary CeO_2, and a minor residual $Ce_2Zr_2O_7$, whose formation mechanisms can be proposed as follows:

$$\begin{aligned} Ti + 2Ce_2Zr_3O_{10} &\rightarrow Ti + (Ce_2Zr_2O_7 + 2CeO_2 + 4ZrO_2 + O) \\ &\rightarrow (Ti + 4ZrO_2 + O) + Ce_2Zr_2O_7 + 2CeO_2 \\ &\rightarrow x\ \alpha\text{-}Ti(O) + (1\text{-}x)\ \beta'\text{-}Ti(Zr, O) + Ce_2Zr_2O_7 + 2CeO_2 \end{aligned} \quad (9)$$

Formation of CeO_2 at the Ti/70Ce30Zr interface. Figure 4.7(b) displays that reaction layer "III" at the Ti/70Ce30Zr interface consisted of α-Ti, CeO_2, and $Ce_2Zr_2O_7$. The EDS analyses indicate that the CeO_2 contained 31.72 at% Ce, 63.92 at% O, 1.82 at% Ti, and 2.54 at% Zr. Compared with reaction layer "III" at the Ti/50Ce50Zr interface, no β'-Ti was found at the Ti/70Ce30Zr interface since less ZrO_2 content in 70Ce30Zr. It was believed that partial $Ce_2Zr_2O_7$ was reacted with Ti, resulting in the formation of α-Ti(O) and secondary CeO_2. The formation mechanisms of α-Ti, $Ce_2Zr_2O_7$, and CeO_2 in reaction layer "III" at the Ti/70Ce30Zr interface can be expressed as follows:

$$\begin{aligned} Ti + Ce_2Zr_2O_7 &\rightarrow Ti + (Ce_2O_3 \cdot 2ZrO_2) \\ &\rightarrow Ti + (Ce_2O_3 + O) + (2Zr + 3O) \\ &\rightarrow (Ti + 2Zr + 3O) + 2CeO_2 \\ &\rightarrow \alpha\text{-}Ti(O) + 2CeO_2 \end{aligned} \quad (10)$$

Reaction layer "IV" at Ti/70Ce30Zr interface also consisted of α-Ti, $Ce_2Zr_2O_7$, and CeO_2. However, the α-Ti phase was spherical and isolated in reaction layer "IV" as shown in Fig. 4.8(b). The α-Ti phase became a minor phase in the inner region of reaction layer "IV" at the Ti/70Ce30Zr interface, since a relatively small amount of Ti could reach at this region.

4.3.6 Mass Transport in Reaction Layers

The phase transformation taking place various reaction layers are caused by different mass transport mechanisms. In the metal side, reaction layers "I" and "II" were caused by the outward diffusion of Zr and O; in the ceramic side, reaction layers "III" and "IV" were formed due to the inward diffusion of Ti and outward diffusion of Zr and O, while the reaction affected zone (reaction layer "V") was caused by the outward diffusion of O.

At the Ti/10Ce90Zr interface. As Ce^{4+} replaces Zr^{4+} in 10Ce90Zr, no extrinsic oxygen vacancies takes place. As a result, oxygen as well as zirconium diffused at a much slower rate in 10Ce90Zr than in an aliovalent cation oxide (e.g., Y_2O_3) stabilized ZrO_2. Upon heating to 1550ºC, O and Zr diffused outwards from 10Ce90Zr and were dissolved in Ti, resulting in the formation of a two-phase (α-Ti + β-Ti) layer. Because CeO_2 remained in the solid solution due to the very limited solubility of CeO_2 in Ti, the increase in the ratio of CeO_2 to ZrO_2 gave rise to the formation of $Ce_2Zr_3O_{10}$ as shown in Fig. 4.9(a). During cooling, the cubic β-Ti was transformed into the orthorhombic β'-Ti.

At the Ti/50Ce50Zr interface. As shown in Fig. 4.9(b), titanium diffused inwards the reaction layer "III" and dissolved a large amount of ZrO_2,

resulting in the formation of (α-Ti + β'-Ti). The dissolution of a large amount of O and Zr from $Ce_2Zr_3O_{10}$ (formed previously during sintering) into Ti resulted in the formation of $Ce_2Zr_2O_7$. Secondary CeO_2 was formed in the reaction layer "III" due to a very limited solubility of CeO_2 in Ti when ZrO_2 was dissolved in Ti. The pyrochlore structure of $Ce_2Zr_2O_7$ possesses a connected channel of oxygen vacancies, so that $Ce_2Zr_2O_7$ is a fast oxygen diffusion path. In contrast, Zr^{+4} cations diffused very slow in $Ce_2Zr_2O_7$.

4.3.7 Phase Transformation Mechanisms in Reaction Affected Zone

In the ceramic side, reaction layer "V" is the so called reaction affected zone, which was caused by the reduction-oxidation reaction between Ti and the ceramics. The phase transformation took place in the reaction affected zone mainly because oxygen ions diffused outwards from this layer to the outer layers.

The reduction-oxidation reaction resulted in the formation of α-Zr, $Ce_2Zr_2O_7$, and CeO_2, and Ce_2O_3, etc, in the reaction affected zone or reaction layer "V," depending on the relative amount of CeO_2 and ZrO_2 in the ceramic samples. Figures 4.10(a)-(d) show the bright field images of reaction layer "V" in the ceramic sides far away from the original interfaces between Ti and 10Ce90Zr, 30Ce70Zr, 50Ce50Zr, and 70Ce30Zr, respectively.

It was attributed that oxygen ions were ready to leave out of or enter into ZrO_2, CeO_2 and their compounds when the environments were changed. While the oxidation-reduction reaction was the predominant reaction mechanism in reaction layer "V," dissolution did not play a significant role. The titanium was not detected by EDS in the reaction affected zone,

indicating that the outward diffusion of oxygen is the solely predominant phase transformation mechanism in the reaction affected zone.

Formation of α-Z and c-ZrO_{2-x} at the Ti/10Ce90Zr interface. Because of a greater affinity with Ti, oxygen ions in ZrO_2 were extracted by Ti, leading to the formation of oxygen deficient zirconia, as mentioned in previous studies. Oxygen ions in zirconia were highly deficient in reaction layer V so that the composition would go into a two-phase (α-Zr + *c*-ZrO_{2-x}) region. In other words, α-Z and *c*-ZrO_{2-x} would be observed in the reaction affected zone at the Ti/10Ce90Zr interface.

Based upon the XRD results, all the CeO_2 went into solid solution in 10Ce90Zr after sintering. However, as shown in Fig. 4.10(a), the *m*-ZrO_2 and *t*-ZrO_2 phases were transformed into *c*-ZrO_{2-x} and *α*-Zr in the reaction affected zone of 10Ce90Zr. The α-Zr particles were located in the grain boudaries of *c*-ZrO_{2-x} at the Ti/10Ce90Zr interface. The reduction-oxidation took place in reaction layer III and V can be expressed be the following equation:

$$\text{Ti}_{\text{(in III)}} + \text{ZrO}_{2\,\text{(in V)}} \rightarrow \text{Ti}_{\text{(in III)}} + [\text{ZrO}_{2-x} + x\text{O}]_{\text{(in V)}} \rightarrow \text{Ti(O)}_{\text{(in III)}} + [\text{ZrO}_{2-x}]_{\text{(in V)}} \quad (11)$$

$$[\text{ZrO}_{2-x}]_{\text{(in V)}} \rightarrow [\text{Zr}_{(1-y)}\text{O}_{2-x} + y\ \alpha\text{-Zr(O)}]_{\text{(in V)}} \quad (12)$$

$$\text{Ti}_{\text{(in III)}} + \text{ZrO}_{2\,\text{(in V)}} \rightarrow \text{Ti(O)}_{\text{(in III)}} + [\text{Zr}_{(1-y)}\text{O}_{2-x} + y\ \alpha\text{-Zr(O)}]_{\text{(in V)}} \quad (13)$$

Formation of $Ce_2Zr_2O_7$ and c-ZrO_{2-x} at the Ti/30Ce70Zr interface. The

$Ce_2Zr_3O_{10}$ in the as sintered 30Ce70Zr was reduced into $Ce_2Zr_2O_7$ in the reaction affected zone. The oxidation state of Ce was changed from +4 to +3. Figure 4.10(b) shows several $Ce_2Zr_2O_7$ grains existed along the grain boundaries of *c*-ZrO_{2-x} in the reaction affect zone of 30Ce70Zr. It is worth noting that no α-Zr was found in 30Ce70Zr, indicating that *c*-ZrO_{2-x} did not become oxygen vacancy supersaturated. It is thus inferred that $Ce_2Zr_3O_{10}$ is more reducible than ZrO_2. The formation mechanisms of $Ce_2Zr_2O_7$ and *c*-ZrO_{2-x} in reaction layer "V" can be expressed as follows:

$$\begin{aligned} Ti_{\text{(in III)}} + Ce_2Zr_3O_{10\,\text{(in V)}} &\rightarrow Ti_{\text{(in III)}} + (2CeO_2{\cdot}3ZrO_2)_{\text{(in V)}} \\ &\rightarrow Ti_{\text{(in III)}} + [(Ce_2O_3{\cdot}2ZrO_2) + O + ZrO_2]_{\text{(in V)}} \\ &\rightarrow Ti(O)_{\text{(in III)}} + [(Ce_2O_3{\cdot}2ZrO_2) + ZrO_2]_{\text{(in V)}} \\ &\rightarrow Ti(O)_{\text{(in III)}} + [Ce_2Zr_2O_7 + xO + ZrO_{2-x}]_{\text{(in V)}} \\ &\rightarrow Ti(O)_{\text{(in III)}} + [Ce_2Zr_2O_7 + ZrO_{2-x}]_{\text{(in V)}} \end{aligned} \quad (14)$$

Formation of $Ce_2Zr_2O_7$ and α-Zr at the Ti/50Ce50Zr interface. Figure 4.10(c) shows the bright field image of $Ce_2Zr_2O_7$ and dense α-Zr in the reaction affected zone of 50Ce50Zr. As mentioned above, $Ce_2Zr_3O_{10}$ in the sintered 50Ce50Zr could preferentially be reduced into $Ce_2Zr_2O_7$. However, 50Ce50Zr contained less $Ce_2Zr_3O_{10}$ than 30Ce70Zr as demonstrated by XRD results in Fig. 4.1. As a result, ZrO_2 was subjected to a greater degree of reduction in 50Ce50Zr than in 30Ce70Zr after most of $Ce_2Zr_3O_{10}$ was reduced to $Ce_2Zr_2O_7$. The dramatic reduction of ZrO_2 in the reaction affected zone of 50Ce50Zr resulted in the formation of α-Zr. The reduction of $Ce_2Zr_3O_{10}$ and ZrO_2 in the reaction affected zone of 50Ce50Zr can be expressed in terms of the following equation:

$$Ti_{(in\ IV)} + Ce_2Zr_3O_{10\ (in\ V)} \rightarrow Ti_{(in\ IV)} + (2CeO_2 \cdot 3ZrO_2)_{(in\ V)}$$
$$\rightarrow Ti_{(in\ IV)} + [(Ce_2O_3 \cdot 2ZrO_2) + O + ZrO_2]_{(in\ V)}$$
$$\rightarrow Ti(O)_{(in\ IV)} + [Ce_2Zr_2O_7 + ZrO_2]_{(in\ V)}$$
$$\rightarrow Ti(O)_{(in\ IV)} + [Ce_2Zr_2O_7 + \alpha\text{-}Zr(O) + xO]_{(in\ V)}$$
$$\rightarrow Ti(O)_{(in\ IV)} + [Ce_2Zr_2O_7 + \alpha\text{-}Zr(O)]_{(in\ V)} \quad (15)$$

Formation of $Ce_2Zr_2O_7$ and CeO_2 at the Ti/70Ce30Zr interface. Figure 4.10(d) shows the bright field image of reaction layer "V" at the Ti/70Ce30Zr interface. Secondary CeO_2 grains were re-precipitated due to the decomposition of $Ce_2Zr_2O_7$ and strong affinity of Zr and O to Ti. The composition of CeO_2 in the reaction affected zone of 70Ce30Zr was measured as 30.2 at% Ce, 66.6 at% O, and 3.2 at% Zr by TEM/EDS. The decomposition of $Ce_2Zr_2O_7$ in 70Ce30Zr can be expressed in terms of the following equation:

$$Ti_{(in\ IV)} + Ce_2Zr_2O_{7\ (in\ V)} \rightarrow Ti_{(in\ IV)} + [x(Ce_2Zr_2O_7) + (1\text{-}x)\ (Ce_2Zr_2O_7)_{(in\ V)}]$$
$$\rightarrow Ti_{(in\ IV)} + [x(Ce_2O_3 \bullet 2ZrO_2) + (1\text{-}x)\ (Ce_2Zr_2O_7)]_{(in\ V)}$$
$$\rightarrow Ti_{(in\ IV)} + [x(Ce_2O_3 + O) + x(2Zr + 3O) + (1\text{-}x)\ (Ce_2Zr_2O_7)]_{(in\ V)}$$
$$\rightarrow [Ti + 2xZr + 3xO]_{(in\ IV)} + [2xCeO_2 + (1\text{-}x)\ (Ce_2Zr_2O_7)]_{(in\ V)}$$
$$\rightarrow Ti(Zr, O)_{(in\ IV)} + [2xCeO_2 + (1\text{-}x)\ (Ce_2Zr_2O_7)]_{(in\ V)} \quad (16)$$

Formation of Ce_2O_3 at the Ti/100Ce interface. While the oxidation state of Ce can be +3 or +4, the Ce^{+4} can be reduced to Ce^{+3} at low oxygen partial pressures, high temperatures, zirconia doping or some reduction environments. An oxygen vacancy is created to maintain charge neutrality for every two Ce^{+4} ions reduced. Because the sintering was operated in Ar atmosphere, $Ce_2Zr_2O_7$ was found in 30Ce70Zr, 50Ce50Zr and 70Ce30Zr,

respectively. The CeO_2 can be reduced into Ce_2O_3 in contact with Ti, which has a great affinity with oxygen. The composition of Ce_2O_3 in the reaction affected zone of 100Ce was measured as 40.03 at% Ce and 59.97 at% O by TEM/EDS.

$$\begin{aligned} Ti_{\text{(in III)}} + 2CeO_{2\text{ (in V)}} &\rightarrow Ti_{\text{(in III)}} + (Ce_2O_3 + O)_{\text{(in V)}} \\ &\rightarrow Ti(O)_{\text{(in III)}} + (Ce_2O_3)_{\text{(in V)}} \end{aligned} \quad (17)$$

4.4 Conclusions

1. The incorporation of more than 50 mol% CeO_2 significantly suppressed the interfacial reactions at the interfaces between Ti and various sintered CeO_2/ZrO_2 samples.
2. On the metal side near the original interface, a relatively large amount of β'-Ti and α-Ti were observed after Ti reacted with 10Ce90Zr or 30Ce70Zr. However, no β'-Ti was found after Ti reacted with 50Ce50Zr or 70Ce30Zr at 1550ºC for 4 h.
3. In 10 mol% CeO_2-ZrO_2, selected dissolution of ZrO_2 into Ti gave rise to the formation of a diffusion zone with a columnar shaped $Ce_2Zr_3O_{10}$. In the 30-50 mol% CeO_2-ZrO_2 samples, Ce^{+4} was reduced to Ce^{+3} after reaction with Ti so that $Ce_2Zr_3O_{10}$ was transformed into $Ce_2Ze_2O_7$. Excess CeO_2 was re-precipitated at the interface between Ti and the samples containing 50-70 mol% CeO_2.
4. A reaction affected zone existed on the ceramic side far from the original interface due to the outward diffusion of oxygen. In the reaction affected zone, ZrO_2 was reduced into spherical α-Zr and ZrO_{2-x} and CeO_2 was reduced into $Ce_2Zr_2O_7$ and Ce_2O_3, depending upon the

relative amounts of CeO_2 and ZrO_2.

5. In the reaction affected zone, α-Zr and *c*-ZrO_{2-x} were formed in the 10 mol% CeO_2 -ZrO_2 sample; $Ce_2Zr_2O_7$ and *c*-ZrO_{2-x} existed in the 30 mol% CeO_2 -ZrO_2 sample; dense α-Zr and $Ce_2Zr_2O_7$ were found in the 50 mol% CeO_2 -ZrO_2 sample; CeO_2 and $Ce_2Zr_2O_7$ resulted in the 70 mol% CeO_2 -ZrO_2 sample; Ce_2O_3 was found in pure CeO_2.

Table 4.1 Designations, Compositions, Sintering Conditions, Relative Densities and XRD Phases of CeO_2/ZrO_2 Samples

Specimens	Composition (mol%)	Sintering conditions	Relative Densities	XRD Phases*
10Ce90Zr	10% CeO_2 + 90% ZrO_2	1400℃/4 h/Air	98.9%	*t*-$ZrO_{2(w)}$, *m*-$ZrO_{2(s)}$
30Ce70Zr	30% CeO_2 + 70% ZrO_2	1400℃/4 h/Air	99.3%	*c*-$ZrO_{2(w)}$, *t*-$ZrO_{2(w)}$, $Ce_2Zr_3O_{10(s)}$, $Ce_2Zr_2O_{7(m)}$
50Ce50Zr	50% CeO_2 + 50% ZrO_2	1400℃/4 h/Air	99.1%	*c*-$ZrO_{2(w)}$, *t*-$ZrO_{2(w)}$, $Ce_2Zr_3O_{10(m)}$, $Ce_2Zr_2O_{7(s)}$
70Ce30Zr	70% CeO_2 + 30% ZrO_2	1400℃/4 h/Air	98.8%	$Ce_2Zr_2O_{7(s)}$, *c*-$CeO_{2(w)}$
100Ce	100% CeO_2	1400℃/4 h/Air	99.5%	*c*-$CeO_{2(s)}$

*The symbols in parentheses indicate the diffracted x-ray intensities: s, strong; m, medium; w, weak.

Table 4.2 Interfacial Reaction Layers between Ti and Various CeO_2/ZrO_2 Samples after Reaction at 1550°C/4 h

Specimens	Interfacial reaction layers and phases				Reaction layer "V" in the Ceramic side
	Ti side		Ceramic side		
	I	II	III	IV	
10Ce90Zr	α-Ti + Ti_2ZrO	α-Ti + Ti_2ZrO, β′-Ti + acicular α-Ti	α-Ti, β′-Ti, $Ce_2Zr_3O_{10}$	None	*c*-ZrO_{2-x}, α-Zr
30Ce70Zr	α-Ti + Ti_2ZrO	α-Ti, β′-Ti + acicular α-Ti	β′-Ti, $Ce_2Zr_2O_7$	None	*c*-ZrO_{2-x}, $Ce_2Zr_2O_7$
50Ce50Zr		α-Ti(O)	α-$Ti_{(major)}$, CeO_2, β′-Ti	α-Ti, CeO_2, β′-Ti, $Ce_2Zr_2O_{7(minor)}$	α-Zr, $Ce_2Zr_2O_7$
70Ce30Zr		α-Ti(O)	α-$Ti_{(major)}$, CeO_2, $Ce_2Zr_2O_7$	α-Ti, CeO_2, $Ce_2Zr_2O_7$	CeO_2, $Ce_2Zr_2O_7$,
100Ce		α-Ti(O)	α-$Ti_{(major)}$, Ce_2O_3	α-Ti, $Ce_2O_{3(major)}$	Ce_2O_3

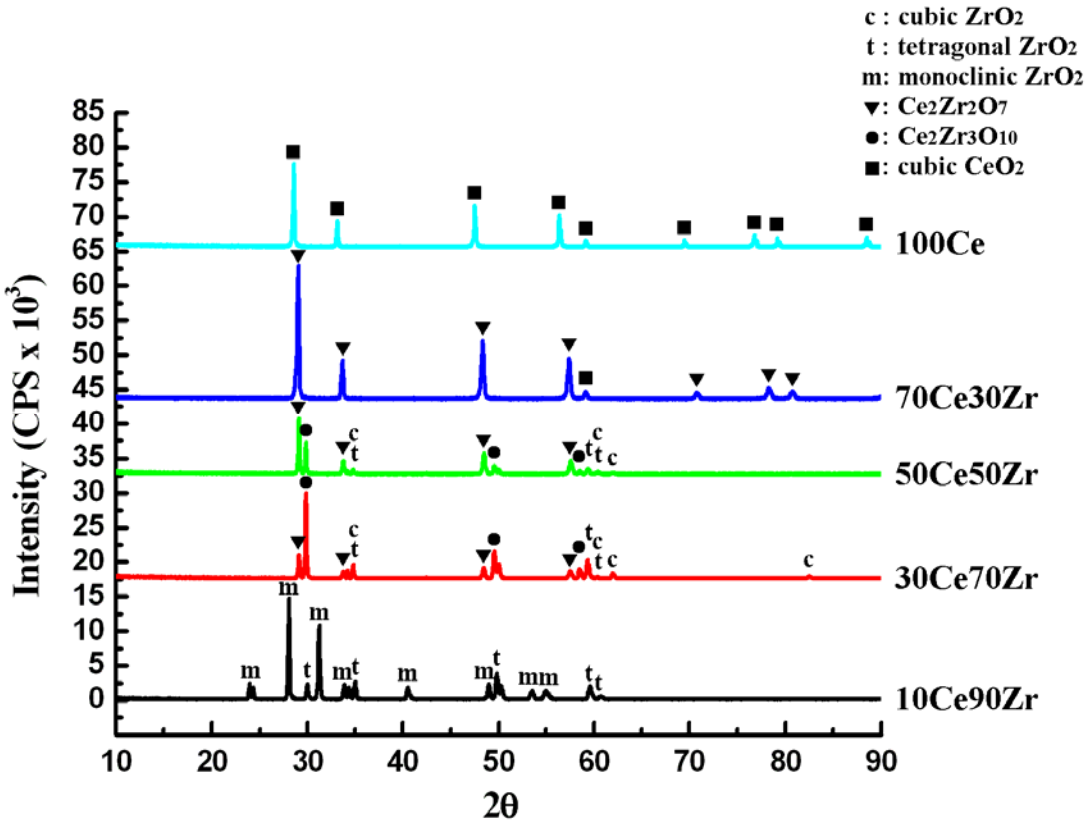

Fig. 4.1 X-ray diffraction spectra of various sintered CeO_2/ZrO_2 samples.

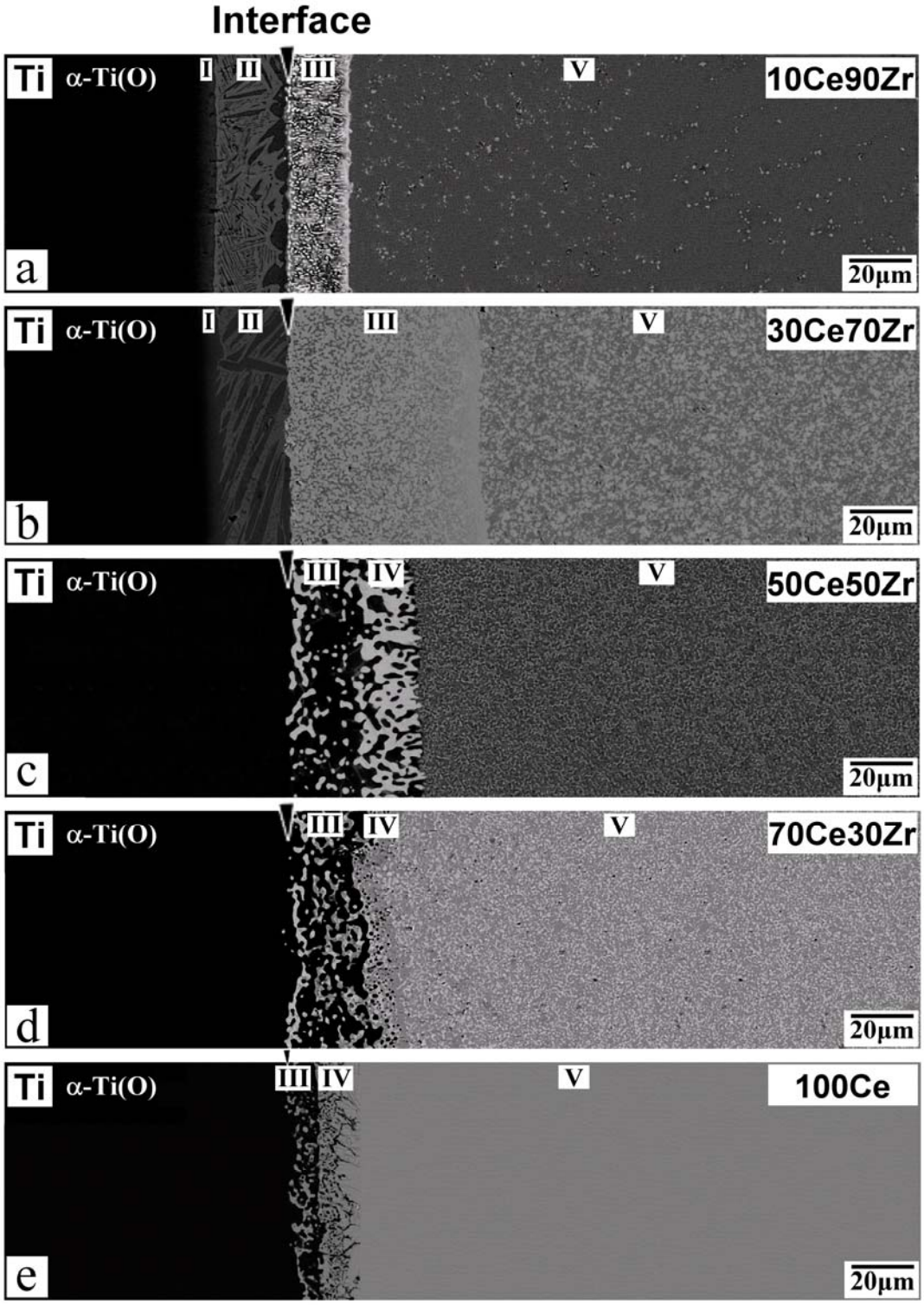

Fig. 4.2 (a)-(e) Backscattered electron images of the interfacial reaction layers between Ti and various sintered CeO_2/ZrO_2 samples after reaction at 1550°C for 4 h. Arrows indicate the original interfaces between Ti and CeO_2/ZrO_2 samples before reaction.

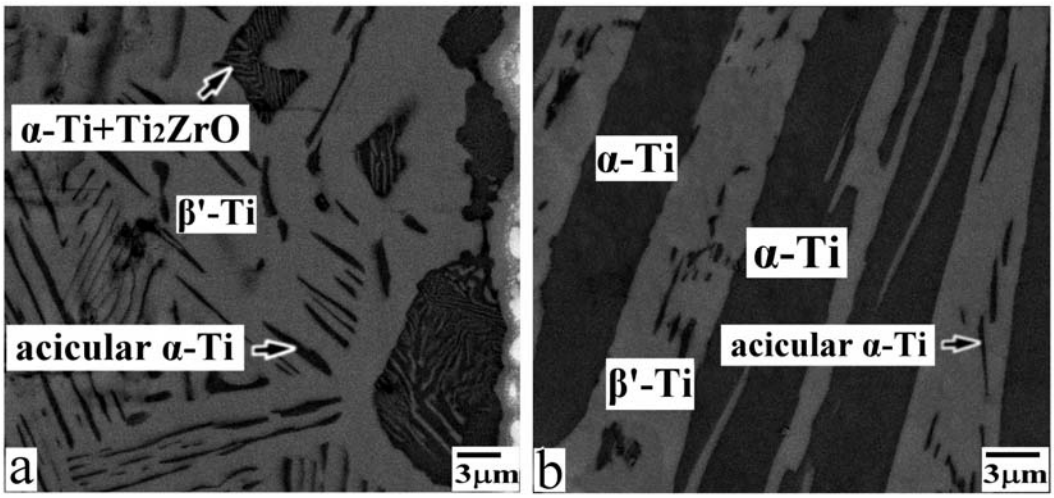

Fig. 4.3 Backscattered electron images of reaction layer "II" in the titanium side near the original interfaces between (a) Ti and 10Ce90Zr and (b) Ti and 30Ce70Zr after reaction at 1550°C for 4 h.

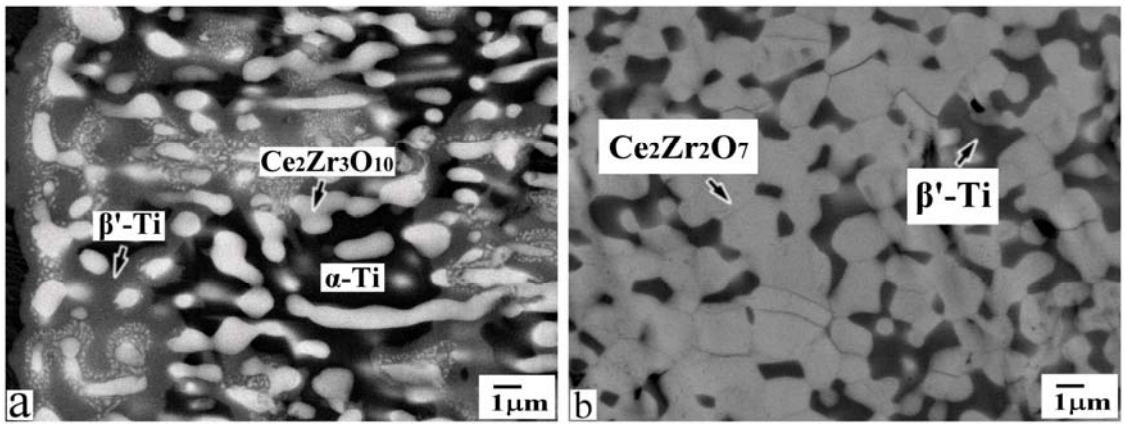

Fig. 4.4 Backscattered electron images of reaction layer "III" in the zirconia side near the original interfaces between (a) Ti and 10Ce90Zr and (b) Ti and 30Ce70Zr after reaction at 1550°C for 4 h.

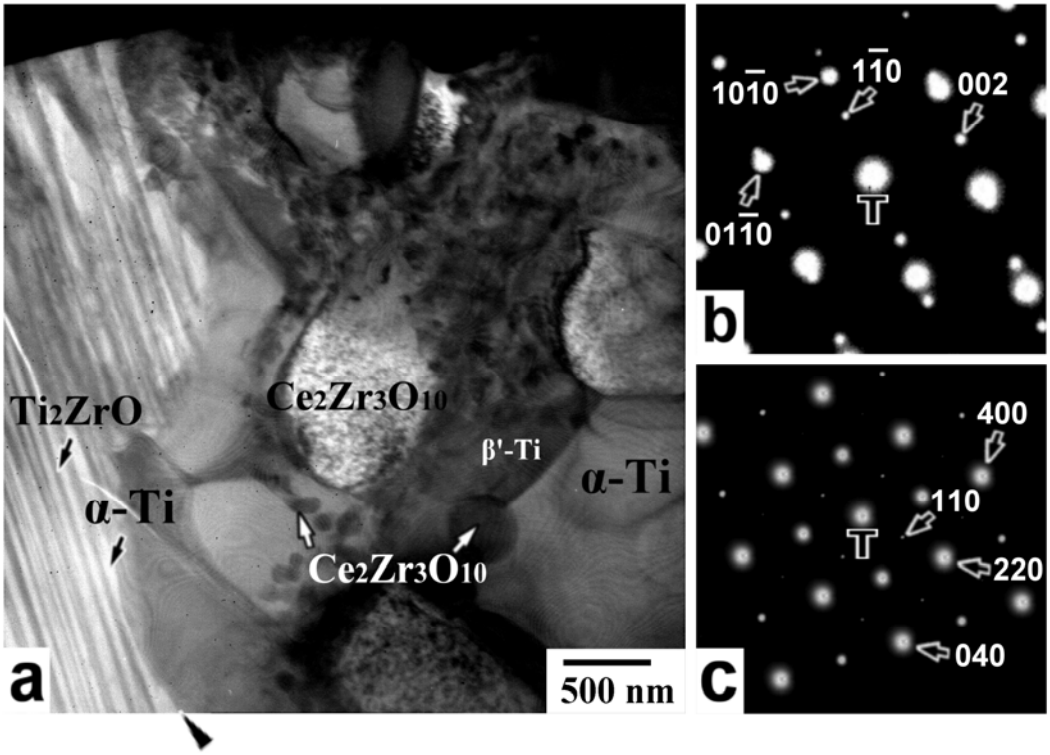

Fig. 4.5 (a) Transmission electron micrograph (bright-field image) of Ti_2ZrO, α-Ti, β′-Ti, and $Ce_2Zr_3O_{10}$ in reaction layers "II" and "III" at the Ti/10Ce90Zr interface after reaction at 1550°C for 4 h; (b) a selected area diffraction patterns of the lamellar Ti_2ZrO in α-Ti matrix, Z = $[110]_{Ti2ZrO}$ //$[0001]_{\alpha\text{-}Ti}$; (c) a selected area diffraction pattern of the $Ce_2Zr_3O_{10}$ with the zone axis [001]. Arrow below the bright-field image indicates the original interface between reaction layers "II" and "III".

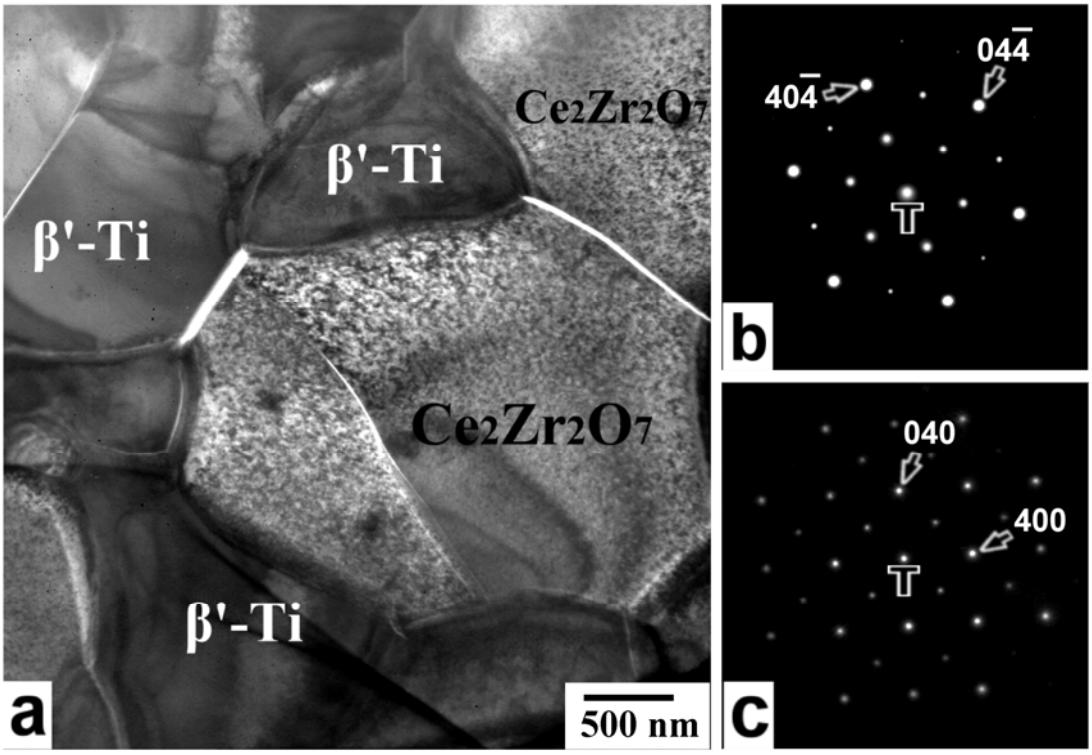

Fig. 4.6 (a) Transmission electron micrograph (bright-field image) of β′-Ti and $Ce_2Zr_2O_7$ in reaction layer "III" at the Ti/30Ce70Zr interface after reaction at 1550°C for 4 h; (b) and (c) the selected area diffraction patterns of the $Ce_2Zr_2O_7$ along the zone axes of [111] and [001], respectively.

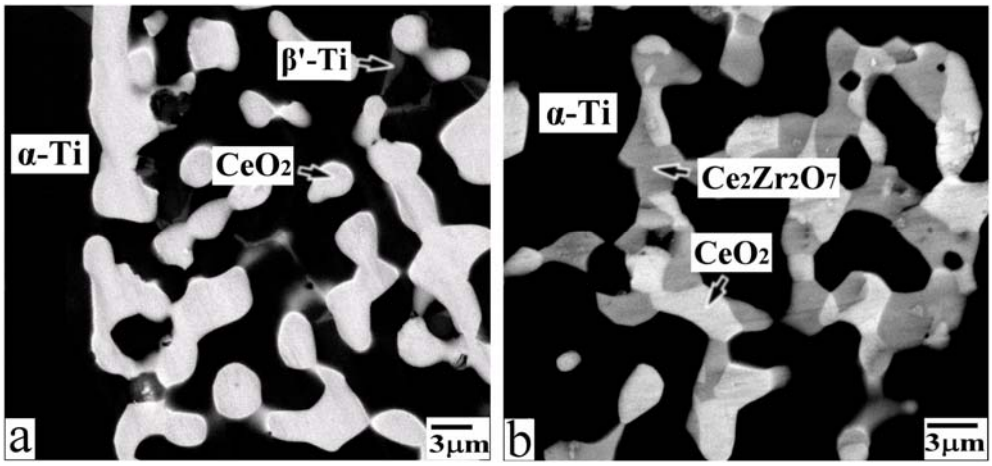

Fig. 4.7 Backscattered electron images of reaction layer "III" in the zirconia side near the original interfaces between (a) Ti and 50Ce50Zr and (b) Ti and 70Ce30Zr after reaction at 1550°C for 4 h.

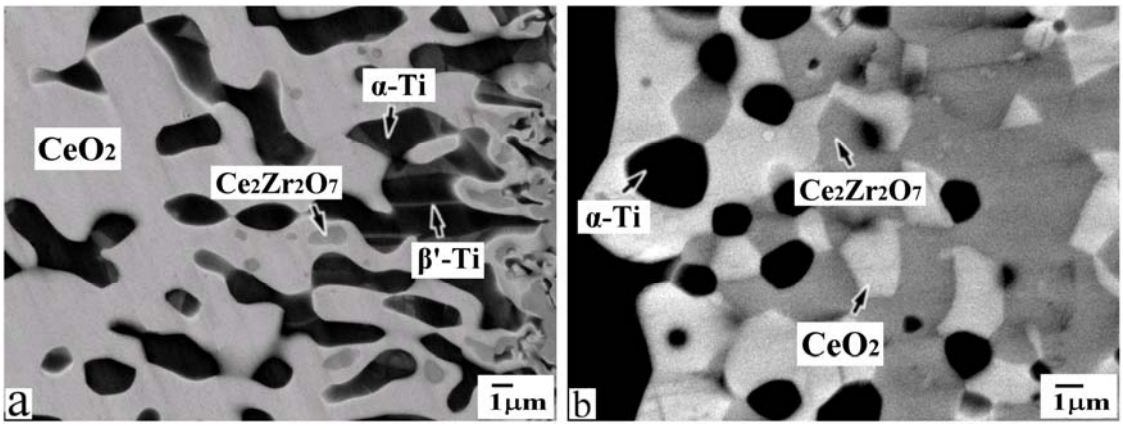

Fig. 4.8 Backscattered electron images of reaction layer "IV" in the zirconia side near the original interfaces between (a) Ti and 50Ce50Zr and (b) Ti and 70Ce30Zr after reaction at 1550°C for 4 h.

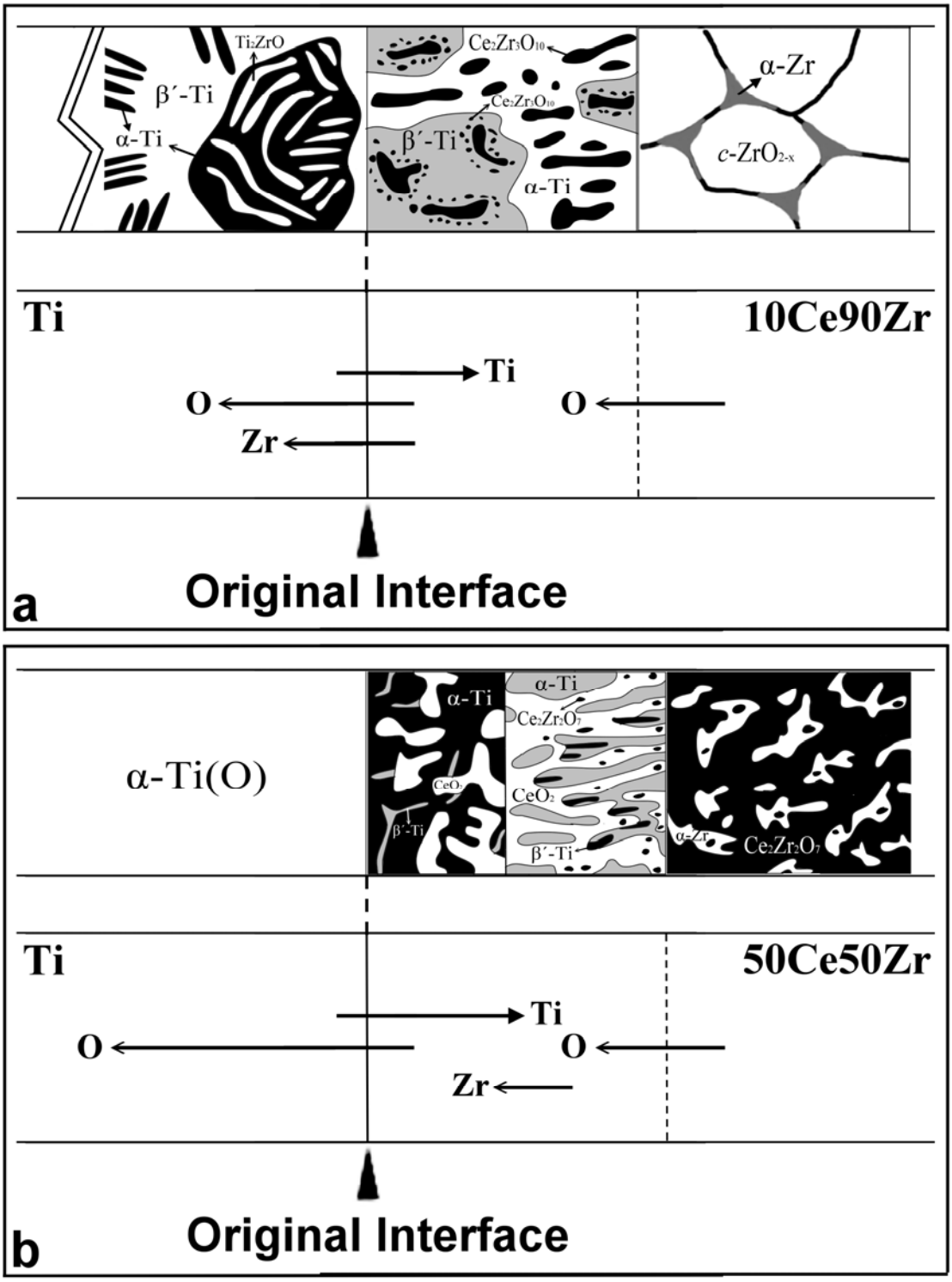

Fig. 4.9 Schematic diagrams indicate the diffusion directions for the individual atoms of O, Zr, and Ti with respect to the original interfaces between (a) Ti and 10Ce90Zr and (b) Ti and 50Ce50Zr after reaction at 1550°C for 4 h.

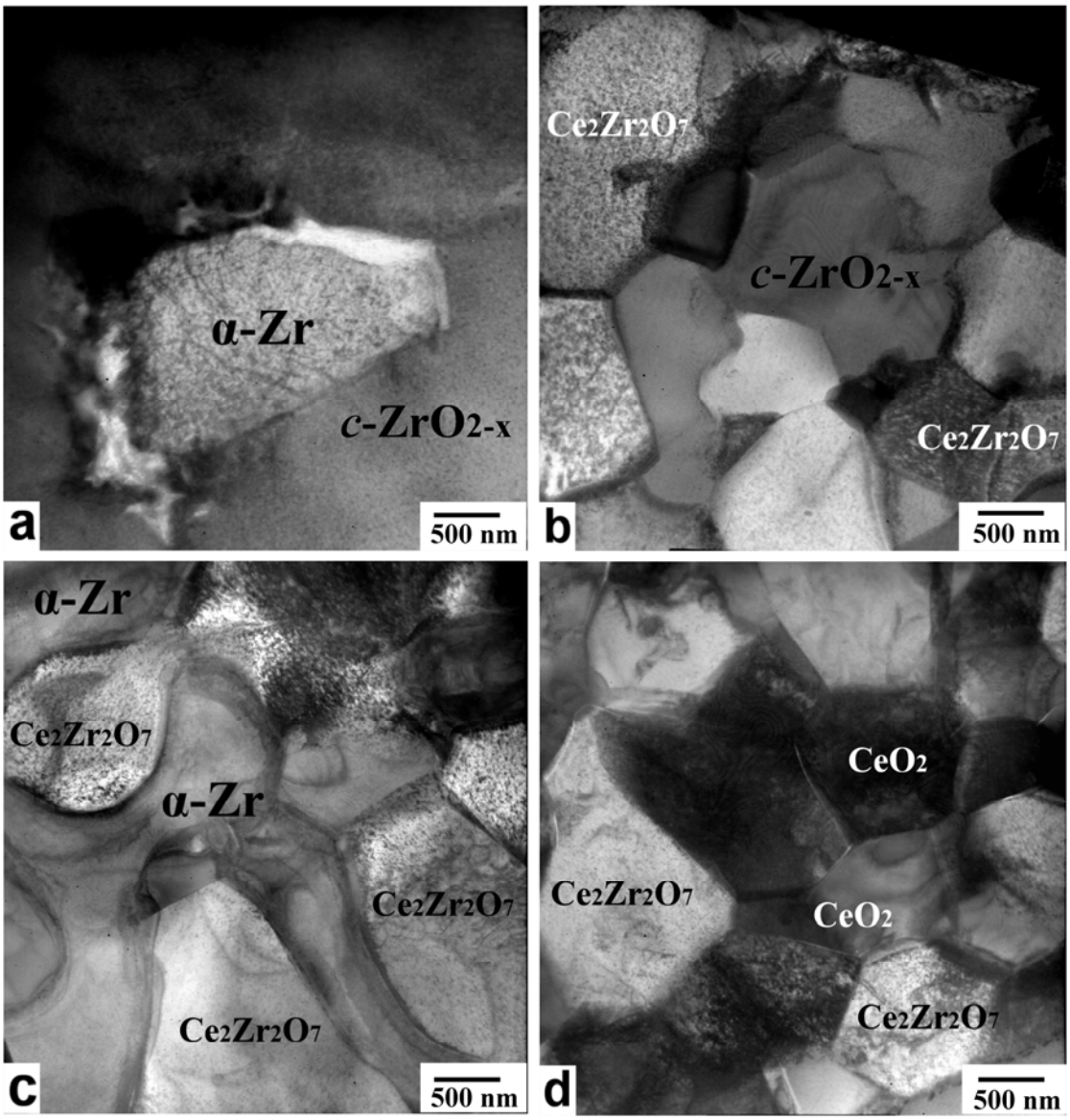

Fig. 4.10 Transmission electron micrographs (bright-field images) of reaction layer "V" in the zirconia side far away from the original interfaces between (a) Ti and 10Ce90Zr, (b) Ti and 30Ce70Zr, (c) Ti and 50Ce50Zr, and (d) Ti and 70Ce30Zr after reaction at 1550°C for 4 h.

Chapter 5
Summary

Concerning the interfacial reaction of Ti with various Y_2O_3/ZrO_2 samples at 1700°C for 10 min, the incorporation of more than 30 vol% Y_2O_3 significantly suppressed reactions at the interfaces between Ti and various Y_2O_3/ZrO_2 samples. In contrast, an extensive reaction occurred at the interface between Ti and 10Y90Z (or a partially stabilized ZrO_2) as mentioned previously. On the metal side, β'-Ti and acicular α-Ti were observed in the α-Ti matrix after Ti melt reacted with 10Y90Z or 30Y70Z. However, only a very small amount of β'-Ti was found in the α-Ti matrix after Ti reacted with 50Y50Z or 70Y30Z. Ti was almost kept intact after reaction with 90Y10Z or Y_2O_3. After reaction, β'-Ti, α-Ti and *c*-ZrO_{2-x} were found in the outermost region of 10Y90Z, while β'-Ti, α-Ti and Y_2O_3 existed in the outermost region of 30Y70Z, 50Y50Z, and 70Y30Z. The formation of Y_2O_3 in this region was caused by the extensive dissolution of ZrO_2 in Ti together with a very limited solubility of Y_2O_3. Dense α-Zr was formed along with residual ZrO_2 (cubic and/or tetragonal) or Y_2O_3 far from the original interface. The amount of α-Zr decreased with increasing amounts of Y_2O_3. Y_2O_3, existing as a solid solution or $Zr_3Y_4O_{12}$ after hot pressing, was re-precipitated in 50Y50Z and 70Y30Z far from the original interface. This was due to the oxidation-reduction reaction and the strong Ti affinity of O and Zr. Some $Zr_3Y_4O_{12}$ grains were retained in the sample containing 50 vol% Y_2O_3.

Concerning the interfacial reaction of Ti with various CaO-stabilized-ZrO_2

samples at 1550°C for 6 h, the 5C95Z shows the best performance due to the formation of a thin layer of TiO which behaves as diffusion barrier between Ti and ZrO_2. In other words, the incorporation of 5 mol% CaO into ZrO_2 could effectively suppress the interfacial reactions between Ti and 5C95Z. However, more complex layers consisting of α-Ti, β'-Ti and Ti_2ZrO were found at interfaces such as Ti/9C91Z and Ti/17C83Z. This indicates that the zirconia with 5 mol% CaO in solid solution is one of the most potential candidates for crucible and mold materials in the Ti-casting industry. Both β'-Ti and spherical $CaZrO_3$ were found at the Ti/9C91Z interface after reaction because of extensive dissolution of O and Zr together with a very limited solubility of Ca in Ti. The outward diffusion of Zr and O, which were subsequently dissolved into Ti, gave rise to a diffusion zone featuring columnar $CaZrO_3$ in the matrix of β'-Ti after the reaction between Ti and 17C83Z. This implies that $CaZrO_3$ is a stable phase and thus as a potential refractory when it is taken into contact with titanium alloys at high temperatures. For 5C95Z and 9C91Z, a large amount of α-Zr grains were excluded from metastable oxygen-deficient ZrO_{2-x} on the zirconia side far away from the original interface. In this reaction affected zone, oxygen-deficient zirconia was partially stabilized as tetragonal in 5C95Z and fully stabilized as cubic in 9C91Z. A very small amount of α-Zr and $CaZrO_3$ was found on grain boundaries of zirconia on the ceramic side far away from the original interface between Ti and 17C83Z. The amount of intergranular α-Zr decreased with increasing CaO content.

Concerning the interfacial reaction of Ti with various CeO_2/ZrO_2 samples at 1550°C for 4 h, the incorporation of more than 50 mol% CeO_2 significantly

suppressed the interfacial reactions at the interfaces between Ti and various sintered CeO_2/ZrO_2 samples. On the metal side near the original interface, a relatively large amount of β'-Ti and α-Ti were observed after Ti reacted with 10Ce90Zr or 30Ce70Zr. However, no β'-Ti was found after Ti reacted with 50Ce50Zr or 70Ce30Zr at 1550ºC for 4 h. On the zirconia side near the original interface, selected dissolution of ZrO_2 into Ti gave rise to the formation of a diffusion zone with a columnar shaped $Ce_2Zr_3O_{10}$ in the 10 mol% CeO_2-ZrO_2 sample. In the 30-50 mol% CeO_2-ZrO_2 samples, Ce^{+4} was reduced to Ce^{+3} after reaction with Ti so that $Ce_2Zr_3O_{10}$ was transformed into $Ce_2Ze_2O_7$. Secondary CeO_2 was re-precipitated at the interface between Ti and the samples containing 50-70 mol% CeO_2. A reaction affected zone existed on the ceramic side far from the original interface due to the outward diffusion of oxygen. In the reaction affected zone, ZrO_2 was reduced into α-Zr and ZrO_{2-x} and CeO_2 was reduced into $Ce_2Zr_2O_7$ and Ce_2O_3, depending upon the relative amounts of CeO_2 and ZrO_2. In the reaction affected zone, α-Zr and *c*-ZrO_{2-x} were formed in the 10 mol% CeO_2 -ZrO_2 sample; $Ce_2Zr_2O_7$ and *c*-ZrO_{2-x} existed in the 30 mol% CeO_2 -ZrO_2 sample; dense α-Zr and $Ce_2Zr_2O_7$ were found in the 50 mol% CeO_2 -ZrO_2 sample; CeO_2 and $Ce_2Zr_2O_7$ resulted in the 70 mol% CeO_2 -ZrO_2 sample; Ce_2O_3 was found in pure CeO_2.

References:

[1]G. R. Daly, "Golf Club Heads Could Become Titanium's largest Commercial Market," *Incast*, [5] 10 (1996).

[2]P. Allen, "Titanium Alloy Development," *Adv. Mat. & Proc.*, [10] 35-7 (1996).

[3]M. J. Donachie, "Titanium: A Technical Guide"; ASM International, Metals Park, OH, 1988.

[4]A. I. Kahveci and G. E. Welsch, "Effect of Oxygen on the Hardness and Alpha/Beta Phase Ration of Ti-6Al-4V Alloy," *Scr. Metall.*, **20** [9] 1287-90 (1986).

[5]P. H. Brace, "Reactions of Molten Titanium With Certain Refractory Oxides," *J. Electrochem. Soc.*, **94** [4] 170-6 (1948).

[6]D. Eylon, F. H. Freos, and R. W. Gardiner, "Developments in Titanium Alloy Casting Technology," *J. Metals*, **35** [2] 35-45 (1983).

[7]S. Bangs, "Precision Titanium Castings Capturing Aircraft Industry," *Precision Metal*, [3] 36-9 (1975).

[8]G. Economos and W. D. Kingery, "Metal-Ceramic Interactions:II, Metal Oxide Interfacial Reactions at Elevated Temperatures," *J. Am. Ceram. Soc.*, **36** [12] 403-09 (1953).

[9]B. C. Weber, W. M. Thompson, H. O. Bielstein, and M. A. Schwartz, "Ceramic Crucible for Melting Titanium," *J. Am. Ceram. Soc.*, **40** [11] 363-73 (1957).

[10]R. Ruh, "Reaction of Zirconia and Titanium at Elevated Temperatures," *J. Am. Ceram. Soc.*, **46** [7] 301-06 (1963).

[11]M. Garfinkle and H. M. Davis, "Reaction of Liquid Titanium With Some Refractory Compounds," *Trans. ASM.*, **58** 520-30 (1965).

[12]R. L. Saha, T. K. Nandy, R. D. K. Misra, and K. T. Jacob, "Evaluation of the Reactive of Titanium with Mould Materials during Casting," *Bull. Mater. Sci.*, **12** [5] 481-93 (1989).

[13]R. L. Saha and K. T. Jacob, "Casting of Titanium and It's Alloy," *Def. Sci.*, **36** [2] 121-41 (1986).

[14]L. Espie, B. Drevet, and N. Eustathopoulos, "Experimental Study of the Influence of Interfacial Energies and Reactivity on Wetting in Metal/Oxide Systems," *Metall. Trans.*, **25A** [3] 599-605 (1994).

[15]R. J. Ackermann, S. P. Garg, and E. G. Rauh, "High-Temperature Phase Diagram for the System Zr-O," *J. Am. Ceram. Soc.*, **60** [7-8] 341-45 (1977).

[16]T. Wahner, R. Kirchheim, and M. Ruhle, "Chemical Reactions at Metal/Ceramic Interfaces During Diffusion Bonding," *Acta Metall. Mater.*, **43** [3] 1053-63 (1995).

[17]R. N. Correia, J. V. Emiliano, and P. Moretto, "Microstructure of Diffusional Zirconia-Titanium and Zirconia-(Ti-6wt%Al-4wt%V) Alloy Joints," *J. Mater. Sci.*, **33** 215-21 (1998).

[18]K. I. Suzuki, S. Watakabe, and K. Nishikawa, "Stability of Refractory Oxides for Mold Material of Ti-6Al-4V Alloy Precision Casting," *J. Jpn. Inst. Met.*, **60** [8] 734-43 (1996).

[19]G. Welsch and W. Bunk, "Deformation Modes of the Alpha-Phase of Ti-6Al-4V as a Function of Oxygen Concentration and Aging Temperature," *Metall. Trans. A*, **13A** [5] 889-99 (1982).

[20]B. C. Weber, H. J. Garrett, F. A. Mauer, and M. A. Schwartz, "Observations on the Stabilization of Zirconia," *J. Am. Ceram. Soc.*, **39** [6] 197-07 (1956).

[21]J. Zhu , A. Kamiya, T. Yamada, W. Shi, K. Naganuma, and K. Mukai,

"Surface tension, Wettability and Reactivity of Molten Titanium in Ti/Yttria-Stabilized ZirconiaSystem," *Mater. Sci. Engng. A*, **327** 117-27 (2002).

[22]C.E. Holcombe and T.R. Serandos, "Consideration of Yttria for Vacuum Induction Melting of Titanium," *Metall. Trans.*, **14B** [9] 497-98 (1983).

[23]K. F. Lin and C. C. Lin, "Transmission Electron Microscope Investigation of the Interface between Titanium and Zirconia," *J. Am. Ceram. Soc.*, **82** [11] 3179-85 (1999).

[24]K. L. Lin and C. C. Lin, "Ti_2ZrO Phases Formed in the Titanium and Zirconia Interface after Reaction at 1550oC," *J. Am. Ceram. Soc.*, **88** [5] 1268-72 (2005).

[25]K. L. Lin and C. C. Lin, "Zirconia-Related Phases in the Zirconia/Titanium Diffusion Couple after Annealing at 1100o to 1550oC," *J. Am. Ceram. Soc.*, **88** [10] 2928-34 (2005).

[26]K. L. Lin and C. C. Lin, "Microstructural Evolution and Formation Mechanism of the Interface Between Titanium and Zirconia Annealed at 1550oC," *J. Am. Ceram. Soc.*, **89** [4] 1400-8 (2006).

[27]K. L. Lin and C. C. Lin, "Effects of Annealing Temperature on Microstructural Development at the Interface Between Zirconia and Titanium," *J. Am. Ceram. Soc.*, **90** [3] 893-9 (2007).

[28]K. F. Lin and C. C. Lin, "Interfacial Reactions between Zirconia and Titanium," *Scr. Metall.*, **39** [10] 1333-38 (1998).

[29]K. F. Lin and C. C. Lin, "Interfacial Reactions between Ti-6Al-4V Alloy and Zirconia Mold During Casting," *J. Mater. Sci.*, **34** 5899-906 (1999).

[30]J. I. Goldstein, "Scanning Electron Microscopy and X-ray

Microanalysis, 2nd ed." 1992.

[31]G. Cliff and G. W. Lorimer, "The Quantitative Analysis of Thin Specimens," *J. Microsc.*, **130** [3] 203-07 (1975).

[32]P. Duran, M. Gonzalez, C. Moure, J. R. Jurado, and C. Pascual, "A New Tentative Phase Equilibrium Diagram For The ZrO_2-CeO_2 System in Air," *J. Mater. Sci.*, **25** 5001-6 (1990).

[33]R. F. Domagala, S. R. Lyon, and R. Ruh, "The Pseudobinary Ti-ZrO_2," *J. Am. Ceram. Soc.*, **56** [11] 584-87 (1973).

[34]G. Broihanne and J. Bannister, "Cold Crucible Melting Gets A New Spin," *Materials World*, **8** [8] 21-23 (2000).

[35]K. Sakamoto, K. Yashikawa, T. Fujisawa, and T. Onaye, "Changes In Oxygen Contents of Titanium Aluminides by Vacuum Induction, Cold Crucible Induction and Electron Beam Melting," *Iron Steel Inst. Jpn. Int.*, **32** [5] 616-24 (1992).

[36]R. L. Saha, T. K. Nandy, R. D. K. Misra, and K. T. Jacob, "On the Evaluation of Stability of Rare Earth Oxides Face Coats for Investment Casting of Titanium," *Metall. Trans.*, **21B** [6] 559-66 (1990).

[37]C. C. Lin, Y. W. Chang, and K. L. Lin, "Effect of Yttria on Interfacial Reactions Between Titanium Melt and Hot-Pressed Yttria/Zirconia Composites at 1700oC," *J. Am. Ceram. Soc*, **91** [7] 2321-27 (2008).

[38]R. C. Garvie, "The Cubic Field in the System ZrO_2-CaO," *J. Am. Ceram. Soc*, **51** [10] 553-56 (1968).

[39]V. S. Stubican and S. P. Ray, "Phase Equilibria and Ordering in the System ZrO_2-CaO," *J. Am. Ceram. Soc*, **60** [11-12] 534-37 (1977).

[40]J. R. Hellmann and V. S. Stubican, "Stable and Metastable Phase Relations in the System ZrO_2-CaO," *J. Am. Ceram. Soc*, **66** [4] 260-64 (1983).

[41]J. R. Hellmann and V. S. Stubican, "The existence and stability of $Ca_6Zr_{19}O_{44}$ compound in the system ZrO_2-CaO," *Mat. Res. Bull.*, **17** [4] 459-65 (1982).

[42]A. H. Heuer and M. Ruhle, "On the Nucleation of the Martensitic Transformation in Zirconia (ZrO_2)," *Acta metall.*, **33** [12] 2101-12 (1985).

[43]H. Hao, Y. Wang, Z. Jin, and X. Wang, "Joining of Zirconia Ceramic to Stainless Steel and to Itself Using $Ag_{57}Cu_{38}Ti_5$ Filler Metal," *J. Am. Ceram. Soc*, **78** [8] 2157-60 (1995).

[44]G. W. Goward and D. H. Boone, "Mechanisms of Formation of Diffusion Aluminide Coatings on Nickel-Base Superalloys," *Oxidation of Metals*, **3** [5] 475-95 (1971).

[45]K. Wang, C. H. Li, Y. H. Gao, X. G. Lu, and W. Z. Ding, "Thermodynamic Reassessment of ZrO_2-CaO System," *J. Am. Ceram. Soc.*, **92** [5] 1098-104 (2009).

[46]G. Roga and M. Potoczek-Dudek, "Determination of the Standard Molar Gibbs Energy of Formation of Calcium Zirconate by a Galvanic Cell Involving Calcium-Ion Conducting Solid Electrolyte," *J. Chem. Thermodyn.*, **33** 77-82 (2001).

[47]J. Tanabe and K. Nagata, "Use of Solid-Electrolyte Galvanic Cells to Determine the Activity of CaO in the CaO-ZrO_2 System and the Standard Gibbs Free Energies of Formation of $CaZrO_3$ from CaO and ZrO_2," *Metall. Mater. Trans. B*, **27B** [8] 658-62 (1996).

[48]K. T. Jacob and Y. Waseda, "Gibbs Energy of Formation of Orthorhombic $CaZrO_3$," *Thermochim. Acta*, **239** 233-41 (1994).

[49]B. R. Brown and K. O. Bennington, "Thermodynamic Properties of Calcium Zirconate," *Thermochim. Acta*, **106** 183-90 (1986).

[50]V. A. Levitski, P. B. Narchuk, J. Hekimov, and J. I. Gerassimov,

"Thermodynamic Study of Some Solid Solutions in CaO-ZrO_2 System by emf Method," *Solid State Chem.*, **20** 119-25 (1977).

[51]E. R. Andrievskaya, A. V. Shevchenko, L. M. Lopato, and Z. A. Zaitseva, "Interactions in the System $CaZrO_3$-Y_2O_3," *Izv. Akad. Nauk SSSR Neorg. Mater.*, **25** [9] 1338-40 (1989).

[52]K. S. Mohandas and D. J. Fray, "Electrochemical Deoxidation of Solid Zirconium Dioxide in Molten Calcium Chloride," *Metall. Mater. Trans. B*, **40B** [10] 685-99 (2009).

[53]R. L. Saha and R. D. K. Misra, "Formation of low-melting eutectic at the metal-mould interface during titanium casting in zircon sand moulds," *J. Mater. Sci. Lett*, **10** 1318-19 (1991).

[54]Y. W. Chang and C. C. Lin, "Compositional Dependence of Phase Formation Mechanisms at the Interface Between Titanium and Calcia-Stabilized Zirconia at 1550oC
" *J. Am. Ceram. Soc.*, (2010).

[55]P. Li, I-W. Chen, and J. E. Penner-Hahn, "Effect of Dopants on Zirconia Stabilization-An X-ray Absorption Study: II, Tetravalent Dopants," *J. Am. Ceram. Soc.*, **77** [5] 1281-88 (1994).

[56]E. Tani, M. Yoshimura, and S. Somiya, "Revised Phase Diagram of the System ZrO_2-CeO_2 Below 1400oC," *J. Am. Ceram. Soc*, **66** [7] 506-10 (1983).

[57]C. L. Lin, D. Gan, and P. Shen, "The Effect of TiO_2 Addition on the Microstructure and Transformation of ZrO_2 with 3 and 6 mol% Y_2O_3," *Mater. Sci. Eng.* , **A129** 147-55 (1990).

[58]V. C. Pandolfelli, J. A. Rodrigues, and R. Stevens, "Effects of TiO_2 Addition on the Sintering of ZrO_2 TiO_2 Compositions and on the Retention of the Tetragonal Phase of Zirconia at Room Temperature," *J. Mater. Sci.*, **26**

5327-34 (1991).

[59]J. Lefevre, "Fluorite-Type Structural Phase Modifications in Systems Having a zirconium or Hafnium Oxide Base," *Ann. Chim.*, **8** 117-49 (1963).

[60]V. C. Pandolfelli, W. M. Rainforth, and R. Stevens, "Tetragonal Zirconia Polycrystals in the ZrO_2-TiO_2-CeO_2 System," [pp. 161-65 in Proceedings of the 1st European Ceramic Society Conference, Vol. 2. Edited by G. Dewith, R. A Terpstra, and R. Metseloar. Elsevier Science Publishing, New York] (1989).

[61]I. Cohen and B. E. Schaner, "A Metallographic and X-ray Study of the UO_2-ZrO_2 System," *J. Nucl. Mater.*, **9** [1] 18-52 (1963).

[62]P. Duwez and E. Loh, "Phase Relationships in the System Zirconia-Thoria," *J. Am. Ceram. Soc.*, **40** [9] 321-24 (1957).

[63]K. Tsukuma, Y. Kubota, and T. Tsukidate, "Thermal and Mechanical Properties of Y_2O_3-stabilized Tetragonal Zirconia Polycrystals"; pp. pp. 382-90 in in Advances in Ceramics, Vol. 12, Science and Technology of Zirconia II. Edited by N. Claussen, M. Ruhle, and A. H. Heuer. American Ceramic Society, Columbus, OH, 1984.

[64]S. B. Bhaduri, A. Chakraborty, and R. M. Rao, "Method of Fabrication Ceria-Stabilized Tetragonal Zirconia Polycrystals," *J. Am. Ceram. Soc.*, **71** [9] C-410-C-11 (1988).

[65]J. G. Duh, H. T. Dai, and B. S. Chiou, "Sintering Microstructure, Hardness, and Fracture Toughness Behaviour of Y_2O_3-CeO_2-ZrO_2," *J. Am. Ceram. Soc.*, **71** [10] 813-19 (1988).

[66]J. Wang, X. H. Zheng, and R. Stevens, "Fabrication and Microstructure-Mechanical Property Relationships in Ce-TZPs," *J. Mater. Sci.*, **27** [19] 5348-56 (1992).

[67]K. H. Heussner and N. Claussen, "Strengthening of Ceria-Doped

Tetragonal Zirconia Polycrystals by Reduction-Induced Phase Transformation," *J. Am. Ceram. Soc.*, **72** 1044-46 (1989).

[68]H. Inaba and H. Tagawa, "Ceria-based Solid Electrolytes " *Solid State Ion.*, **83** [1-2] 1-16 (1996).

[69]M. Mogensen, N. M. Sammes, and G. A. Tompsett, "Physical, Chemical and Electrochemical Properties of Pure and Doped Ceria " *Solid State Ion.*, **129** [1-4] 63-94 (2000).

[70]J. V. Herle, R. Ihringer, N. M. Sammes, G. Tompsett, K. Kendall, K. Yamada, C. Wen, T. Kawada, M. Ihara, and J. Mizusaki, "Concept and Technology of SOFC For Electric Vehicles," *Solid State Ion.*, **132** [3-4] 333-42 (2000).

[71]A. Atkinson and A. Selcuk, "Mechanical Behaviour of Ceramic Oxygen Ion-Conducting Membranes " *Solid State Ion.*, **134** [1-2] 59-66 (2000).

[72]C. Tian and S. W. Chan, "Ionic Conductivities, Sintering Temperatures and Microstructures of Bulk Ceramic CeO_2 Doped With Y_2O_3 " *Solid State Ion.*, **134** [1-2] 89-102 (2000).

[73]O. Bellon, N.M. Sammes, and J. Staniforth, "Mechanical Properties and Electrochemical Characterisation of Extruded Doped Cerium Oxide for Use as An Electrolyte for Solid Oxide Fuel Cells," *J. Power Sources* **75** 116-21 (1998).

[74]S. Roitti and V. Longo, "Investigation of Phase Equilibrium Diagrams Among Oxides by means of Electrical Conductivity Measurements. Application of the Method to the System CeO_2-ZrO_2," *Ceramurgia Int.*, **2** [2] 97-102 (1972).

[75]V. Longo and D. Minichelli, "X-Ray Characterization of $Ce_2Zr_3O_{10}$," *J. Am. Ceram. Soc*, **56** [11] 600 (1973).

[76]T. Sasaki, M. Shiroyama, M. Furukawa, T. Masaki, and M. Ohno, "Analytical Study of black colored Y_2O_3-Stabilized Tetragonal Polycrystals," pp. 78-79 in Extended Abstracts of Zirconia '86 Tokyo, Sept. 9-11 (1986).

[77]Z. C. Kang, "Phases in $Ce_{0.5}Zr_{0.5}O_{2-x}$ System," *J. Alloys and Compounds*, **408-12** 1103-07 (2006).

[78]G. Vicario, G. Balducci, S. Fabris, S. D. Gironcoli, and S. Baroni, "Interaction of Hydrogen With Cerium Oxide Surfaces: A Quantum Mechanical Computational Study," *J. Phys. Che. B*, **110** [39] 19380-5 (2006).

[79]K. A. Gschneider and L. Eyring, "Handbook on The Physics and Chemistry of Rare Earths"; North-Holland: Amsterdam, 1979.

[80]T. Negas, R. S. Roth, C. L. McDaniel, H. S. Parker, and C. D. Olson, "Influence of K_2O on the Cerium Oxide-ZrO_2 System," 605-14 (1976).

[81]T. Xu, P. Wang, P. Fang, Y. Kan, L. Chen, V. Jef, V. D. B. Omer, and V. L. Jef, "Phase Assembly and Microstructure of CeO_2-doped ZrO_2 Ceramics Prepared by Spark Plasma Sintering," *J. Eur. Ceram. Soc*, **25** [15] 3437-42 (2005).

List of Publications

1. Chien-Cheng Lin, Yao-Wen Chang, and Kun-Lin Lin, "Effect of Yttria on Interfacial Reactions Between Titanium Melt and Hot-Pressed Yttria/Zirconia Composites at 1700°C," *J. Am. Ceram. Soc.*, **91** [7] 2321-2327 (2008).

2. Yao-Wen Chang and Chien-Cheng Lin, "Compositional Dependence of Phase Formation Mechanisms at the Interface Between Titanium and Calcia-Stabilized Zirconia at 1550°C," *J. Am. Ceram. Soc.*, in press.

3. Yao-Wen Chang and Chien-Cheng Lin, "Formation Mechanisms of Interfacial Reaction Layers Between Titanium and Ceria/Zirconia Ceramics at 1550°C," to be submitted to *J. Am. Ceram. Soc.* (2010)